Photodiagnostics

CePOF paper collection

ELSEVIER

Fluorescence Spectroscopy in Renal Ischemia and Reperfusion: Noninvasive Evaluation of Organ Viability

M.F. Cassini, M.M. da Costa, V.S. Bagnato, L.F. Tirapelli, G.E.B. Silva, C.A.F. Molina, A.C.P. Martins, and S. Tucci Jr

ABSTRACT

Background. Damage provoked by ischemia in renal transplants is difficult to quantify. To determine whether a donated organ is fit for transplantation. We sought to correlate the findings of fluorescence spectroscopy (FS) with histologic evidence of ischemic injury and organ viability.

Methods. Kidneys of 33 rats were submitted to FS of the upper and lower poles as well as the middle third. Excitation was generated by the laser's wavelengths of 408, 442, and 532 nm. Rats were randomized into groups with the 30, 60, and 120 minutes warm ischemia before analysis by FS, that was repeated at 5 minutes after reperfusion.

Results. FS results in the reperfusion phase correlated with ischemia time and degree of histologic injury. After 60 or 120 minutes of ischemia, the excitation lasers of 532 and 442 nm resented a significant negative correlation coefficient with the histological grade ($r = -0.61$ and $r = -0.73$, respectively).

Conclusions. There was a strong correlation between FS and histologic changes only in the reperfusion phase after renal ischemia. The method was thus unable to assess the viability of organs before transplantation.

KIDNEY transplantation is widely recognized to be the best treatment for patients who require renal replacement therapy.[1] The continuous increase in waiting times raises the need to increase the number of donors. The transplant team frequently faces the difficult question of determining whether organs from marginal cadaver donors or those after cardiac arrest are fit for transplantation. It is difficult to quantify the intensity of damage in the graft provoked by ischemia, especially when the donor has shown signs and symptoms of hemodynamic instability reducing significantly tissue perfusion and reducing graft survival. In addition to ischemia, which promotes anerobic cell metabolism, edema, acidosis, and the risk of necrosis, reperfusion can also cause acute cell injury and renal dysfunction due to inflammatory reactions mediated by oxidants and free radicals.[2–4]

Fluorescence spectroscopy measures tissue changes by quantitating alterations in tissue spectral properties. Biological tissue absorbs, emits, and dissipates light at various wavelengths. Measurements can be performed rapidly with no organ manipulation, in contrast with a biopsy, which provides a static, focal evaluation. Evaluations by fluorescence spectroscopy do not suffer interference by the methods of hypothermic preservation because they do not involve enzymatic tests. The ideal time to assess graft viability is during hypothermic preservation and not during the post-transplant period. At present, in view of the lack of fully reliable and safe methods for the evaluation of ischemic damage before transplantation,[5] we sought to assess the technique of laser, induced fluorescence spectroscopy, an objective, noninvasive, rapid, and real-time technique, which might in the future be applied to human renal transplantations. The objective of the present study was to correlate laser-induced fluorescence spectroscopy it with histologic evidence of ischemic damage affecting organ viability.

From the Division of Urology, Department of Surgery and Anatomy, Ribeirao Preto Medical School, University of Sao Paulo, Sao Paulo, Brazil.

Address reprint requests to Marcelo Ferreira Cassini, PhD, MD, Division of Urology, Department of Surgery and Anatomy, Ribeirao Preto Medical School, University of Sao Paulo (USP), Av. dos Bandeirantes 3900 - Monte Alegre, Ribeirao Preto – Sao Paulo – Brazil. E-mail: marcelo.cassini@globo.com

0041-1345/–see front matter
http://dx.doi.org/10.1016/j.transproceed.2012.10.054

MATERIALS AND METHODS

Thirty-three adult male albino Wistar rats (*Rattus norvegicus*) weighing 200–250 g were anesthetized using intraperitoneal thiopental (20 U/100 g body weight) before a longitudinal median laparotomy to approach the left kidney. The 33 kidneys were subjected to fluorescence spectroscopy of the cortex (control group). The tip of the laser was placed on the upper and lower poles and in the middle third of the kidneys. The excitations were generated by laser beams of 408, 442, and 532 nm wavelengths. Next, the renal vascular pedicles were dissected, isolated, and controlled with a vascular mini-clamp. The animals were randomized into 3 groups that underwent 30, 60, or 120 minutes warm ischemia. During the ischemia time the kidneys were subjected to new cortical readings. New readings were obtained at 5 minutes of reperfusion after observation of the return of the pulse in the renal artery, patency of the renal vein and complete, uniform kidney reperfusion, with return to the initial color. The left kidneys were then excised for histologic study. At zero time of warm ischemia, 4 animals chosen randomly underwent contralateral nephrectomy as the histologic control group.

The study performed according to the regulations of the Brazilian College of Animal Experimentation was approved by our Ethics Committee (protocol 041-2010).

Histologic and Statistical Analysis

After staining with hematoxylin and eosin and Masson trichrome, the ischemic injuries in proximal tubular cells were classified according to the histologic grading proposed by Goujon et al (1999).[6,7] This method of evaluation is based on 7 morphologic patterns typical of proximal tubular injuries: vacuolization of the apical cytoplasm, tubular necrosis, tubular dilatation, cell detachment, brush border integrity, intracellular edema, and basement membrane denudation. Scores included a 5-point scale: 1 (no abnormality), 2 (mild injuries in ≤10% of renal tissue), 3 (injuries affecting 10%–25% of renal tissue), 4 (injuries affecting 25%–50% of renal tissue) and 5 (injuries in >50% of the renal tissue studied).

Light-View-Med (LVM.exe) software was used to acquire spectroscopy data, together with the Origin-Lab (8.Ink) software to produce and store the graphs.

Statistical analysis was performed using GraphPad PRISM software, version 4.0 (GraphPad Software Inc, San Diego, Calif). Continuous variables were compared using the nonparametric Kruskal–Wallis test followed by the Dunn multiple comparisons post-test. Associations between parameters were analyzed by linear regression. One-way analysis of variance (ANOVA) was used to evaluate renal damage, correlation coefficients were calculated and multiple comparisons corrected by Bonferroni post-tests. The level of significance was set at $P < .05$.

RESULTS

To validate the fluorescence spectroscopy method, we first analyzed the mean graphic readings obtained during phases of autofluorescence, ischemia and renal reperfusion (Fig 1). A post hoc Bonferroni test revealed the mean result of autofluorescence to be significantly higher ($P < .001$) compared with ischemia and reperfusion phases with the latter significantly greater than the ischemia phase. Ischemia of increased times (eg, from 30 to 60 minutes), showed a significant decrease in the peaks of fluorescence spectroscopy during the reperfusion phase (Fig 2).

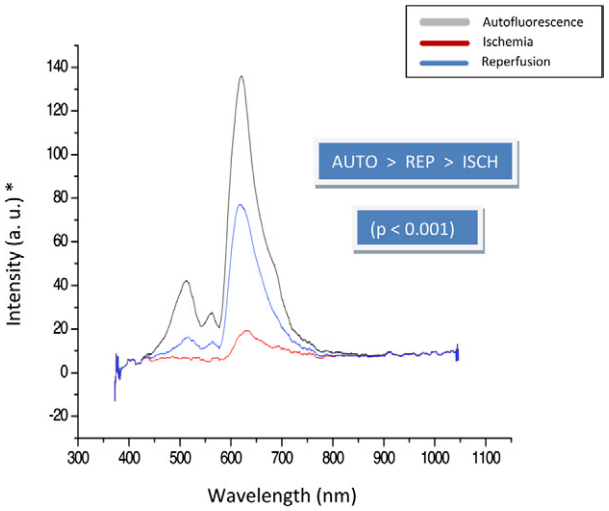

Fig 1. Mean renal fluorescence values obtained at autofluorescence (AUTO), ischemia (ISCH), and reperfusion (REP) regardless of the laser excitation wavelength. *a.u., arbitrary unit.

The correlation between histologic grading and ischemia time was positive ($r = 0.81$); that is, the longer the time of ischemia, the higher the histological grade of injury (Table 1). As expected, histologic analysis of the control group showed no change (grade 1). The grades for kidneys undergoing 30 minutes of ischemia were 3 and 4, while those after 60 or 120 minutes were 4 and 5. Grade 4 was observed more frequently among kidneys undergoing to 60 minutes and grade 5, 120 minutes of ischemia (Fig 3). Because the time of ischemia showed a strong effect on histologic grading, we sought to correlate histologic grades with the various wavelengths (excitation laser) for each ischemia time using 1-way ANOVA. At 30 minutes of ischemia, no wavelength (excitation lasers, 408, 442, and 532 nm) correlated with histologic grading. At 60 minutes, the 532-nm excitation laser (in the reperfusion phase) showed a significant, negative correlation coefficient ($r = -0.61$) with the histologic grade, namely, the lower the peak reading by spectroscopy (reperfusion, 532 bm), the higher the histological grading. At 120 minutes of ischemia, the 442-nm laser (in the reperfusion phase) showed a significant negative correlation coefficient ($r = -0.73$) with the histologic grade, namely, the lower the peak reading by spectroscopy (reperfusion, 442 nm), the higher the histologic grade (Fig 4).

DISCUSSION

The use of spectroscopy to study ischemia is not new. Spectroscopy for tissue analysis was introduced in 1955 by Chance and Williams,[8] who evaluated changes in tissue fluorophores, such as mitochondrial nicotinamide adenine dinucleotide, during the process of cell respiration with production of adenosine triphosphate.

The present study showed that laser-induced fluorescence spectroscopy of rat renal tissue of was able to detect

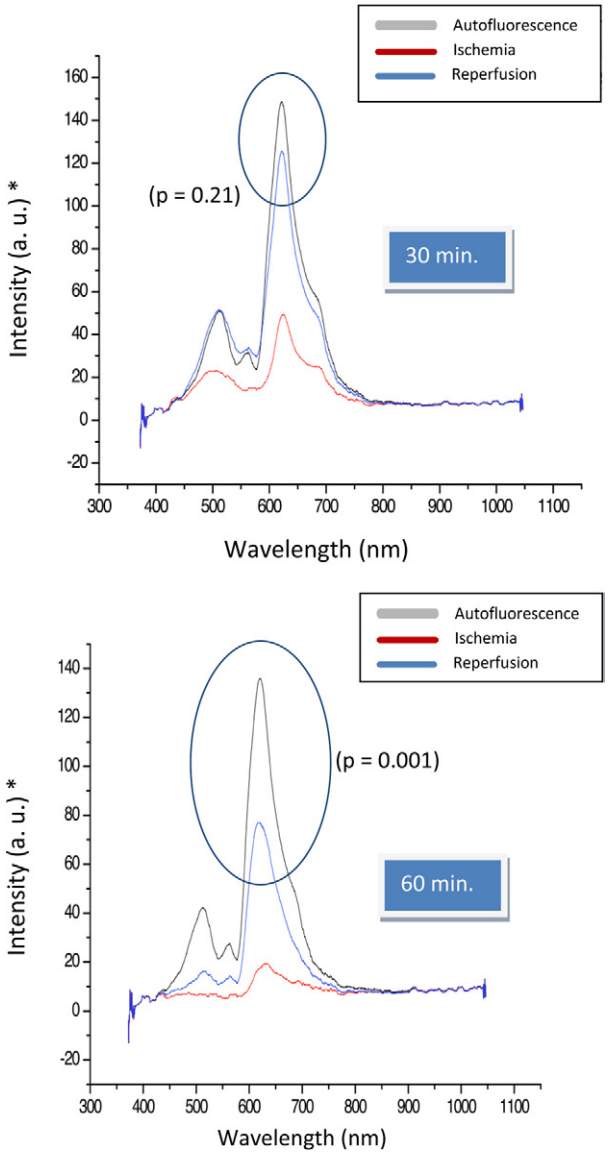

Fig 2. Reperfusion curve showing a significant decrease with an increased in ischemia time from 30 to 60 minutes, compared with the control curve (autofluorescence). *Arbitrary unit.

changes during the phases of normal perfusion (autofluorescence) as well as of ischemia and reperfusion. A significant difference was detected between the decreased curve

Table 1. Correlation Between Ischemia Time and Histologic Grade

Histologic grade	Correlation coefficient	1.000
	Sig. (2-tailed)	
	n	37
Ischemia time	Correlation coefficient	.806**
	Sig. (2-tailed)	.000
	n	33

**Significant correlation at .01 ($r = 0.81$).

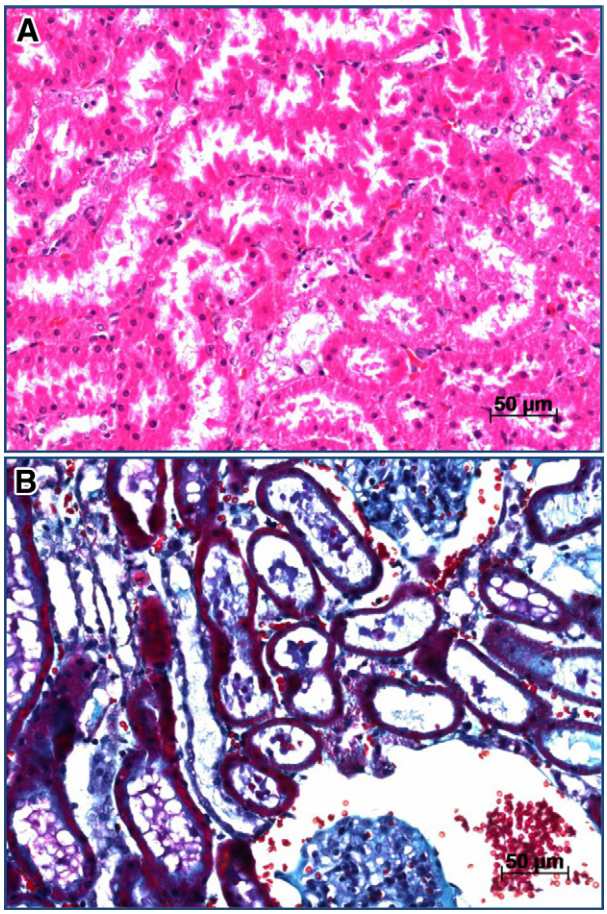

Fig 3. Typical aspect of acute tubular necrosis (ATN) with cell desquamation toward the lumen (**A;** stain: hematoxylin and eosin; original magnification, ×400). Dilatation of the proximal tubules with brush border loss (**B;** Stain; Masson Trichrome; original magnification, ×200).

peaks during ischemia, versus recovery during reperfusion, depending on the ischemic increasing length of time, regardless of the excitation wavelength, as also reported by Fitzgerald et al in 2004.[9] This result suggests that all biological fluorophores behave in a similar manner in response to ischemia regardless of the wavelengths, possibly as a consequence of intense changes in pH, which reduce the efficiency of fluorescence emission by biological compounds.[10] In addition, during ischemia the organ becomes excessively rich in carboxyhemoglobin (cyanotic), further increasing the absorptive properties of hemoglobin compared with the pink color under normal perfusion.[11] The origin of changes in signal intensity during ischemia and reperfusion phases has not been identified; this subject possibly requires monitoring of additional parameters, such as dispersal of excitation and emission or even intracelullar pH.[12] An important result also obtained in the present study was that with increasing time of ischemia (from 30 to 60 minutes, for example), there was a significant fall in the

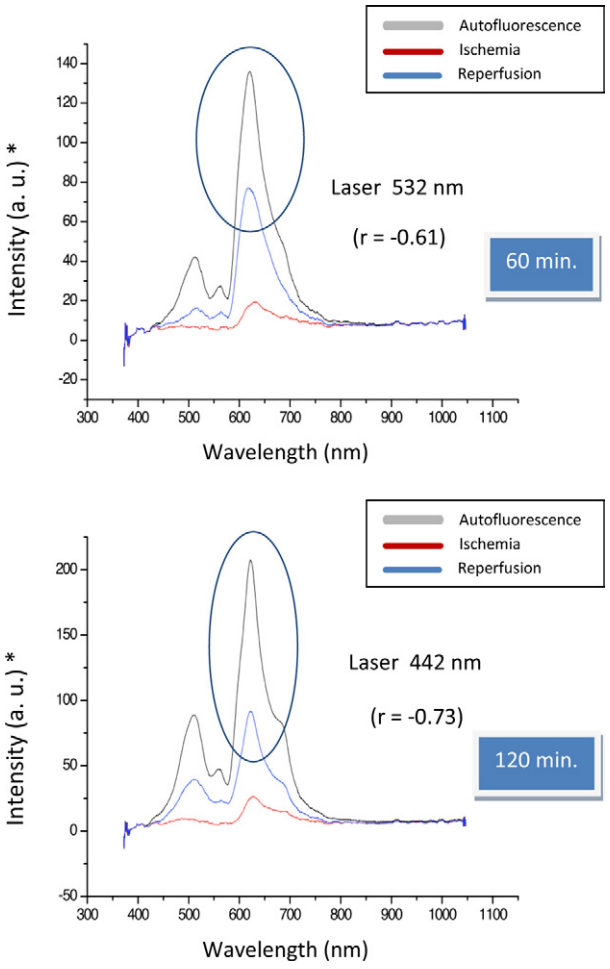

Fig 4. At 60 and 120 minutes of ischemia, the laser excitation of 532 and 442 nm, were significantly correlated, in the reperfusion phase, with histologic injury degree ($r = -0.61$ and $r = -0.73$), respectively. *a.u., arbitrary unit.

peak of fluorescence curves during reperfusion. This fall was significantly correlated with the ischemia time (Fig 2). This observation suggests that the molecular changes in ischemic tissue are continuous and progressive. As time passes, there is a progressive increase among absorbing chromophores, such as carboxyhemoglobin, and a worsening of metabolic acidosis, which reduces fluorescence at the expense of tissue fluorophores (fluorescent structures).

The present study showed a direct association between the severity of the histologic tissue injury and the warm renal ischemia time (30–120 minutes), in agreement with previous reports.[13,14] G1 and G3 animals showed histologic changes of morphologic damage, especially after 60 minutes of ischemia. Particularly important was the denudation of the basement membrane, which suggested that, after 60 minutes, the injuries caused by ischemia were probably irreversible broadly supporting the previous literature.[13,15–17]

Injuries mediated by ischemia and reperfusion were more evident when examined by light microscopy at 24 hours after the ischemic insult.[13] The true extent of the structural changes to cells was observed only at a few days after reperfusion.[18] Because the present samples were obtained 5 minutes after reperfusion, the observed changes were certainly less evident both from a structural and a metabolic viewpoint; this possibly explains why kidneys submitted to 30 or 60 minutes of ischemia showed similar histologic grades.

In the present study, we were unable to find an excitation wavelength among 408, 442, and 532 nm that correlated in a significant manner with the histologic injuries secondary to the biphasic process of renal ischemia and reperfusion. Indeed, the laser with a 408-nm wavelength did not prove to be effective for this purpose, regardless of the ischemia time or the histologic grade. After 30 minutes of ischemia, no wavelength (excitation lasers, 408, 442, and 532 nm) showed a correlation with histologic grade, in contrast with the results reported by Tirapelli et al in 2009.[19]

Conversely, in the present study we observed a significant correlation between determined wavelengths and certain ischemia times. Thus, after 60 minutes of ischemia, during reperfusion the laser delivering 532 nm wavelength showed the greatest correlation with the histologic grade, namely, the reduced peak of the reading curve (fluorescence) with the greater histologic injury. A similar, significant correlation was observed between the 442-nm laser during renal reperfusion after 120 minutes of ischemia.

An important detail of our study was the significant results obtained during the reperfusion phase in contrast with some previous reports.[19,20] Cell changes seem to occur according to time of ischemia, becoming more evident by fluorescence spectroscopy during reperfusion, which confirms the significant biochemical changes known to mediate reperfusion lesions.

From a practical viewpoint, our study using current methods was unable to demonstrate that laser-induced fluorescence spectroscopy was a safe, reliable method to organ viability for transplantation, for example using a graft from a marginal donor. The organ would have to first be implanted and reperfused to obtain a reliable fluorescence reading to correlate with the probable degree of histologic damage. In addition, it is difficult to extrapolate our results to humans; when using a 442-nm wavelength excitation laser (during reperfusion), we would have to ask what time 120 minutes ischemia in rats corresponds to ischemia in a human kidney.

In conclusion, there was a strong correlation between the fluorescence spectroscopy data and the histologic changes in renal ischemia in rats, specifically after 60 or 120 minutes of ischemia using 532 or 442 nm excitation lasers, respectively. Since the effect was only observed in the reperfusion phase, the method would be unable to assess organ viability before transplantation.

REFERENCES

1. Nankivell BJ, Kuypers DR. Diagnosis and prevention of chronic kidney allograft loss. *Lancet*. 2011;378:1428–1437.
2. Thadhani R, Pascual M, Bonventre JV. Acute renal failure. *N Engl J Med*. 1996;334:1448–1460.
3. Schrier RW, Wang W, Poole B, et al. Acute renal failure: definitions, diagnosis, pathogenesis, and therapy. *J Clin Invest*. 2004;114:5–14.
4. Perico N, Cattaneo D, Sayegh MH, et al. Delayed graft function in kidney transplantation. *Lancet*. 2004;364:1814–1827.
5. Hall AM, Crawford C, Unwin RJ, et al. Multiphoton imaging of the functioning kidney. *J Am Soc Nephrol*. 2011;22:1297–1304.
6. Goujon JM, Hauet T, Menet E, et al. Histological evaluation of proximal tubule cell injury in isolated perfused pig kidneys exposed to cold ischemia. *J Surg Res*. 1999;82:228–233.
7. Solez K, Colvin RB, Racusen LC, et al. Banff's 2005 meeting report: differential diagnosis of chronic allograft injury and elimination of chronic allograft nephropathy ("CAN"). *Am J Transplant*. 2007;7:518–526.
8. Chance B, Williams GR. Respiratory enzymes in oxidative phosphorylation in the kinetics of oxygen utilization. *J Biol Chem*. 1955;217:383.
9. Fitzgerald JT, Demos S, Michalopoulou A, et al. Assessment of renal ischemia by optical spectroscopy. *J Surg Res*. 2004;122:21–28.
10. Lin HJ, Herman P, Lakowicz JR. Fluorescence lifetime-resolved pH imaging of living cells. *Cystometry*. 2003:52:77.
11. Gryczynski Z, Gryczynski L, Lakowicz JR. Fluorescence sensing methods. *Methods Enzymol*. 2003;360:44.
12. Raman RN, Pivetti CD, Matthews DL, et al. Quantification of in vivo autofluorescence dynamics during renal ischemia and reperfusion under 355 nm excitation. *Optics Express*. 2008;16: 4930–4944.
13. Jablonsky P, Howden BO, Rae DA, et al. An experimental model for assessment of renal recovery from warm ischemia. *Transplantation*. 1983;35:198–204.
14. Morin D, Pires F, Plin C, et al. Role of the permeability transition pore in cytochrome *C* release from mitochondria during ischemia-reperfusion in rat liver. *Biochem Pharm*. 2004;68:2065–2073.
15. Riera M, Herrero I, Torras J, et al. Ischemic preconditioning improves post-ischemic acute renal failure. *Transplant Proc*. 1999; 31:2346–2347.
16. Torras J, Herrero-Fresneda I, Lloberas N, et al. Promising effects of ischemic preconditioning in renal transplantation. *Kidney Int*. 2002;61:2218–2227.
17. Lima LVS. Associação da ciclosporina A ao pré-condicionamento isquêmico em rim de ratos submetidos à isquemia normotérmica e reperfusão. Doctoral Thesis. Ribeirão Preto (SP): Universidade de São Paulo, 2004.
18. González-Flecha B, Boveris A. Mitochondrial sticks of hydrogen peroxide production in reperfused rat kidney cortex. *Biochim Biophys. Acta*. 1995;1243:361–366.
19. Tirapelli LF, Trazzi BFM, Bagnato VIS, et al. Histopathology and laser autofluorescence of ischemic kidneys of rats. *Lasers Med Sci*. 2009;24:397–404.
20. Fitzgerald JT, Michalopoulou A, Pivetti CD. Real-time assessment of in vivo renal ischemia using laser autofluorescence imaging. *J Biomedical Optics*. 2005;10:44018–44018(7).

Two-photon excitation microscopy using the second singlet state of fluorescent agents within the "tissue optical window"

Yang Pu,[1] Lingyan Shi,[2] Sebastião Pratavieira,[1,3] and R. R. Alfano[1,a)]
[1]*Institute for Ultrafast Spectroscopy and Lasers, Departments of Electrical Engineering and Physics, The City College of New York, 160 Convent Ave, New York, New York 10031, USA*
[2]*Department of Biomedical Engineering, The City College of New York, 160 Convent Ave, New York, New York 10031, USA*
[3]*Instituto de Física de São Carlos, Universidade de São Paulo, São Carlos, Brazil*

(Received 7 August 2013; accepted 1 October 2013; published online 15 October 2013)

Two-photon (2P) excitation of the second singlet (S_2) state of a group of fluorescent agents with near infrared emission was used to extend the optical excitation and imaging regime of 2P microscope into "tissue optical window" (650–1100 nm). As the first step to achieve deeper optical imaging, Chlorophyll *a* and Indocyanine green are investigated and demonstrated as imaging agents using 2P S_2 excitation at 800 nm for microscope imaging at 685 nm. The salient feature is to drive both the 2P excitation and emission wavelengths of the imaging agents to fall into the "tissue optical window." © *2013 AIP Publishing LLC*. [http://dx.doi.org/10.1063/1.4825319]

I. INTRODUCTION

One of the main challenges of the biomedical optical community is to image deeper layer of tissue.[1] By exciting the first singlet (S_1) state of endogenous or exogenous fluorophores in the visible range, two-photon (2P) technique can achieve deeper imaging in tissue over conventional fluorescence microscope.[2] Moreover, the 2P imaging technique has more advantages: diminishing the scattering caused by short wavelength and decreasing the out-of-focus background associated with single-photon (1P) excitation.[3] A conventional two-photon microscope (2PM) imaging systems usually operates in the near infrared (NIR) for excitation and in visible range for emission from either intrinsic fluorophores (e.g., collagen, elastin, and flavin)[4] or extrinsic agents (e.g., fluorescein dye); therefore, the penetration depth of current 2P imaging techniques are still limited by the scattering and re-absorption of the imaging signal light in the visible range.[2] Additionally, the visible endogenous fluorescence hinders advantages of molecular imaging when targeting contrast agents are applied, particularly when the target concentrations are low.[5]

Selecting the appropriate imaging wavelength according to light attenuation caused by tissue provides a means of increasing the imaging depth. As shown in Fig. 1(a), the "tissue optical window" from the far-red to NIR range (650–1100 nm) allows light to penetrate into deep tissue.[6] In the ultraviolet (UV) to visible, the limitation of imaging depth in tissue is due to the scattering caused by extracellular and nuclear structures and the attenuation of blood (both oxyhemoglobin and deoxyhemoglobin). Above 1100 nm, strong absorption of water causes the large loss of the light intensity. In order to increase the penetration depth, the ideal condition for tissue imaging is to have both the pumping and emission wavelengths within this "tissue optical window." However, the conventional 2P S_1 excitation cannot achieve this goal. Since the current 2P imaging methods excite S_1 state of the endogenous fluorophores or fluorescent dyes, it can just have either the pumping[2] or imaging[3] wavelength fall in the NIR "tissue optical window," but not both of them. This dilemma can be illustrated by the absorption spectrum (solid line) and the emission spectrum (dot line) of Indocyanine green (ICG) shown as Fig. 1(b). The 2P exciting S_1 band of 779 nm for ICG by a laser at ~1552 nm is not in the NIR "tissue optical window," but in the strong absorption spectral tail due to water at ~1440 nm. There is a need for 2P imaging technique to force the wavelengths of both pumping and imaging falling into the NIR "tissue optical window."

To overcome these problems, the second singlet (S_2) state of the contrast fluorescent agents, such as Chlorophyll a (Chl *a*) and ICG, are utilized to achieve deeper imaging with 2PM. Chl *a* is vital for photosynthesis, easy to be obtained and not toxic. ICG is one of the most important medical imaging contrast agents since it is the only US Food and Drug Administration (FDA)-approved dye in NIR range.[5] The 2P S_2 excitation of these fluorescent agents using Ti:Sapphire laser centered at ~800 nm makes it possible to drive the wavelengths of both excitation and emission of the imaging agents falling in NIR "tissue optical window." This study will investigate the possibility of this innovated approach of 2P pumping of S_2 of Chl *a* and ICG dyes for the first time to make both absorption and emission wavelengths in NIR "tissue optical window."

II. SAMPLES AND EXPERIMENTAL METHODS

The samples to be imaged were Chl *a*- and ICG-stained uncoated pore glass beads, which size is ~20 to 40 μm and pore diameter is ~24 nm from Pierce Biotechnology INC (Rockford, IL 61005). ICG was purchased from MP Biomedicals, LLC (Solon, OH 44139) and Chl *a* was extracted from fresh spinach leaves using Ethyl Alcohol. All the sample preparations and measurements were performed

a)Author to whom correspondence should be addressed. Electronic mail: ralfano@sci.ccny.cuny.edu

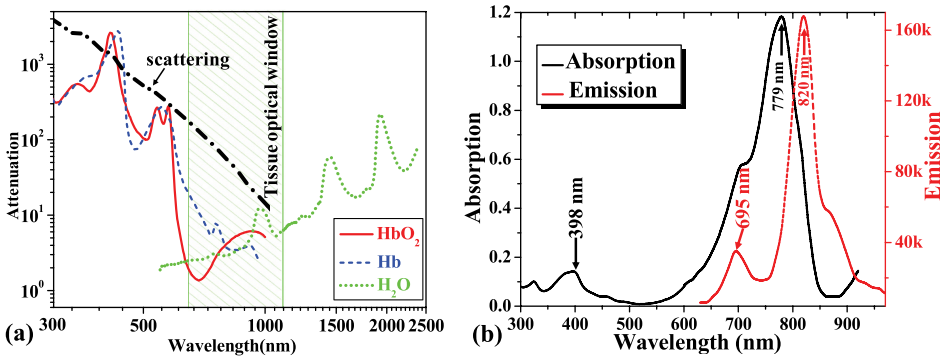

FIG. 1. (a) Optical attenuation caused by the absorption of principal tissue chromophores and the scattering of extracellular and nuclear structures in the spectral region of 300–2500 nm to show the existence of the NIR "tissue optical window"; and (b) The absorption (solid line) and fluorescence (dashed line) spectra of ICG.

at room temperature. The beads were soaked in the Chl *a*-Ethyl solution and ICG-DMSO (20% aqueous Dimethyl Sulfoxide) solution with concentration of ~0.75 mg/ml for overnight. It is well-known that Chl *a* strongly absorbs red and blue-violet light from S_1 and S_2 bands, respectively, for giving green color of leaves.[7] Figure 2 illustrates the mechanism of 1P and 2P excitation of S_1 and S_2 bands of Chl *a* using the Jablonski energy level diagram (left side) and the measured absorption and fluorescence spectra (right side) of Chl *a*. The absorption spectrum (solid line) was measured using UV-VIS-NIR spectrophotometer (Cary 500 Scan) and the emission spectrum (dot line) was acquired by FluoroMax-3 spectrometer (Horiba Jobin Yvon). The absorption of photons could drive the molecules of Chl *a* from the ground (S_0) state to the S_1 and S_2 excited states, converting photon energy into electronic excitation. The scheme of light absorption and energy decay of Chl *a* caused by 1P excitation is well known that the emission of Chl *a* in far-red light of ~680 nm can be achieved by excitation of S_1 caused by red light at ~629 nm band or by violet light at ~404 nm (Soret band) using S_2 excitation.[7] The Chl *a* decaying to the S_0 may also be achieved by emitting photons from S_1 after 2P excitation given nonradiative process for S_2 to S_1 following 2P excitation.

ICG was also investigated as a potential S_2 fluorescent agent since ICG and its derivative dyes are widely used in optical vessel imaging, cancer detection, and surgery cancer margin assessment. The potential of ICG S_2 excitation is possible because a weak S_2 band exists at ~398 nm and dual fluorescence peaks from S_1 at 695 nm (weak) and 820 nm (strong) were observed in Fig. 1(b).

A Multiphoton Microscopy System (Prairie Tech., Inc., W.I.) with Coherent Ultima 130 femtosecond duration laser pulses light source was used to investigate 2P S_2 excitation of Chl *a* and ICG, which is schematically shown in Fig. 3. The laser power is 10 mW. The excitation of 800 nm was used to achieve the 2P pumping S_2 band of 400 nm to accomplish fluorescence imaging in spectral range around 680 nm for both Chl *a* and ICG. This is the optimal condition for the study of 2P S_2 excitation of Chl *a* because of the strong S_1 band absorption and strong emission at ~680 nm of Chl *a* as shown in Fig. 2. Corresponding to the absorption and

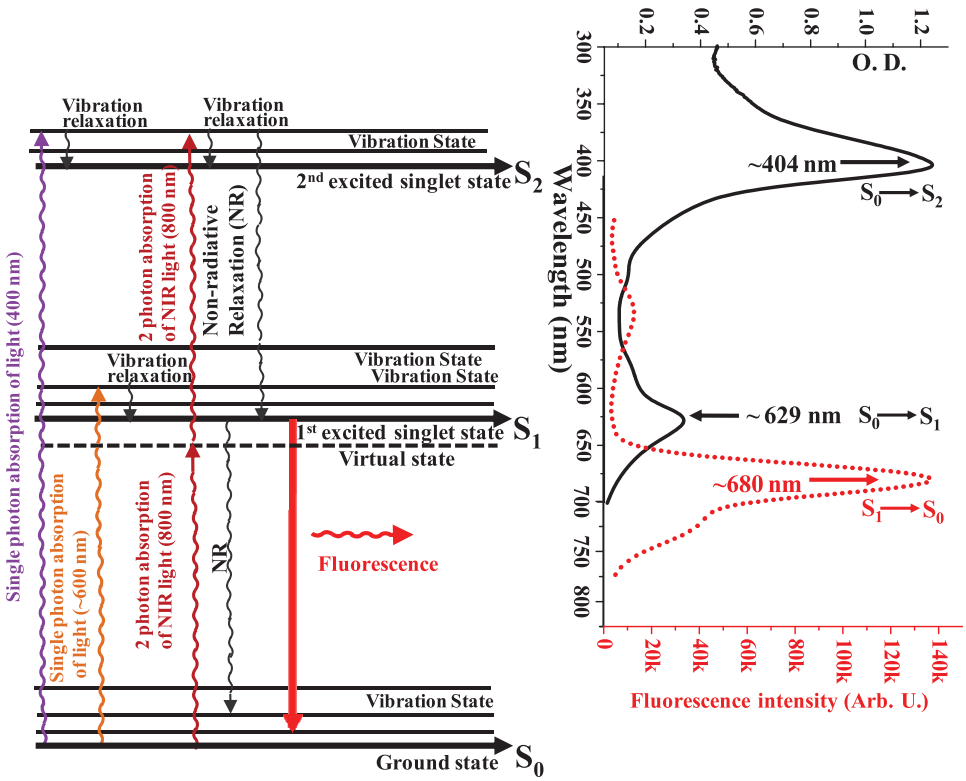

FIG. 2. Jablonski energy level diagram for Chl *a* to be pumped to 1st and 2nd excited singlet state by the possible ways in one- or two-photon absorption (left side); Measured absorption (solid line) and fluorescence (dot line) spectra of Chl *a* (right side).

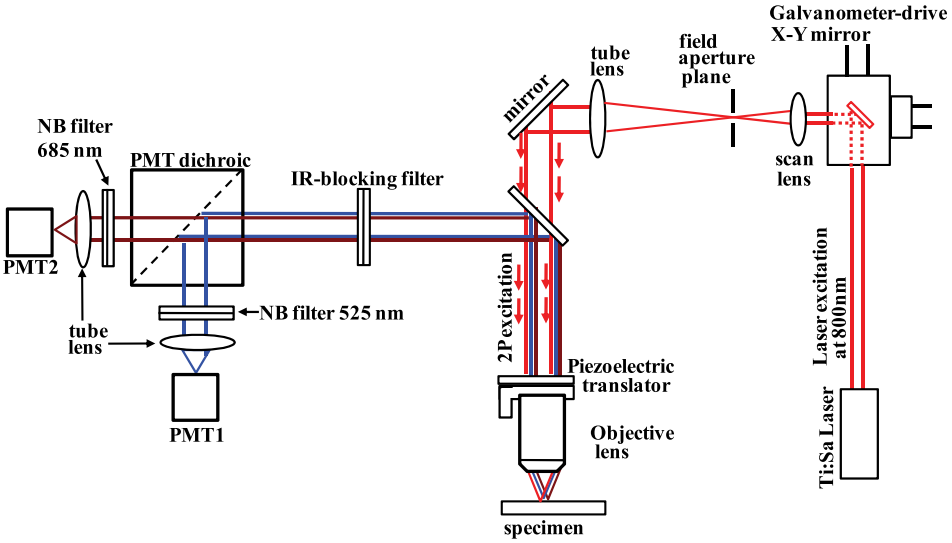

FIG. 3. The schematic diagram of the two-photon microscopy system used for demonstrating the ideas of the second singlet state excitation.

emission spectra of ICG, our 2PM S_2 imaging study is not perfect to investigate ICG as a 2P S_2 imaging agent. One reason forced us to investigate the weaker emission of ICG at ~695 nm is that an unmountable IR-blocking filter see Fig. 3 in front of the PMT of the 2PM Prairie system cuts the strong emission of ICG at ~820 nm and just allows the visible light pass through.

III. EXPERIMENTAL RESULTS AND DISCUSSION

The 2PM of Chl *a* and ICG-stained beads were imaged using the channel outfitted with wide band filter of 685 ± 40 nm from Chroma (Brand name) with a 40× lens (N.A. = 0.8, water immersion, Olympus). Images were taken by another channel with filter of 525 ± 35 nm for control study while other imaging parameters (such as laser power, amplification of the PMT, and scanning speed, etc.) were kept constant between control (525 nm) and imaging (685 nm) channel.

Figures 4(a) and 4(b) show the 2P microscope image of Chl *a*-stained beads under imaging and control channel, respectively. The 2P microscope images of ICG-stained beads under imaging and control channel were displayed in Figs. 4(c) and 4(d), respectively. The potential application of Chl *a* and ICG for 2P S_2 imaging was validated by observing the fluorescence images of the Chl *a*- and ICG-stained beads under the channel of 685 nm, which is close to the emission peak of Chl *a* and ICG while no fluorescence images of beads can be acquired under the control channel of 525 nm, which is far from the emission peak of Chl *a* and ICG. The 2PM images of Chl *a*- and ICG-stained beads can be clearly seen under the imaging channel, but no visible profiles of bead are under the control channel. The much stronger emission intensity of the Chl *a*- and ICG-stained beads under the imaging channel over the control channel can be more clearly visualized by Figs. 4(e)–4(h), which is the corresponding spatial intensity profiles of the image obtained by

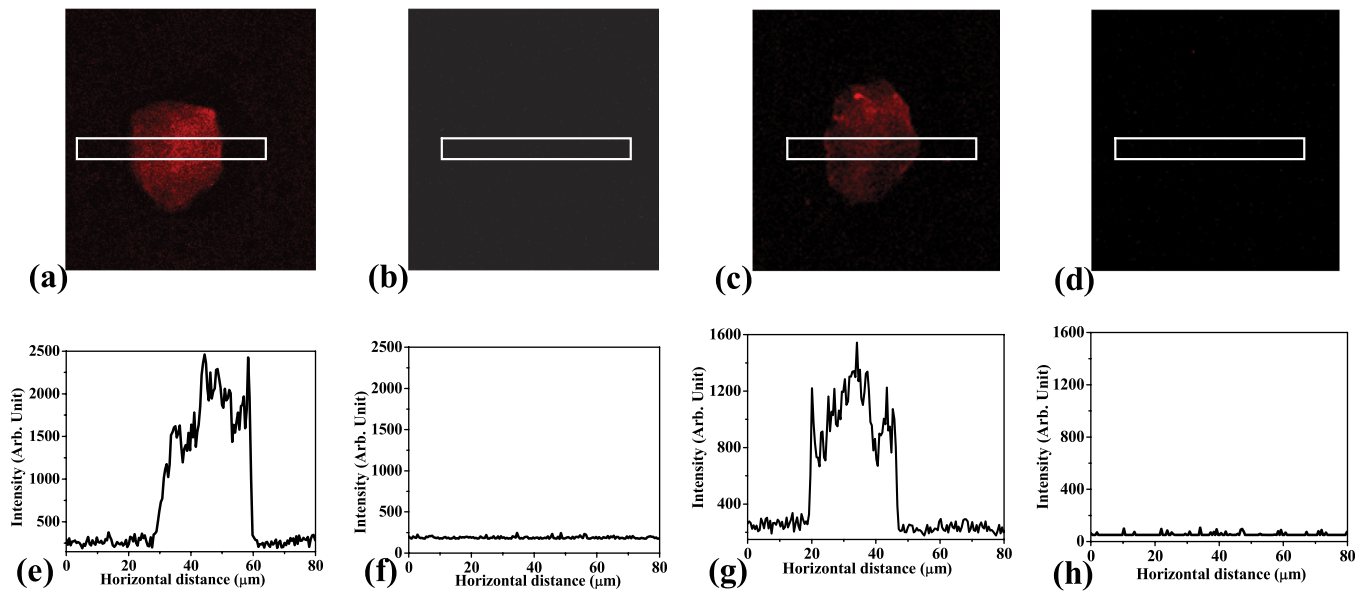

FIG. 4. The 2P microscope image of (a) Chl *a*-stained beads under imaging (685 nm) and (b) control (525 nm) channel, (c) ICG-stained beads under imaging (685 nm), and (d) control (525 nm) channel; (e), (f), (g), and (h) are the corresponding digital spatial cross section intensity distribution of the image shown in (a), (b), (c), and (d), respectively. The femtosecond laser excitation wavelength was 800 nm.

TABLE I. The potential S_2 2PM fluorescent agent.

Fluorescent agents	Solvent	S_2 or S_n	S_1	Emission peak
Diprotonated-tetraphenylporphyrin	Chloroform + HCl	446	662	687
MgOEP	Toluene	410	582	638
N-Confused tetraphenylporphyrin	Chloroform	439	730	750
Octaethylporphyrin	Benzene	402	621	689
Pheophorbide a	Ethanol	410	669	674
Porphin	Toluene	396	566	684
Pyropheophorbide a methyl ester	Dichloromethane	413	666	674
Pyropheophorbide a	Dichloromethane	412	668	675
TBP-beta-octa(COOBu)-Fb	DMF	433	675	750
TBP-beta-octa(COOBu)-Zn	DMF	453	644	709
TBP-meso-tetra(4-COOMe-phenyl)-Fb	DMF	469	642	807
TBP-meso-tetra(4-COOMe-phenyl)-Zn	DMF	469	659	741
Tetrakis(2,6-dichlorophenyl) porphyrin	Toluene	418	592	717
Tetrakis (o-aminophenyl) porphyrin	Toluene	406	633	717
Tetramesitylporphyrin [TMP]	Toluene	426	603	721

integrating the horizontal area shown by the rectangle in Figs. 4(a)–4(d). These results show that the optimized 2PM imaging of Chl *a*- and ICG-stained beads under 2P excitation of 800 nm is the channel of 685 nm, which is exactly the strong fluorescence peak of Chl *a*, and close to the second strong emission peak of ICG at 685 nm. This indicates that the recorded microscope image is indeed formed from emission of the 2P S_2 fluorescent agent (Chl *a* and ICG in our case) because of the rapid nonradiative relaxation from S_2 to S_1. Chl *a* and ICG can be used as potential 2P S_2 fluorescents agent to enhance the imaging depth by two-photon microscope.

There are many fluorescent agents with similar spectral profiles as Chl *a* and ICG that can be used as potential 2P S_2 fluorescent imaging agents. Extensive absorption and emission spectra of dyes agents have been studied by Oregon Medical Laser Centre.[8] All these fluorescent agents have stronger absorption S_2 band or even higher singlet (S_n) state over the S_1 band. Although their toxicity is still needed to be investigated, for the interest of the researchers, spectral characteristics of these agents are listed in Table I.

IV. CONCLUSION

The 2P S_2 excitation properties of two most important fluorescent agents, Chl *a* and ICG, were characterized using 2PM technique. The 2P S_2 imaging technique allows for the wavelength of both exciting and emitting of these imaging agents into NIR "tissue optical window." The strong emission intensities of 2P microscope images of Chl *a*- and ICG-stained beads were observed under the imaging channel of 685 nm, which indicates they can be used to as potential 2P S_2 fluorescent agents to enhance the imaging depth. The outcome of this paper will be the first step for deeper tissue imaging using S_2 excitation 2PM techniques.

ACKNOWLEDGMENTS

This research is supported in part by the President Seed program of the City College of New York, and U.S. Army Medical Research and Material Command (USAMRMC) under Grant of # W81XWH-11-1-0335 (CUNY RF # 47204-00-01).

[1]Y. Pu, W. Wang, M. Xu, J. Eastham, G. Tang and R. R. Alfano, "Characterization and three-dimensional localization of cancerous prostate tissue using backscattering scanning polarization imaging and independent component analysis," J. Biomed. Opt. **17**(8), 081419-1-8 (2012).
[2]Y. Guo, P. P. Ho, F. Liu, Q. Z. Wang, and R. R. Alfano, "Noninvasive Two-photon-excitation imaging of tryptophan distribution in highly scattering biological tissues," Opt. Commun. **154**, 383–389 (1998).
[3]M. Berezin, C. Zhan, H. Lee, C. Joo, W. Akers, S. Yazdanfar, and S. Achilefu, "Two-photon optical properties of near-infrared dyes at 1.55 μm excitation," J. Phys. Chem. B **115**, 11530–11535 (2011).
[4]Y. Pu, W. B. Wang, Y. Yang, and R. R. Alfano, "Native fluorescence spectra of human cancerous and normal breast tissues analyzed with nonnegative constraint methods," Appl. Opt. **52**(6), 1293–1301 (2013).
[5]Y. Pu, W. B. Wang, G. C. Tang, F. Zeng, S. Achilefu, J. H. Vitenson, I. Sawczuk, S. Peters, J. M. Lombardo, and R. R. Alfano, "Spectral polarization imaging of human prostate cancer tissue using near-infrared receptor-targeted contrast agent," Technol. Cancer Res. Treat. (TCRT) **4**, 429–436 (2005).
[6]R. R. Anderson and J. A. Parrish, "The optics of human skin," J. Invest. Dermatol. **77**, 13–19 (1981).
[7]S. Frigerio, R. Bassi, and G. M. Giacometti, *Light conversion in photosynthetic organisms—Chapter One of Biophotonics*, edited by L. Pavesi (Springer-Verlag, Berlin, 2008).
[8]S. Jacque and S. Prahl "125 PhotochemCAD Spectra!," http://omlc.ogi.edu/spectra/PhotochemCAD/index.html, Accessed on April 6, 2013.

Photodiagnosis and Photodynamic Therapy (2014) 11, 409—415

Available online at www.sciencedirect.com

ScienceDirect

journal homepage: www.elsevier.com/locate/pdpdt

Identification of skin lesions through aminolaevulinic acid-mediated photodynamic detection

C.T. Andrade[a,*], J.D. Vollet-Filho[a], A.G. Salvio[b], V.S. Bagnato[a], C. Kurachi[a]

[a] *Physics Institute of Sao Carlos, University of Sao Paulo, Brazil*
[b] *Amaral Carvalho Hospital Foundation, Jahu, Brazil*

Available online 2 June 2014

KEYWORDS
Fluorescence;
Photodynamic detection;
Skin lesion;
Aminolaevulinic acid;
Diagnosis

Summary Non-melanoma skin cancer is the most common cancer lesion worldwide. In Brazil, it represents 95% of all skin cancer lesions, and 25% of all tumor types. Early diagnosis allows treatment at initial stages of the disease, improving patient's prognosis. Thus, it is of great importance the development of techniques to aid diagnosis, such as marked fluorescence, which we propose here for early detection of skin cancer lesions. In this study, we use a photosensitive substance, aminolaevulinic acid (ALA), as biomarkers, and analyze its *in situ* fluorescence response to light excitation. The use of ALA as a biomarker precursor is interesting because it shows selectivity for protoporphyrin IX production/concentration in abnormal cells. Protoporphyrin IX shows high fluorescence yield when excited with UV-blue light. In this study, ALA solutions (at 5% and 10% concentrations) were applied to malignant (basal cell carcinoma) and potentially malignant skin lesions (actinic and seborrheic keratoses), aiming to investigate our ability in detecting and distinguishing them by using this technique. At regular time intervals (15, 30, 45 and 60 min), fluorescence images were collected with a prototype system for wide-field fluorescence imaging. ALA has provided a marked fluorescence that allowed significant discrimination of normal and tumor. Potentially malignant and benign lesions were all well-identified by their autofluorescence; photodynamic detection did not improve diagnostics. This technique also provided a better delineation of the lesion margins, which is very important for an effective treatment of malignant, potentially malignant and benign skin lesions.

* Corresponding author at: Cintia Teles de Andrade, Instituto de Física de São Carlos, Universidade de São Paulo, Grupo de Óptica, Laboratório de Biofotônica, Av. Trabalhador São-carlense, n° 400, Centro, 13566-590 São Carlos, — SP, Brazil. Tel.: +55 1633739810; fax: +55 1633739810.
E-mail addresses: cintya_teles@yahoo.com.br, cintyateles@gmail.com (C.T. Andrade).

http://dx.doi.org/10.1016/j.pdpdt.2014.05.006
1572-1000/

Introduction

Skin cancer can be classified in two major groups: non-melanoma and melanoma. Non-melanoma lesions are the most common ones, with estimative between 2 and 3 million cases per year around the world [1,2].

The most common non-melanoma skin cancer is the basal cell carcinoma (BCC), originated in the basal layer of epidermis. Its occurrence is higher in middle-aged and elderly people with skin phototype I or II, and its appearance is directly related to prolonged exposure to solar radiation throughout life. It is usually observed at body areas exposed to the sun, such as arms, face and neck [2—6].

Others non-malignant, but also important, skin lesions — due to the large occurrence and possibility of misdiagnosis — are actinic keratosis (AK) and seborrheic keratosis (SK). Actinic keratosis is a skin epidermal dysplasia that develops due to the cumulative effect of ultraviolet radiation from sun exposure. It is more prevalent at the same population group as for skin cancer and presents a higher incidence on face, scalp, arms and hands. The seborrheic keratosis, usually associated to genetic origin, affects mainly the chest and face, but it can occur also in the limbs. These lesions have a warty appearance, irregular surface and a soft consistency [3—5]. Therefore, being able to differentiate these lesions is of relevance for clinical diagnosis.

Prevention and detection are the major challenges in dealing with skin cancer: prevention depends mainly on the use of sunscreen and avoidance of exposure to high ultraviolet irradiation, and early diagnosis improves patient prognosis, and reduces patient morbidity, as well as treatment complexity and costs [4,5,7,8].

Skin diagnosis is initiated with whole body visualization under illumination with white light sources, during the clinical examination. If any lesion is identified, a dermatoscopic examination is performed to obtain additional details. This equipment magnifies the visualization field in 10 up to 40 times. When a malignant condition is suspected, a biopsy is performed. Histopathological analysis is ''gold standard'' for tissue diagnosis. Clinical characteristics of benign lesions and carcinomas at early stage are similar, and the large variability of professional skills to recognize early malignant features result in a non-efficient inter-lesion discrimination. Biopsy is an invasive technique which does not provide information of lesion margins, which is relevant for treatment planning, since surgical resection of the lesion has to be performed beyond the clinically apparent margin for the malignant conditions. For the lesions in areas of cosmetic relevance or in surgically complex anatomic regions, especially in face and scalp, the treatment must consider removing the least possible amount of healthy tissue [9,10].

The detection of lesions using illumination parameters distinct to the conventional white light, and the fluorescence visualization has the potential to increase *in situ* tissue discrimination. Among optical techniques for tissue diagnostics, one of the most investigated one is autofluorescence [11—14], because tissue biochemical and structural changes that take place during cancer development and progression alter the light—tissue interactions. Tissue fluorescence patterns also depend on these interactions. Thus, fluorescence is capable of detecting such changes. At skin, autofluorescence helps in the detection and delineation of tumor margins, limiting damage caused by the tumor recurrence due to an incomplete surgical removal [11]. The use of skin fluorescence also aids in distinguishing tumor from healthy tissue [12] and benign lesions [13].

The photodiagnosis using an exogenous marker can increase the contrast resolution between abnormal and healthy tissue. In photodynamic diagnosis, a solution of aminolaevulinic acid (ALA) is topically placed on lesion surface. ALA is a protoporphyrin IX (PpIX) precursor which is an endogenous photosensitizer (PS) that naturally occurs in the cellular heme biosynthetic pathway. After ALA is localized into the cell, it enters in the heme biosynthesis and stimulates the PpIX production. This PS has fluorescence properties, and accumulates preferentially in abnormal tissues, allowing its use as a complementary diagnostic tool [14,15]. A higher ALA-PpIX production at malignant cells has been observed at several studies [14,16,17], supporting ALA use as a potential marker for photodynamic diagnosis.

For diagnostic applications, after ALA solution is administered to the target tissue, a time interval is required for enough PpIX production and accumulation allowing its fluorescence visualization at the interrogated tissue. Then, skin is illuminated using light at the UV-blue spectral range, in order to excite the PpIX molecules inside the tumor cells and to induce their fluorescence emission. Under this excitation range, the PpIX shows an intense orange-red fluorescence, which strongly contrasts with the green autofluorescence of the biological tissues.

In this clinical study, the efficacy of ALA photodynamic detection (ALA-PDD) of malignant, potentially malignant and benign skin lesions was investigated. To the best of our knowledge, there is no analysis evaluating the best ALA concentration for the photodynamic detection of skin lesions. The aim of the present study was to evaluate the efficacy of a clinical protocol for the ALA-PDD for the detection of skin lesions.

Material and methods

Patient accrual

In this study, 43 patients of both genders, Caucasian, between 45 and 91 years old, with BCC, AK, and SK were investigated between May 2010 and June 2011. A total of 71 lesions were imaged: 29 BCC, 31 AK, and 11 SK.

All lesions were clinically diagnosed, and BCC was confirmed by histopathology. All patients were evaluated at the Skin Department of Amaral Carvalho Hospital, and all underwent surgery after fluorescence evaluation. This research was approved by the Review Board on Ethics in Research from the Amaral Carvalho Hospital Foundation (CEPFHAC 123/2010). Patients and their respective caregivers signed an informed written consent for participation in the clinical study.

Photosensitization

The pro-drug used was 5-aminolevulinic acid (5-ALA — FSUESCC ''NIOPIIK'' B SADAVAYAd. 1k4, Moscow, Russia) manipulated at concentrations of 5% and 10% in Milli-Q water solution with 3% of dimethylsulfoxide (DMSO) and

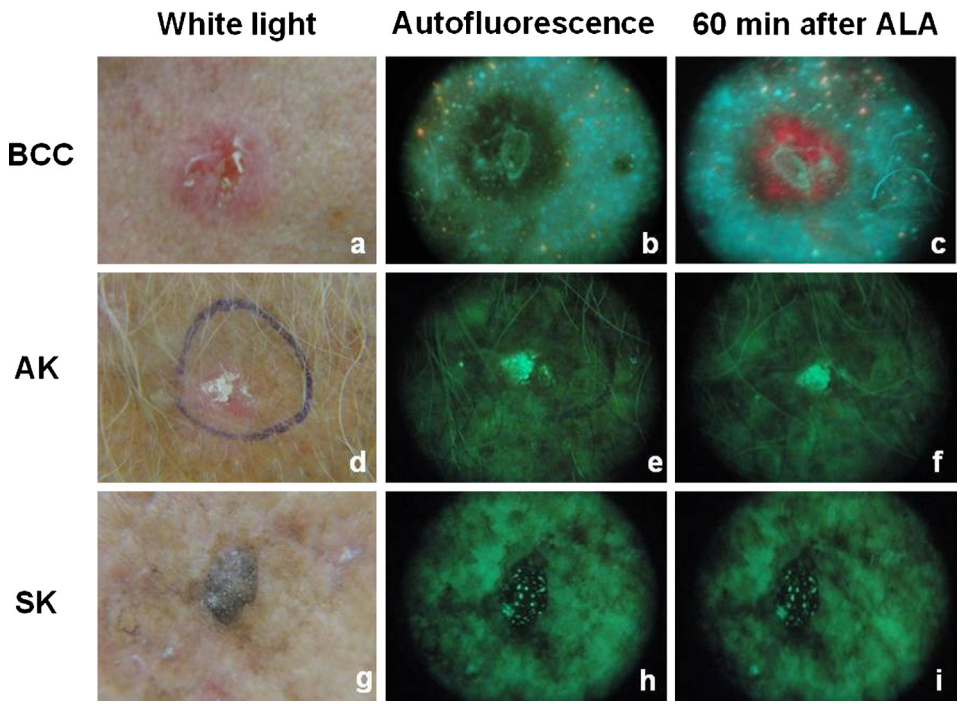

Figure 1 Skin lesions images using white light illumination (left column), autofluorescence (central column) and 1 h after application ALA (right column). The lines show typical images for: BCC (top), AK (center), and SK (bottom).

1 mM ethylenediaminetetraacetic acid (EDTA). DMSO is an enhancer of ALA penetration in tissue, and EDTA inhibits the enzyme ferrochelatase, resulting in a higher concentration of PpIX in cells. The PpIX production occurs inside the mitochondria, and it is induced by the ALA present in the biosynthetic heme pathway [18—20].

Fluorescence device

The fluorescence evaluation was performed using a homemade handheld device for widefield fluorescence imaging. The illumination system is composed of a set of LED arrays with emission between 380—420 nm, with peak in 400 nm and irradiance at 50 mW/cm^2. Three optical components are used: a filter at the excitation path (band-pass filter between 390 nm and 460 nm), a dichroic mirror (reflection of the blue spectrum and transmission of the green—red spectrum), and a filter at the collection path (long-pass filter, over 475 nm). This optical arrangement was designed to improve the contrast visualization (difference between colors and intensities) of light in green and red regions of the visible spectrum, main fluorescence emissions of the biological tissue and PpIX, respectively. A digital color camera (Sony DSC-H50) was coupled at the device through an adapter for image acquisition [21].

Clinical protocol

The skin lesions were initially evaluated under conventional white light and dermatoscopy by a certified dermatologist (AGS), and the clinical characteristics described at the patient chart.

Solutions of ALA 5% or 10% were prepared, and immersed in a warm bath for total dissolution of ALA. After that, the solution was kept at room temperature, protected from light until the moment of use.

Lesions were cleaned with chlorhexidine soap, and cleansed with NaCl 0.9% solution. No curettage procedure was performed in the interrogated lesions, because our aim was to analyze the efficacy of the photodynamic diagnostics without any invasive procedure, so variations due to the inherent lesion characteristics, like surface keratin and dead cell layers, could not be avoided.

Five percent ALA solution was applied on 54 lesions (21 BCCs, 22 AK, and 11 SK). In order to determine if a higher pro-drug concentration could improve the photodynamic detection, 10% ALA solution was applied on 17 lesions (8 BCCs and 9 AK), and the same analysis parameters were performed.

The ALA solution was applied over the lesion surface, covering all clinical margins. After the pro-drug application, the lesions were protected from light exposure using an occlusive curative with PVC plastic film, aluminum foil and bandage. Images were collected at regular time intervals (15, 30, 45 and 60 min) in a dark room. At each time interval, the curative was removed for image collection, and replaced just after imaging.

The images were processed using an algorithm written in Matlab® 7.5 (MathWorks, USA) for evaluation of PpIX fluorescence emission. This algorithm determines the number of pixels for the component R (''red'') in the RGB matrix for each image, attributing them to red light intensity, which was associated to the photosensitizer fluorescence.

Statistics

Data are expressed as average values and standard deviations. The Shapiro–Wilk test was used to determine the normality of the data. To compare differences between lesions and normal tissue, before and after ALA application paired Student's *t*-test was used, and for discrimination between lesion and normal tissue, unpaired Student's *t*-test was applied.

The software Statistica for Windows, release 7 (Statsoft, Tulsa, OK) was used for the statistical analysis and the significance level was set at 5% ($p < 0.05$).

Results

ALA 5%

The image sequence in Fig. 1 shows the PpIX production over time in a BCC at right temporal (Fig. 1a–c), an AK at the right forearm (Fig. 1d–f) and a SK at the chest (Fig. 1g–i). The left column shows the image of skin lesions under white light illumination (Fig. 1a, d, g); the central column their autofluorescence (Fig. 1b, e, i); and the right column, typical lesion photodynamic fluorescence, one hour after ALA application.

Healthy tissue shows fluorescence at the green region of the spectrum, and abnormal tissues, as BCC, AK, and SK, show loss of fluorescence emission (LOF), visualized as a darker region. The red fluorescence at Fig. 1c, is observed at the same regions previously associated with LOF. The visualized bright spots correspond to areas of high fluorescence emission (Fig. 1e and f) from hyper-keratinized areas of the lesion surface. It can be noted that SK does not fluoresce (Fig. 1h), visualized as a dark region with several fluorescent points. This autofluorescence pattern is related to a high melanin content that extensively absorbs both excitation and fluorescence lights, and to the corneal structures inside the lesion, resulting in LOF and highly fluorescent spots, respectively [9,22]. No qualitative visualization of the PpIX production could be observed at the AK and SK.

To quantify the PpIX showed in the images, regions at both normal and lesion tissue were selected, and the intensity of red fluorescence was calculated for each image. Then, intensity was normalized by its background red intensity (the red emission present at tissue autofluorescence), to obtain only the contribution of the PpIX emission in the tissue fluorescence after the ALA treatment. Fig. 2 shows graphs of PpIX intensity emission as a function of time of the three lesions shown in Fig. 1. It is possible to observe that the PpIX fluorescence intensity increases with time for BCC, while remains almost constant for the other lesions, enhancing the qualitative analysis.

Statistical tests were performed to determine whether there was significant difference between the fluorescence of the lesion and normal tissue (before and after ALA application) and between these lesions before and after ALA application. In order to show that the PpIX production occurs preferentially in abnormal cells, tests were also performed by evaluating normal tissue before and after ALA application.

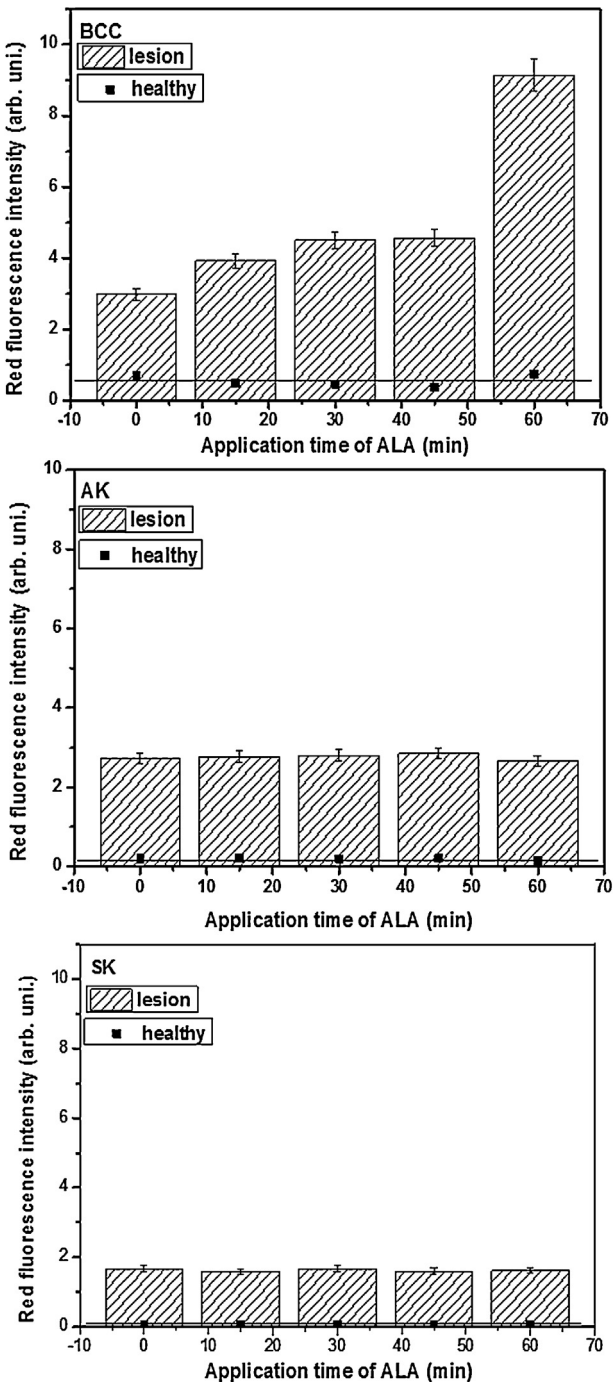

Figure 2 Graphics of red fluorescence intensity *versus* application time of ALA for lesions shown in Fig. 1. BCC, AK and SK, respectively. The line corresponds to the red fluorescence present in fluorescence from the healthy skin.

In the comparison between lesion and normal tissue prior to ALA application (autofluorescence), there was significant difference in all cases ($p < 0.01$). The same was true when comparing the lesion and normal tissue 60 min after ALA application ($p < 0.01$).

When the lesion autofluorescence was compared with the values of fluorescence 60 min after ALA application, there was significant difference ($p < 0.01$) only for the BCC. Comparison between normal tissue before and 60 min after

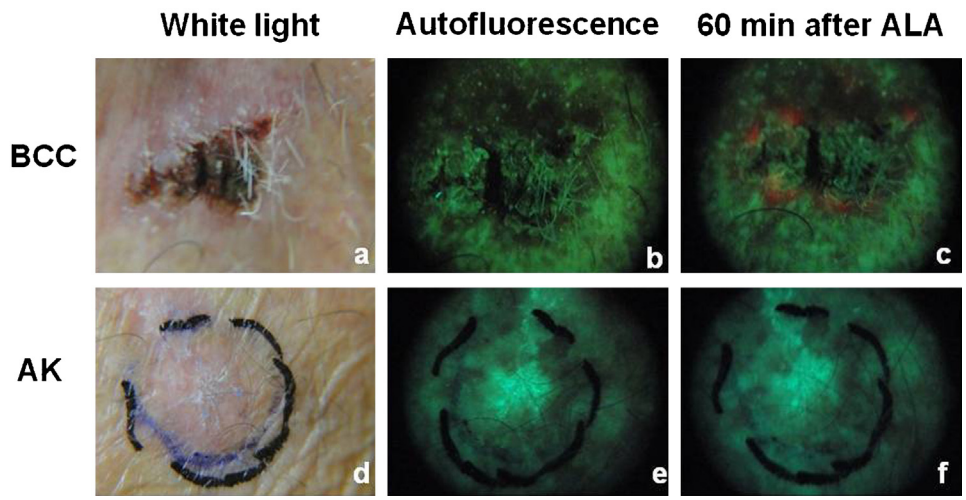

Figure 3 Skin lesions images using white light illumination (left column), autofluorescence (central column) and 1 hour after application ALA (right column). The lines show typical images for: BCC (top) and AK (bottom).

ALA application showed no statistical significance for any group.

ALA 10%

The images in Fig. 3 show PpIX fluorescence emission over time in a BCC lesion (Fig. 1a—c) and an AK lesion (Fig. 1d—f). The left column shows the skin lesions under white light illumination (Fig. 1a and d); the central column, their autofluorescence (Fig. 1b and e); and the right column, lesion fluorescence one hour after ALA application.

For AK lesion, the result was similar to 5% ALA. For BCC lesion, however, a reduced production of PpIX was observed, although the quantitative analysis showed an increase in PpIX fluorescence intensity (Fig. 4), it was preferentially located at the lesion borders as showed in Fig. 3c. Here it is important to point out that this BCC lesion, in comparison to the one in Fig. 1a, showed a higher necrotic tissue at lesion surface, preventing an efficient penetration of the ALA solution, due to a non-curettage of these lesions, the PpIX emission was observed at the lesion regions of less keratinized surface.

The statistical tests for comparison between lesion and normal tissue, both prior to ALA application (autofluorescence) and 60 min after, showed significant differences in all cases ($p < 0.01$). When lesion and normal tissues' autofluorescence was compared to fluorescence intensity values 60 min after ALA application, no significant difference was observed.

Discussion

The observed LOF from the abnormal skin has been also described in other studies [12,23,24], and this is mainly justified by the decrease in collagen fluorescence caused by fiber linkage breakdown [25]. Others skin components such as flavins do not have a great contribution due to the excitation wavelength, which is not within the absorption wavelengths of these components [26].

Fluorescence images after the ALA application show preferential accumulation of PpIX in skin areas associated or within the BCC lesions, representing a potential aid to the cancer diagnosis, since it increases the visualization contrast between normal and abnormal tissue. With this increase in contrast, an improved discrimination of the lesion superficial margins is provided, information highly important for the treatment planning and execution.

The difference between the autofluorescence from normal and abnormal tissue is noticeable. This observation is in agreement with other studies in literature which demonstrate a reduction of the green fluorescence at skin, and an increase in the red fluorescence for lesions [16,17,27]. After application of the ALA solution, the difference between tissues is more evident with time, when considering the red fluorescence emission. The use of the photodynamic diagnosis only showed a response for BCC lesion, but there was no improvement at the visual discrimination to the autofluorescence detection.

A possible reason for the lesions in which there was no increase in the red fluorescence emission is the ineffective penetration of ALA solution; mainly caused by areas of hyper-keratinization and necrotic tissue.

Several lesions of BCC and AK present extensive keratinization on the surface, which behaves as physical barrier to the penetration of ALA solution [28]. The result is a large number of lesions which showed no increase in PpIX fluorescence even 60 min after ALA application. However, this keratin layer can be removed by curettage, which is a simple medical procedure. Indeed, the curettage is performed in ALA-photodynamic therapy (PDT) for the removal of the keratin and dead cells layers to improve the pro-drug penetration [29,30]. In the investigated protocol, the curettage was not performed, since the aim was to verify the efficacy of the photodynamic detection using a procedure with the least possible number of steps. Based on the present results, an improved performance and diagnostic resolution may be achieved, if the curettage is performed previously to ALA solution placement.

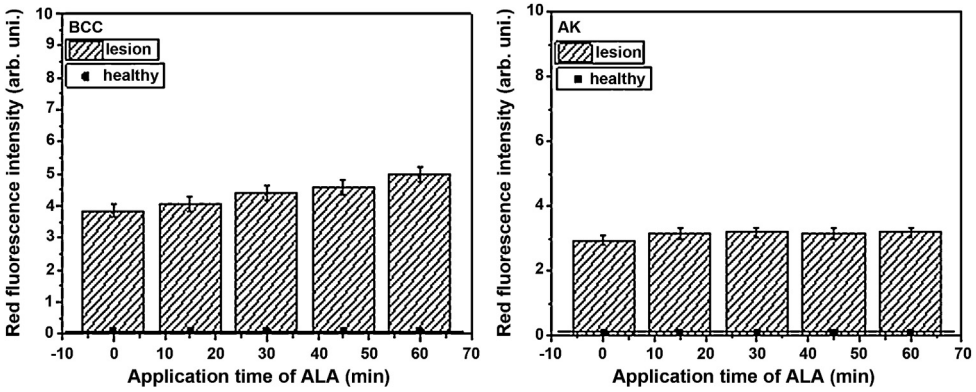

Figure 4 Graphics of red fluorescence intensity *versus* application time of ALA for BCC and AK lesions showed in Fig. 3. The line corresponds to the red fluorescence in fluorescence from the healthy skin.

For SK, the high light absorption by melanin hinders fluorescence visualization, in both autofluorescence and photodynamic detection.

However, for SK and AK lesions, the autofluorescence detection presents already an improved visualization of the lesion. The photodynamic detection did not show a significantly increase in the red fluorescence intensity. Therefore, sensitization has shown to be important only for BCC lesions.

The autofluorescence for SK lesions may help on the differential diagnostics to melanoma. The corneum pseudocysts, a tissue structure that differentiates the SK from melanoma, become evident in autofluorescence images [22,31]. In melanoma lesions, the autofluorescence pattern is an evident LOF, visualized as a dark area without any fluorescent spots.

The anatomical site also plays an important role on the penetration of the ALA solution. Lesions that are located in the arm and forearm usually present a thicker layer of keratin than those located in the head and neck, reducing the pro-drug penetration. In arm/forearm cases, the PpIX fluorescence emission was less intense in the lesions borders, as well as less intense when compared to cases in head and neck.

Even when the ALA concentration is increased from 5% to 10%, most of the lesions did not show enough accumulation of PpIX, reinforcing the hypothesis of the physical barrier impairing an efficient tissue photosensitization [15,32,33].

Although curettage has been already used for other protocols as a safe and effective practice [29,30], this study aimed to verify how feasible this technique could be with no application of any invasive procedure.

Conclusion

Fluorescence investigation of BCC lesions, using both autofluorescence and photodynamic detection techniques, showed ability to significantly differentiate normal from tumor tissue. PpIX accumulation in skin lesions increases visual contrast between healthy and abnormal tissues. This contrast allows for improved identification of lesion margins.

For detection of non-malignant skin lesions, AK and SK, the use of autofluorescence images only proved to be sufficient; no additional information was provided by using photodynamic diagnosis. In the case of AK, due to excessive keratin at lesion surface, ALA solution did not adequately penetrate into the tissue to induce PpIX production. For SK lesions, with higher melanin content, autofluorescence images result in tissue LOF, with highly fluorescent spots inside the lesion. These spots are corneum pseudocysts, which are characteristic structures at those lesions. Therefore, observing them contributes to diagnosis, especially to differentiate them from melanoma.

Increasing concentration of ALA form 5% to ALA 10% for BCC and AK showed that the low PpIX production was not due to low concentration, but to the limited penetration of the pro-drug solution, which might be managed by performing curettage on lesions prior to ALA administration.

Widefield fluorescence imaging is, therefore, a potential auxiliary tool for skin diagnosis, helping to define the lesions margins; and ALA-mediated photodynamic detection showed to be able to increase visual contrast of BCC lesions.

References

[1] INCA — Nacional Institute of Cancer Rio de Janeiro. Ações nacionais integradas para prevenção e controle do câncer [14 Nov 2011]; 2011, available from www.inca.gov.br
[2] Non melanoma Skin Cancer São Paulo. Hospital A.C. Camargo [14 nov 2011]; 2011, available from http://www.hcanc.org.br/index.php?idTipoCancer=28&page=14
[3] Successful treatment of actinic keratosis Brasil. Dermatologia Online — Saúde e beleza da pele [15 set 2009]; 2009, available from http://www.dermatologia.net/medicos_nova/mednews/news2006_11b.shtml
[4] Neves R, Lupi O, Talhari S. Câncer da pele. Med Brasil 2001.
[5] Schwartz RA. Skin Cancer Recognition and Management. 2nd ed. Estados Unidos: Blackwell Publishing; 2008.
[6] Fitzpatrick, all e. Dermatology in General Medicine. 7th ed. USA: Mc Graw Hill Medical; 2008.
[7] INCA — Nacional Institute of Cancer. Ações de Prevenção Primárias e Secundárias no Controle de Câncer. Rio de Janeiro; 2008. p. 139—50.
[8] Curettage Brasil. Plástica e Dermatologia [15 set 2009]; 2009, available from http://www;plasticaedermatologia.com.br/d6.htm

[9] Costa MM, Andrade CT, Inada NM, Ventura L, Kurachi C, Bagnato VS. Desenvolvimento e Aplicação de Equipamento para Diagnóstico por Fluorescência. Jornal brasileiro de laser 2010;2:8—12.
[10] Fritsch C, BeckerWegerich PM, Menke H, Ruzicka T, Goerz G, Olbrisch RR. Successful surgery of multiple recurrent basal cell carcinomas guided by photodynamic diagnosis. Aesthet Plast Surg 1997;21(6):437—9.
[11] Neuss S, Gambichler T, Bechara FG, Wohl S, Lehmann P. Preoperative assessment of basal cell carcinoma using conventional fluorescence diagnosis. Arch Dermatol Res 2009;301(4):289—94.
[12] Brancaleon L, Durkin AJ, Tu JH, Menaker G, Fallon JD, Kollias N. In vivo fluorescence spectroscopy of nonmelanoma skin cancer. Photochem Photobiol 2001;73(2):178—83.
[13] Panjehpour M, Julius CE, Phan MN, Vo-Dinh T, Overholt S. Laser-induced fluorescence spectroscopy for in vivo diagnosis of non-melanoma skin cancers. Laser Surg Med 2002;31(5):367—73.
[14] Torezan L, Niwa ABM, Neto CF. Terapia fotodinâmica em dermatologia: princípios básicos e aplicações. An Bras Dermatol 2009;84(5):445—59.
[15] Pottler R, Krammer B, Baumgartiner R, Stepp H. Phodynamic therapy with ALA: a clinical handbook. 1st ed. Europa: RCS Publishing; 2006.
[16] Smits T, van Laarhoven AIM, Staassen A, van de Kerkhof PCM, van Erp PEJ, Gerritsen MJP. Induction of protoporphyrin IX by aminolaevulinic acid in actinic keratosis, psoriasis and normal skin: preferential porphyrin enrichment in differentiated cells. Br J Dermatol 2009;160(4):849—57.
[17] Valentine RM, Ibbotson SH, Brown CTA, Wood K, Moseley H. A quantitative comparison of 5-aminolaevulinic acid-and,ethyl aminolevulinate-induced fluorescence photobleaching and pain during photodynamic therapy. Photochem Photobiol 2011;87(1):242—9.
[18] De Rosa FS, Marchetti JM, Thomazini JA, Tedesco AC, Lopes MV, Bentley B. A vehicle for photodynamic therapy of skin cancer: influence of dimethylsulphoxide on 5-aminolevulinic acid in vitro cutaneous permeation and in vivo protoporphyrin IX accumulation determined by confocal microscopy. J Control Release 2000;65(3):359—66.
[19] Panfilo BML [Dissertação de mestrado] Técnicas de imagem para triagem de melanoma. Botucatu: Universidade Estadual Paulista ''Júlio de Mesquita Filho''; 2012.
[20] Liu HF, Xu SZ, Zhang CR. Influence of $CaNa_2$ EDTA on topical 5-aminolaevulinic acid photodynamic therapy. Chin Med J-Peking 2004;117(6):922—6.
[21] Costa Mmd [Dissertação] Desenvolvimento de um sistema por imagem de fluorescência óptica para uso médico-odontologico. São Carlos: Universidade de São Paulo; 2010.
[22] Panfilo BML [Dissertação de mestrado] Técnicas de imagem para triagem de melanoma. Botucatu: Universidade Estadual Paulista ''Júlio de Mesquita Filho'';; 2012.
[23] de Veld DCG, Skurichina M, Wities MJH, Duin RPW, Sterenborg HJCM, Roodenburg JLN. Autofluorescence and diffuse reflectance spectroscopy for oral oncology. Laser Surg Med 2005;36(5):356—64.
[24] de Leeuw J, van der Beek N, Neugebauer WD, Bjerring P, Neumann HAM. Fluorescence detection and diagnosis of non-melanoma skin cancer at an early stage. Laser Surg Med 2009;41(2):96—103.
[25] Pavlova I, Williams M, El-Naggar A, Richards-Kortum R, Gillenwater A. Understanding the biological basis of autofluorescence imaging for oral cancer detection: high-resolution fluorescence microscopy in viable tissue. Clin Cancer Res 2008;14(8):2396—404.
[26] DaCosta RS, Andersson H, Wilson BC. Molecular fluorescence excitation-emission matrices relevant to tissue spectroscopy. Photochem Photobiol 2003;78(4):384—92.
[27] Allison RR, Sibata CH. Photodiagnosis for cutaneous malignancy: a brief clinical and technical review. Photodiagn Photodyn 2008;5(4):247—50.
[28] McLoone N, Donnelly RF, Walsh M, Dolan OM, McLoone S, McKenna K, et al. Aminolaevulinic acid diffusion characteristics in 'in vitro' normal human skin and actinic keratosis: implications for topical photodynamic therapy. Photodermatol Photoimmunol Photomed 2008;24(4):183—90.
[29] Berroeta L, Clark C, Dawe RS, Ibbotson SH, Fleming CJ. A randomized study of minimal curettage followed by topical photodynamic therapy compared with surgical excision for low-risk nodular basal cell carcinoma. Brit J Dermatol 2007;157(2):401—3.
[30] Christensen E, Skogvoll E, Viset T, Warloe T, Sundstrom S. Photodynamic therapy with 5-aminolaevulinic acid, dimethylsulfoxide and curettage in basal cell carcinoma: a 6-year clinical and histological follow-up. J Eur Acad Dermatol 2009;23(1):58—66.
[31] Pratavieira S, Andrade CTd, Salvio AG, Bagnato VS, Kurachi C. Optical imaging as auxiliary tool in skin cancer diagnosis. skin cancers — risk factors. Prev Ther: InTech 2011:159—71.
[32] Ibbotson S, Jong C, Lesar A, Ferguson J, Padgett M, O'Dwyer M, et al. Characteristics of 5-aminolaevulinic acid-induced protoporphyrin IX fluorescence in human skin in vivo. Photodermatol Photoimmunol Photomed 2006;22(2):105—10.
[33] Berroeta L, Clark C, Dawe R, Ibbotson S, Fleming C. A randomized study of minimal curettage followed by topical photodynamic therapy compared with surgical excision for low-risk nodular basal cell carcinoma. Br J Dermatol 2007;157(2):401—3.

IOP Publishing | Astro Ltd Laser Physics
Laser Phys. **24** (2014) 085604 (5pp) doi:10.1088/1054-660X/24/8/085604

Monitoring scaling and dental calculus removal with an optical fluorescence system

G Sivieri-Araujo[1,3], C R Fontana[2], M M Costa[3], A N S Rastelli[4], L P C Pereira[5], C Kurachi[3] and V S Bagnato[3]

[1] Department of Restorative Dentistry, Discipline of Endodontics, Dental School of Araraquara, São Paulo State University-UNESP, Rua Humaitá, 1680, PO 331, CEP 14.801-903, Araraquara, São Paulo, Brazil
[2] Department of Clinical Analysis, Araraquara School of Pharmaceutical Sciences-FcFAr, Univ. Estadual Paulista-UNESP, Araraquara, São Paulo, Brazil
[3] Department of Physics and Materials Science, Physics Institute of São Carlos-IFSC, University of São Paulo-USP, São Paulo, Brazil
[4] Department of Restorative Dentistry, Araraquara School of Dentistry-FOAr, Univ. Estadual Paulista-UNESP, Araraquara, São Paulo, Brazil
[5] MMOptics, São Carlos, São Paulo, Brazil

E-mail: gustavosivieri@uol.com.br

Received 25 August 2013
Accepted for publication 25 February 2014
Published 18 June 2014

Abstract

Fluorescence results from a process that occurs under certain conditions in molecules known as fluorophores, fluorochromes or fluorescent dyes when they absorb light. The molecule is excited to a higher energy state and emits fluorescent light. The emission wavelength is always higher than the excitation wavelength. Optical diagnoses by fluorescence can be used in medicine and dentistry. It does not cause injury to tissues because it is a noninvasive method and can add benefits to clinical treatments. The aim of this case report was to apply an optical fluorescence system for wide-field image viewing and visual monitoring of the management of plaque and dental calculus before and after periodontal scaling to improve the diagnoses and follow-up of patients with periodontal disease. The results suggest that it is possible to observe, with a fluorescence system, residual plaque and calculus that were not easily seen by the naked eye during oral inspection. Thus, the optical technique can potentially improve periodontal screening efforts, especially in patients undergoing periodontal maintenance.

Keywords: optical diagnosis, fluorescence, dental calculus, dental plaque, biofilm, dental scaling

1. Introduction

The optical fluorescence technique provides an excellent way to simplify clinical diagnosis. The high velocity and sensitivity to differentiate tissue variations allow simple implementation of this tool [1, 2] to obtain good clinical results.

Being a nonaggressive and nondestructive technique [3–5], the fluorescence can be used in medicine for diagnosis purposes or monitoring degradation of some drugs used in cancer treatment modalities. The biochemical composition and structure of biological tissues influence the light–tissue interaction. Thus, healthy tissue compared with injured tissue or contaminated by microorganisms will present different optical characteristics [6, 7].

In dentistry, a similar system was developed for detection of oral cancer, soft tissue alterations [8, 9], incipient caries [10], identification of dental calculus, and for other applications [11, 12].

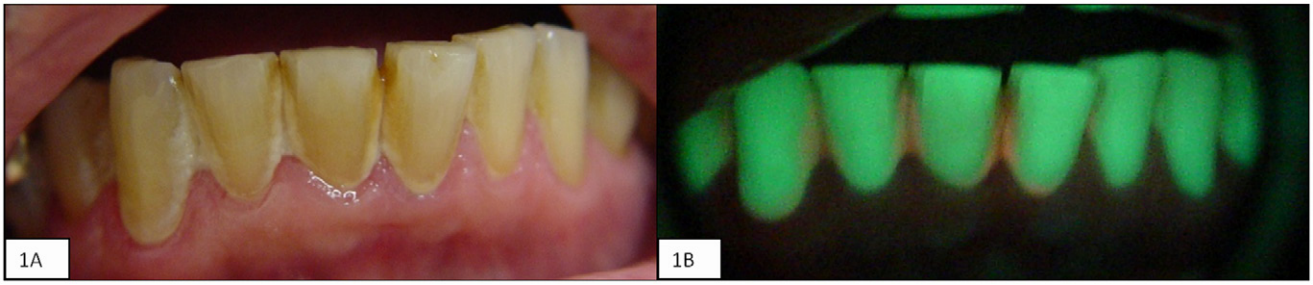

Figure 1. Images of teeth with and without fluorescence. Presence of bacterial plaque and calculus (A). Red (B) shows plaque and calculus with fluorescence.

Periodontal disease is one of the major infections of the oral cavity and is a major cause of tooth loss. During periodontal treatment it is important to conduct a thorough scraping with the aim of removing any calculus that can be attached to the tooth surface [13]. To perform periodontal treatment correctly, visual inspection and tactile sensitivity are fundamental to prevent residual calculus; unfortunately, this kind of skill is possessed only by a periodontal specialist (periodontist) with experience [14].

The use of optical diagnosis as an adjunctive of dental calculus detection becomes especially appropriate for the general practitioner to minimize the difficulty in residual calculus detection that may still persist after periodontal scaling [15].

The purpose of this case report was to demonstrate the use of optical fluorescence as an important tool for nonperiodontists to use to perform visual plaque and calculus monitoring before and after periodontal scaling.

2. Materials and methods

This case report was approved by the Ethics Committee in Research of University Center of Araraquara-UNIARA (protocol number: 1200/10). To perform visualization of scraping and dental calculus removal by optical fluorescence, we examined 30 patients who were instructed verbally and with reading materials who subsequently signed a consent form. Clinical examination and image registers before and after dental procedures were performed at a dental office at The Health Center of Physics Institute of Sao Carlos, University of Sao Paulo, Sao Carlos, Sao Paulo, Brazil.

The system (prototype) used for fluorescence imaging was developed in partnership with the Engineering School of Sao Carlos Laboratory of Biophotonics at Physics Institute of Sao Carlos, both from University of Sao Paulo, Sao Carlos, Sao Paulo, Brazil, and the company MMOptics (Sao Carlos, Sao Paulo, Brazil).

The instrument consists of three different systems. The first is the optical system, consisting of high-intensity LED lights, with emission centered at 405 and 450 nm and five optical filters. The second is the electronic system, which controls and powers the lighting system. The third is the detection system, comprising an attached camera and/or webcam. The excitation wavelength is from 405 to 420 nm. Filters allow the capture of the fluorescence signal fairly well, as well as appropriate contrast in the display of images. To observe hard tissue (teeth), a power of 20 mW was used; to observe the soft tissue (gingival), the power was increased to 140 mW to improve the view of the present structures.

Initially, the clinical examinations were performed and photographs were obtained throughout the oral cavity. The images were obtained using a distance approximately 10 cm from the oral cavity. All patients were photographed with and without the fluorescence system before the beginning of scaling and root planning.

Then, the periodontal treatment was performed by a general dentist (nonperiodontist) with an ultrasound device (Gnatus Medical and Dentistry Equipments, Ribeirao Preto, Sao Paulo, Brazil) to remove supragingival calculus visualized by the fluorescence system. After periodontal scaling, new inspections were performed throughout the oral cavity and new pictures were obtained. Subsequently, a comparison of the images was made before and after periodontal scraping.

3. Results

Calculus within the periodontal pocket is a complicated and potentially delicate structure to be detected with radiographic examinations and dental probe inspections. Our results using an optical fluorescence imaging method was helpful to improve calculus detection and, consequently, dental cleaning.

In addition, clinical appointments have shown that the intervention using optical fluorescence as an additional tool for periodontal treatment had a favorable influence on patient compliance.

Figures 1–4 show the results obtained from the teeth in the buccal region teeth. Figure 1(A) shows the presence of dental calculus without needing help of the fluorescence diagnosis system. Using optical fluorescence, dental calculus can be seen in red in figure 1(B). Both images were taken before the procedure of dental scaling. Figures 2(A) and (B) were taken after periodontal treatment. Figures 1(B) and 2(B) show the images using the fluorescence system. Likewise, in figures 3(A) and (B), it was possible to observe the lingual region of the lower teeth before periodontal treatment. Figures 4(A) and (B) illustrate images after treatment.

4. Discussion

Fluorescence properties of supragingival and subgingival calculus may provide a way to accurately assess presence of

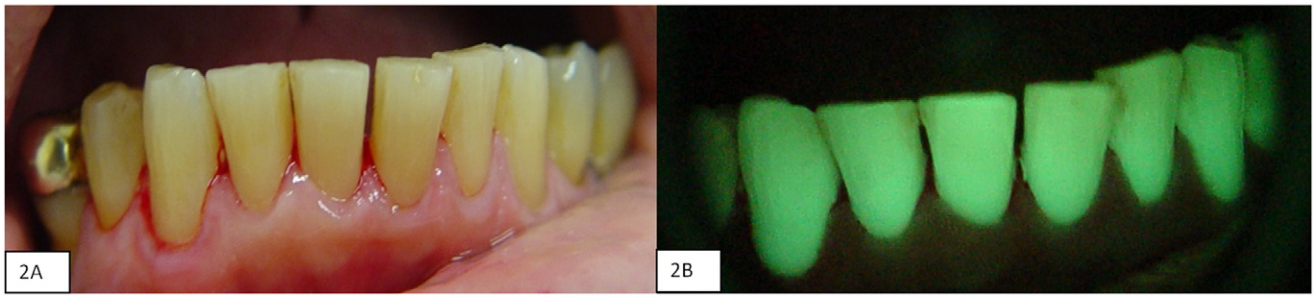

Figure 2. Images of teeth with and without fluorescence after periodontal scaling. Absence of residual calculus is shown (A), (B).

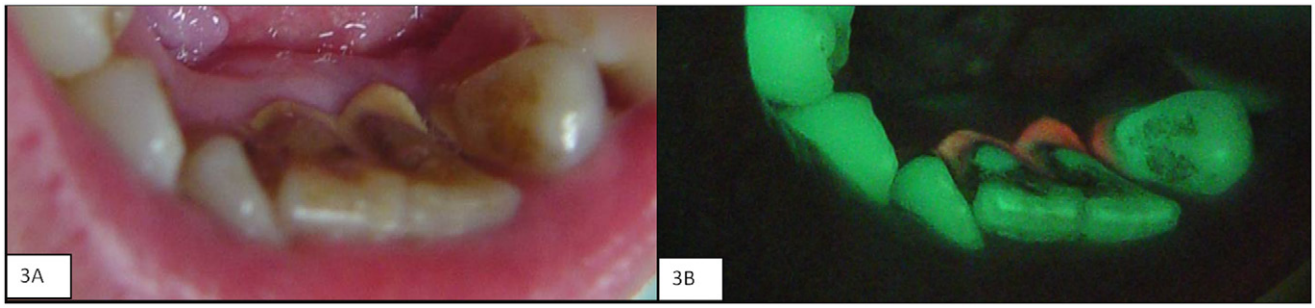

Figure 3. Images without fluorescence show presence of plaque and calculus (A). Using the fluorescence system, plaque and calculus can be seen (red, (B)).

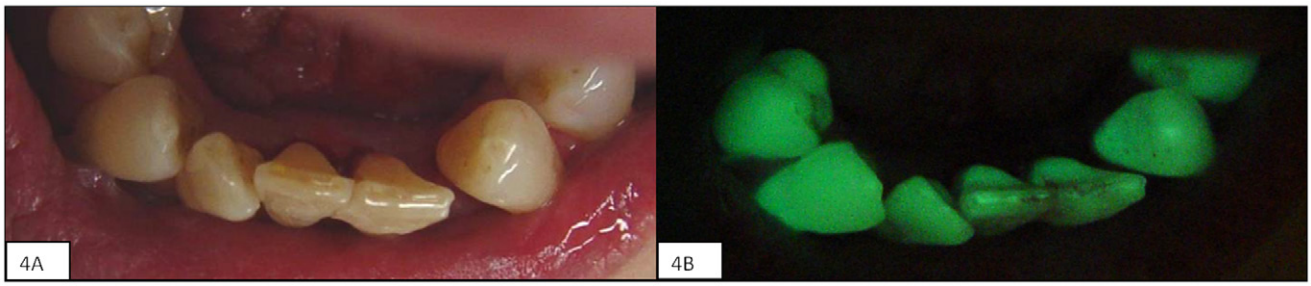

Figure 4. Images after periodontal scaling (A) and (B). Absence of dental plaque and calculus confirmed by optical fluorescence (B).

these deposits in regions not directly seen or that are difficult to reach by periodontal probing. In the present study, fluorescence spectra were recorded directly from patients with solid calculus and periodontal disease [16, 17].

Presence of multiple fluorophores that cover a wide range of excitation and emission maxima and simultaneous quenching and reabsorption effects may change peaks caused by fluorescence [18].

Peaks in the red spectral region between 570 and 740 nm present in calculus preserve their wavelength position independently of the excitation wavelength. A red light is absorbed by organic and inorganic matter on teeth and then are re-emitted from the organic material as near-infrared fluorescent light [19]. Near-infrared fluorescence excited by 655 nm LASER irradiation has shown the feasibility of detecting clinical subgingival calculus [6, 7].

A mixture of different fluorescent chromophores is present in human calculus, as has already been suggested [17, 20]. Supragingival calculus may have porphyrin derivatives noticeable by the Soret bands at approximately 405 nm and by less intense Q bands at higher wavelengths [17, 20, 21].

Ribeiro-Figueiredo *et al* [22] compared the fluorescence spectra obtained at three LASER excitation wavelengths from intact enamel, sound dentin and carious dentin. The results showed that carious enamel usually presents Zn-protoporphyrin and protoporphyrin IX. It is known that porphyrin fluorescence found in dental calculus and in carious dental hard tissue is closely linked to high bacterial activity [23]. Some bacteria rely on hemin iron-containing molecules as a source of iron, such as hemin or hemoglobin, and the inflammatory gingival condition may be a source of blood and an important source for porphyrin derivatives [24].

Carvalho *et al* [25] studied the influence of efforts used to modify patient behavior regarding periodontal maintenance. The irregular compliers and noncompliers were subjected to the usual procedures and strategies, such as reminders of the next visit, information regarding periodontal disease and importance of maintenance, and motivation for those who showed an improvement in compliance. We believe that the optical diagnosis method in this case is a great tool to increase compliance with periodontal treatment.

In this study, the fluorescence imaging system proved to be a good adjunct tool not only for clinical diagnosis by images but also for assisting in the monitoring and visualization of periodontal scaling, in agreement with other studies [8–10, 22].

The light interactions with biological tissues influence biochemical structures that build tissues. Hard tissues fluoresce differently than soft tissues, and the same phenomenon occurs for disease and organisms. Our results regarding detecting the presence of plaque and calculus and fluorescing at red wavelengths were also found in other studies [6–8, 24, 26–29].

Even though dental calculus and plaque are not the only cause of periodontal disease, they deserve special attention. A complete removal procedure is considered crucial for the success of periodontal therapy [27]. The ability to detect subgingival calculus *in vitro* was tested in 20 freshly extracted teeth affected by periodontitis, and the results were compared with clinical and histological findings [27, 28].

It has been well-documented that thorough subgingival scaling and root planning will result in a reduction of periodontal bacteria. However, in the presence of supragingival calculus, rapid subgingival colonization will occur within a few weeks. Hence, a thorough mechanical debridement to ensure complete removal of this pathogenic calculus is mandatory and will also help prevent progression of periodontitis [28, 29].

Traditional methods of calculus detection are typically explorer, periodontal probe and radiographic examinations. Although widely used, traditional methods of diagnosis of dental calculus after scaling and root planning, especially when performed by nonspecialists, may present difficulty in realization and detection [30–34]. In view of its potential for dental diagnostics, fluorescence spectroscopy in the optical range has been the subject of research for years [34–38].

The wavelengths between 405 and 420 nm used in this case report proved to be effective for dental plaque and calculus detection when performed before and after scaling. Our results were similar to those of Buchalla *et al* [20], who used a light wavelength between 400 and 420 nm.

Although optical fluorescence has been recognized for some time [39], only recently have systematic investigations been performed [20, 40]. In our case report, images were recorded directly from mouth of each patient in real time.

The aim of this case report was mainly to focus on qualitative assessment of optical fluorescence properties for dental applications. We could not find a correlation between the thickness of calculation and intensity of fluorescence signal, which may be attributable to the high optical density of dental calculus. However, this system has been used in medicine [1, 2, 4] and dentistry [17, 20, 27, 28] because of its high sensitivity, simplicity, and less time required for obtaining results.

This new tool is quite simple to use, fast, secure and serves as a new aid to determine, monitor and visualize images. The essential component of conventional periodontal therapy is the effective removal of bacterial deposits from the root surface, along with calculus deposits, to create a biologically compatible root surface. This optical instrument can be used to optimize the diagnosis of residual plaque and calculus, thus improving therapy results. The use of optical fluorescence in dental diagnosis before and after periodontal scaling contributes to better detection of residual calculus.

5. Conclusion

We conclude that clinicians can observe the subgingival root surface, tooth structure and residual calculus in real time. This new system of optics diagnosis by fluorescence is simple to use, fast, secure and serves as a new guide for viewing, monitoring, and diagnosis of plaque and dental calculus.

Acknowledgments

We thank CNPq (National Counsel of Technological and Scientific Development), INCT (National Institute of Science and Technology) and MMOptics for financial and engineering support for this work.

References

[1] Perelman L T 2006 *Expert Rev. Med. Devices* **3** 787
[2] Yu C C *et al* 2008 *Opt. Express*. **16** 16227
[3] Gonchukov S, Biryukova T, Sukhinina A and Vdovin Yu 2010 *Laser Phys. Lett*. **7** 812
[4] Badizadegan K, Backman V, Boone C W, Crum C P, Dasari R R and Georgakoudi I 2004 *Faraday Discuss*. **126** 265
[5] Costamagna G and Marchese M 2010 *Eur. Rev. Med. Pharmacol. Sci*. **14** 272
[6] Iwami Y, Yamamoto H, Hayashi M and Ebisu E 2011 *Laser Med. Sci*. **26** 439
[7] Huff K, Stark P C and Solomon L W 2009 *Gen. Dent*. **57** 34
[8] Kerr A R, Sirois D A and Epstein J B 2006 *J. Clin. Dent*. **17** 59
[9] Williams P M, Poh C F, Hovan A J, Ng S and Rosin M P 2008 *J. Can. Dent. Assoc*. **74** 275
[10] Meller C, Heyduck C, Tranaeus S and Splieth C 2006 *Caries Res*. **40** 90
[11] Borisova E, Uzunov T and Avramov L 2006 *Laser Med. Sci*. **21** 34
[12] Paula A B, Campos J A D B, Diniz M B, Hebling J and Rodrigues J A 2011 *Laser Med. Sci*. **26** 1
[13] Deo V and Bhongade M L 2010 *Dent. Today* **29** 60
[14] Roberts F A, Hacker B M, Oswald T K, Mourad P D and McInnes C 2010 *Am. J. Dent*. **23** 65
[15] Tung O H, Lee S Y, Lai Y L and Chen H F 2008 *Conf. Proc. IEEE Engineering Medicine and Biology Society* (*Vancouver*) vol 2008, p 4051
[16] Meisner G and Kocher T 2011 *Periodontology 2000* **55** 189
[17] Ptaszek M 2013 *Prog. Mol. Biol. Translational Sci*. **113** 59
[18] Wilder-Smith P, Holtzman J, Epstein J and Le A 2010 *Oral Dis*. **16** 717
[19] Buchalla W, Lennon A M and Attin T 2004 *J. Periodontal Res*. **39** 327
[20] Kasaj A, Moschos I, Röhrig B and Willershausen B 2008 *Int. J. Dent. Hygiene* **6** 143
[21] Ribeiro-Figueiredo A C, Kurachi C and Bagnato V S 2005 *Caries Res*. **39** 393
[22] Lane P M, Gilhuly T, Whitehead P, Zeng H, Poh C F, Ng S, Williams P M, Zhang L, Rosin M P and MacAulay C E 2006 *J. Biomed. Opt*. **11** 024006
[23] Carvalho V F, Okuda O S, Bernardo C C, Pannuti C M, Georgetti M A, De Micheli G and Pustiglioni F E 2010 *J. Appl. Oral Sci*. **18** 215

[24] Tsui I F, Garnis C and Poh C F 2009 *Am. J. Surg. Pathol*. **33** 1732
[25] Krause F, Braun A and Frentzen M 2003 *Laser Med. Sci*. **18** 32
[26] Krause F, Braun A, Jepsen S and Frentzen M 2005 *J. Periodontol*. **76** 1202
[27] Kurachi C, Fontana C R, Rosa L E and Bagnato V S 2008 *J. Biomed. Opt*. **3** 034018
[28] Eberhard J, Ehleres H, Falk W, Acil Y, Albers H-K and Jepsen S 2003 *J. Clin. Periodontol*. **30** 511
[29] Meisner G, Oehme B, Strackeljan J and Kocher T 2006 *J. Clin. Periodontol*. **33** 195
[30] Rees J S, Addy M and Hughes J 1999 *J. Clin. Periodontol*. **26** 106
[31] Tugnait A, Clerehugh V and Hirschmann P N 2000 *J. Dent*. **28** 219
[32] Kocher T, Strackeljan J and Behr D 2000 *J. Dent. Res*. **79** 829
[33] Sim Y C, Maeng I and Son J-H 2009 *Curr. Appl. Phys*. **9** 946
[34] Sinyaeva M L, Mamedov A A,Vasilchenko S Yu, Volkova A I and Loschenov V B 2004 *Laser Phys*. **14** 1132
[35] Chen Q G, Lin B, Chen Z B, Zhu H H and Chen H 2010 *Laser Phys. Lett*. **7** 752
[36] Bakhmutov D, Gonchukov S, Kharchenko O, Nikiforova O and Vdovin Yu 2004 *Laser Phys. Lett*. **1** 565
[37] Bakhmutov D, Gonchukov S, Kharchenko O, Voytenok O and Zubov B 2008 *Laser Phys. Lett*. **5** 375
[38] Bakhmutov D, Gonchukov S and Sukhinina A 2010 *Laser Phys. Lett*. **7** 384
[39] Benedict H C1928 *Science* **67** 442
[40] Askaroglou E, Kavvadia K, Lagouvardos P and Papagiannoulis L 2011 *Laser Med. Sci*. **26** 29

Biomedical Optics EXPRESS

Time-resolved fluorescence lifetime for cutaneous melanoma detection

Layla Pires,* Marcelo Saito Nogueira, Sebastião Pratavieira, Lilian Tan Moriyama, and Cristina Kurachi

Universidade de São Paulo, Instituto de Física de São Carlos – IFSC/USP, Av. Trabalhador São Carlense,400 - São Carlos, SP, Brazil
**laylabtu@gmail.com*

Abstract: Melanoma is the most aggressive skin cancer type. It is characterized by pigmented lesions with high tissue invasion and metastatic potential. The early detection of melanoma is extremely important to improve patient prognosis and survival rate, since it can progress to the deadly metastatic stage. Presently, the melanoma diagnosis is based on the clinical analysis of the macroscopic lesion characteristics such as shape, color, borders following the ABCD rules. The aim of this study is to evaluate the time-resolved fluorescence lifetime of NADH and FAD molecules to detect cutaneous melanoma in an experimental *in vivo* model. Forty-two lesions were analyzed and the data was classified using linear discriminant analysis, a sensitivity of 99.4%, specificity of 97.4% and accuracy of 98.4% were achieved. These results show the potential of this fluorescence spectroscopy for melanoma detection.

OCIS codes: (300.6500) Spectroscopy, time-resolved; (170.3650) Lifetime-based sensing; (170.3890) Medical optics instrumentation; (170.6510) Spectroscopy, tissue diagnostics; (170.6935) Tissue characterization.

References and links

1. D. S. Rigel, J. Russak, and R. Friedman, "The Evolution of Melanoma Diagnosis: 25 Years Beyond the ABCDs," CA Cancer J. Clin. **60**(5), 301–316 (2010).
2. C. Garbe, T. K. Eigentler, U. Keilholz, A. Hauschild, and J. M. Kirkwood, "Systematic Review of Medical Treatment in Melanoma: Current Status and Future Prospects," Oncologist **16**(1), 5–24 (2011).
3. R. Marchesini, A. Bono, C. Bartoli, M. Lualdi, S. Tomatis, and N. Cascinelli, "Optical imaging and automated melanoma detection: questions and answers," Melanoma Res. **12**(3), 279–286 (2002).
4. S. Seidenari, F. Arginelli, C. Dunsby, P. M. W. French, K. König, C. Magnoni, C. Talbot, and G. Ponti, "Multiphoton laser tomography and fluorescence lifetime imaging of melanoma: morphologic features and quantitative data for sensitive and specific non-invasive diagnostics," PLoS ONE **8**(7), e70682 (2013).
5. C. Gerhäuser, "Cancer cell metabolism, epigenetics and the potential influence of dietary components – A perspective," Biomed. Res. **23**(1), 1–21 (2012).
6. D. A. Scott, A. D. Richardson, F. V. Filipp, C. A. Knutzen, G. G. Chiang, Z. A. Ronai, A. L. Osterman, and J. W. Smith, "Comparative metabolic flux profiling of melanoma cell lines: beyond the Warburg effect," J. Biol. Chem. **286**(49), 42626–42634 (2011).
7. K. Koenig and I. Riemann, "High-resolution multiphoton tomography of human skin with subcellular spatial resolution and picosecond time resolution," J. Biomed. Opt. **8**(3), 432–439 (2003).
8. M. C. Skala, K. M. Riching, A. Gendron-Fitzpatrick, J. Eickhoff, K. W. Eliceiri, J. G. White, and N. Ramanujam, "In vivo multiphoton microscopy of NADH and FAD redox states, fluorescence lifetimes, and cellular morphology in precancerous epithelia," Proc. Natl. Acad. Sci. U.S.A. **104**(49), 19494–19499 (2007).
9. M. S. Islam, M. Honma, T. Nakabayashi, M. Kinjo, and N. Ohta, "pH dependence of fluorescence lifetime of FAD in solution and in cells," Int. J. Mol. Sci. **14**(1), 1952–1963 (2013).
10. R. Martínez-Zaguilán, E. A. Seftor, R. E. Seftor, Y. W. Chu, R. J. Gillies, and M. J. Hendrix, "Acidic pH enhances the invasive behavior of human melanoma cells," Clin. Exp. Metastasis **14**(2), 176–186 (1996).
11. M. L. Wahl, J. A. Owen, R. Burd, R. A. Herlands, S. S. Nogami, U. Rodeck, D. Berd, D. B. Leeper, and C. S. Owen, "Regulation of intracellular pH in human melanoma: potential therapeutic implications," Mol. Cancer Ther. **1**(8), 617–628 (2002).
12. M. G. Vander Heiden, L. C. Cantley, and C. B. Thompson, "Understanding the Warburg Effect: The Metabolic Requirements of Cell Proliferation," Science **324**(5930), 1029–1033 (2009).

#214104 - $15.00 USD Received 16 Jun 2014; revised 8 Aug 2014; accepted 10 Aug 2014; published 22 Aug 2014

13. P. V. Butte, B. K. Pikul, A. Hever, W. H. Yong, K. L. Black, and L. Marcu, "Diagnosis of meningioma by time-resolved fluorescence spectroscopy," J. Biomed. Opt. **10**(6), 064026 (2005).
14. A. Green, N. Martin, G. McKenzie, J. Pfitzner, F. Quintarelli, B. W. Thomas, M. O'Rourke, and N. Knight, "Computer image analysis of pigmented skin lesions," Melanoma Res. **1**(4), 231–236 (1991).
15. A. Green, N. Martin, J. Pfitzner, M. O'Rourke, and N. Knight, "Computer image analysis in the diagnosis of melanoma," J. Am. Acad. Dermatol. **31**(6), 958–964 (1994).
16. S. Tomatis, C. Bartoli, A. Bono, N. Cascinelli, C. Clemente, and R. Marchesini, "Spectrophotometric imaging of cutaneous pigmented lesions: discriminant analysis, optical properties and histological characteristics," J. Photochem. Photobiol. B **42**(1), 32–39 (1998).
17. M. Elbaum, A. W. Kopf, H. S. Rabinovitz, R. G. B. Langley, H. Kamino, M. C. Mihm, Jr., A. J. Sober, G. L. Peck, A. Bogdan, D. Gutkowicz-Krusin, M. Greenebaum, S. Keem, M. Oliviero, and S. Wang, "Automatic differentiation of melanoma from melanocytic nevi with multispectral digital dermoscopy: a feasibility study," J. Am. Acad. Dermatol. **44**(2), 207–218 (2001).

1. Introduction

Annually, 2-3 millions non-melanoma and around 132,000 melanoma skin cancers occur globally and, unfortunately, these numbers are increasing, according to the World Health Organization. Surgical resection is only effective for initial lesions, and its recurrence can vary from 7 to 51%. In Brazil, approximately 6,000 lesions are diagnosed per year, and melanoma is responsible for 80-85% of all deaths caused by skin cancer. Melanoma is the most aggressive skin cancer type, which is characterized by pigmented lesions with high metastatic potential. The early detection of melanoma is extremely important to improve patient prognosis and decrease mortality rate. Presently, the melanoma diagnosis is based on the clinical analysis of the macroscopic lesion characteristics such as shape, color, borders following the ABCD rule. The ABCD rule states for: A (asymmetry), B (border irregularity), color (non-homogenous color distribution), and D (diameter greater than 6 mm). The lesion progression and site location are also considered for clinical diagnosis [1].

As soon as the clinical examination indicates a potential melanoma, an excision is performed and then, the histology is evaluated. If melanoma cells are detected in the border of the lesion, another excision is performed with a larger resection margin. Chemotherapy and radiotherapy are also indicated for the cases of possible metastatic stage [2]. Anyway, early detection of melanoma is highly dependent on the clinician training and expertise on recognizing initial melanoma signs. Optical techniques for diagnosis have been already used for melanoma detection such as epiluminescence microscopy, reflectance spectrophotometry, fluorescence spectroscopy, fluorescence imaging and optical coherence tomography [3, 4].

Melanoma cells are characterized by high proliferative and metabolic rates, but the most common variation between normal and cancer cells is the high rate of aerobic glycolysis or the Warburg effect. The Warburg effect describes the cancer respiratory pathway that, when in the presence of oxygen, shows a high rate of glycolysis, followed by the lact acid fermentation in citosol, in contrast to the normal cells that present a lower glycolysis rate, followed by oxidation of pyruvate in mitochondria. In normal tissue, the glucose metabolism pathway is described by the Pasteur Effect, which determines the metabolism pathway with plentiful and limited oxygen [5, 6]. NADH (nicotinamide adenine dinucleotide) and FAD (flavin adenine dinucleotide) are the primary electron acceptor and donor, respectively, in oxidative phosphorylation, the most efficient means of energy production in cells. Changes in the NADH/FAD rates and their relative amounts of free and protein-bound states depend on the glycolysis and oxidative phosphorylation ratio. This suggests that tissues with different metabolic rates can be discriminated by comparing short and long lifetime fluorescence decays of NADH (the average lifetimes for free and protein-bound NADH are approximately 0.3 ns and 2 ns, respectively) and FAD (for free FAD is around 5 ns and, for protein-bound FAD, approximately 1 ns) and the relative amount of free and protein-bound states [7]. Although NADH and FAD are the mainly molecules used as biomarkers for tumor metabolism, the fluorescence lifetime technique reveals changes in the tumor microenvironment, and is influenced by others fluorophores present in tissue. The individual

#214104 - $15.00 USD Received 16 Jun 2014; revised 8 Aug 2014; accepted 10 Aug 2014; published 22 Aug 2014

fluorescence analysis of specific molecules in tissue measurements is a complex task, since the overall spectrum presents the contribution of several biomolecules, including absorbers and scatterers, and is modified by attenuation coefficient at the visible spectrum. Anyway, the detection of these overall changes in tumor microenvironment is an important factor for tumor and margin evaluation.

Fluorescence lifetime analysis has been presented as a sensitive technique for tissue characterization for diagnosis purposes. The fluorescence lifetime can discriminate free and protein-bound components of fluorophores. One of the main advantages of the fluorescence techniques is the *in situ* and non-destructive evaluation of tissues with fast response. This makes the fluorescence lifetime technique quite suitable for clinical applications. Targeting NADH and FAD from cutaneous melanoma lesions may present diagnostic information. The aim of the present study is to evaluate the efficacy of the time-resolved fluorescence spectroscopy on the diagnostics of the induced cutaneous melanoma in an animal model.

2. Materials and methods

Cell line: The B16F10 murine melanoma cells (Rio de Janeiro Cell Bank, Rio de Janeiro, Brazil) were cultured in DMEM medium supplemented with 10% bovine fetal serum and 1% penicillin-streptomycin solution under 5% CO_2 at 37°C.

Animals: Forty-two nude balb/c mice (Centro de Bioterismo - Universidade de São Paulo – São Paulo, Brasil) were housed in micro-isolator cages, with food and water *ad libitum*.

Experimental melanoma: The animal was anesthetized using 2% isofluorane mask. An intradermal injection of 10^7 B16F10 cells in 100 μL of PBS was performed into the right and left animal flank regions. The mice were examined daily to monitor any changes in systemic conditions as loss of weight or signs of metastasis. This study was approved by the Ethical Committee of the Universidade Federal de São Carlos – São Carlos/Brazil.

Characterization of optical properties of the experimental melanoma: The light distribution in the induced tumor was evaluated by reflectance, fluorescence and transmission spectroscopy measurements. For the reflectance and fluorescence measurements, the optical fiber coupled to 378nm or 445nm laser was positioned on the top of the tumor, and the reflectance was radially collected scanning the total lesion surface, or until the signal absence, in steps of 0.1mm. Then, the animal was euthanized and the tumor was removed for transmittance evaluation. For experimental purposes, an optical fiber was positioned at the top of the lesion, and the collect fiber was positioned at the tumor base to collect the transmission light. The diffuse and transmitted reflectance spectra were plotted and the total attenuation coefficients were determined based on the dimensional lesion characteristics. Fluorescence spectra were also plotted and the maximum distance at the lesion surface from the excitation site was determined. Based on these measurements, an estimated interrogated tissue volume for this experimental melanoma was defined.

Fluorescence system: The time-resolved fluorescence spectroscopy system is composed of two diode lasers, one emitting at 378 nm and another at 445 nm (BDL-375-SMC and BDL-445-SMC, Becker and Hickl, Berlin, Germany). The 378 nm is used to excite NADH, and the 445 nm to excite FAD. Both lasers have a repetition rate of 20, 50, 80 MHz and a temporal pulse duration of 50-100 ps. A bifurcated fiber (Ocean Optics, Dunedin, Florida, USA) was used to deliver the light to the tissue and to collect the tissue fluorescence. A bandpass filter at (440 ± 40) nm (Semrock, Rochester, New York, USA) was used with 378 nm excitation, and a bandpass filter at (514 ± 30) nm (Semrock, Rochester, New York, USA), for 445 nm excitation. The fluorescence signal was detected using a high-speed hybrid PMT detector (HPM-100-50, Becker and Hickl, Berlin, Germany). The data were collected and processed using the TCSPC Software (Becker and Hickl, Berlin, Germany). The impulse response function (IRF) of the system is about 230 ps.

Fluorescence lifetime measurements: Lesions of 2 up to 30 mm in diameter were interrogated. The mice were anaesthetized with 2% iso⟩urane in oxygen using a mask. The

#214104 - $15.00 USD Received 16 Jun 2014; revised 8 Aug 2014; accepted 10 Aug 2014; published 22 Aug 2014

optical fiber was positioned at the surface of the experimental melanoma lesion or on the normal skin and the fluorescence measurements were collected. At least three measurements were taken from each lesion with both excitation lasers. Each flank region where the melanoma cells were inoculated was monitored daily, and the measurements were performed with lesions size between 2 and 15mm. A total of 42 lesions were investigated.

Data processing: The raw data of the photon counting with time resolution was processed using the SPCImage Software (Becker and Hickl, Berlin, Germany). SPCImage software provides an "estimation" of the IRF by calculating the first derivative of the rising part of the fluorescence lifetime spectrum and, then, it calculates a function model for the measured intensity by the convolution of the IRF and the exponential decay fitting. So, the decay curve of the model function was fitted by a bi-exponential function:

$$F(t) = a_1 e^{\frac{t}{\tau_1}} + a_2 e^{\frac{t}{\tau_2}}, \quad [1]$$

using the average fluorescence lifetime values τ_1 and τ_2, ccorresponding to short and long lifetime components, respectively, and relative coefficients a_1 and a_2, where $a_1 + a_2 = 100$.

In order to compare the collected data from normal skin and cutaneous melanoma, scatter plots and box plots graphs were constructed using Origin 9.0 (OriginLab. Corporation, Northampton, MA, USA) using a_1, a_2, τ_1 and τ_2 parameters of each measurement. This comparison allowed a better discrimination for measurements using 378 nm or 445 nm excitation wavelengths.

Statistical analysis: It was used unpaired *t* test. Exact *p* values were computed, all *p* values are two-sided, and a $p < 0.001$ was considered statistically significant.

Data analysis: a classification was performed with the linear discrimination analysis of MATLAB software (version R2012a, Mathworks, Natick, MA, USA) to determine the combination of predictor variables that accounts for most of the differences in the behaviors of the normal skin and cutaneous melanoma groups. The classification algorithms were then evaluated based on sensitivity, specificity and accuracy values. For diagnostics classification, histopathology of HE slides was used as gold standard.

3. Results

Experimental melanoma: the induced cutaneous lesion shows a fast progression characterized by dark pigmentation and metastatic potential. Twenty-four hours after the injection it is possible to observe a small pigmented lesion with an average of 2-3mm in diameter. At 48 hours after the melanoma induction, the lesions reach up to 1cm of diameter. After 7 days, the tumor shows a diameter of 4-5cm. During this development, no significant changes were observed in the animal overall conditions, as loss of body weight or changes in behavior. Ten days after the induction, metastasis can be observed. In the first 48 hours of development, some lesions present a thin layer of normal epidermis over the tumor. It constitutes a limitation for optical measurements such as fluorescence lifetime, especially with ultraviolet-violet excitation, since the detected signal has also the contribution of normal tissue presented. The induced lesion rises at the surface until approximately 72 hours, becoming similar to a spontaneous lesion. After 10 days it starts to invade deeper tissues, reaching muscle and spreading to all the body. Even before invasion, the lesion area observed on the skin surface was smaller than that observed in dermis deeper layers. During this period, angiogenesis is also observed, but this is not sufficient to feed the whole tumor mass and the lesion center become necrotic. For experimental purposes, no measurements were performed in the necrosis area, due to the absence of lesion diagnostic information. In the histology one can observe melanoma cells surrounded by a collagen fiber and numerous blood vessels.

Characterization of experimental melanoma optical properties: the 378nm laser reflectance measurements showed that the light is completely absorbed by the tissue and so, no reflectance was observed at the surface. On the other hand, it was possible to observe the

#214104 - $15.00 USD Received 16 Jun 2014; revised 8 Aug 2014; accepted 10 Aug 2014; published 22 Aug 2014

tissue fluorescence as a function of the radial distance. The decays were fitted and the attenuation coefficient determined. Then, an interrogated volume was estimated in about 0.079 ± 0.009 mm^3. For the 445nm laser, due to its low efficiency for tissue excitation, it was not possible to detect the fluorescence signal. However, the reflectance measurements were enough to estimate the probed volume to 0.017 ± 0.002 mm^3. Due to the lesion thickness between 2.4mm and 4mm, transmittance signal was not detected for none excitation lasers.

Time-resolved fluorescence lifetime spectra: the fluorescence lifetime is sensitive to fluorophore microenvironment and provides a method for discriminating free and protein-bound components of NADH and FAD. The NADH molecules show a short lifetime component when it is free and a longer lifetime component when it is protein-bounded. For FAD molecules, short lifetime component is present for protein-bounded and longer lifetime component for its free state. These molecules states are related to aerobic and anaerobic processes: oxidative phosphorylation and glycolysis. In Fig. 1 one can observe the decay curve for (mainly) NADH and FAD molecules in normal skin and melanoma.

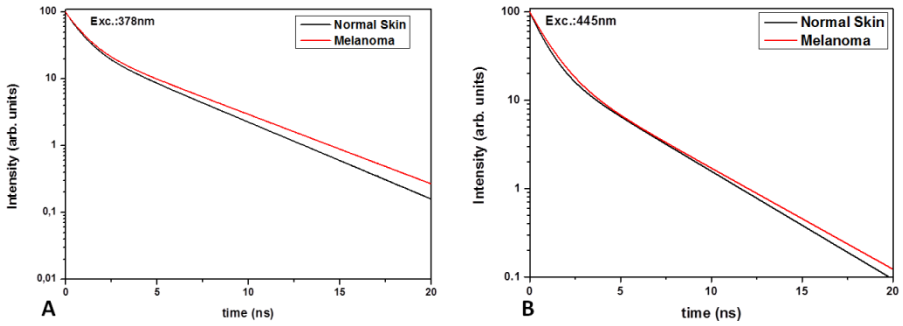

Fig. 1. Representative fluorescence decay profiles of NADH (A) and FAD (B) molecules in normal skin and melanoma.

Despite the fact that the system excites targeting NADH and FAD molecules, it is complex to evaluated individually the contribution of these molecules in the *in* vivo fluorescence spectrum. Other biomolecules also contribute for the collected spectrum such as melanin, collagen, elastin and keratin.

Data processing: The results obtained for the 378nm excitation is shown in Fig. 2. One can observe that for the a_1 and a_2 parameters there were no significant difference between normal skin and cutaneous melanoma (Fig. 2(A) and 2(B)). It was not observed in the melanoma, probably due to the thin normal epidermis layer present over the experimental lesion. In addition to its contribution to the collected fluorescence signal, this thin skin layer also reduces the laser penetration and resulted excitation of the target tissue.

On the other hand, the parameters τ_1 and τ_2 that refers to the average lifetime fluorescence values showed a statistical significant discrimination between normal skin and melanoma ($p < 0.001$)(Fig. 2(C) and 2(D)). Both, short and long lifetime components, increased in melanoma when compared to normal skin. If the results agreed with the Warburg effect, the melanoma fluorescence lifetime would be diminished due to the presence of higher concentration of free NADH molecules when compared to protein-bound molecules. However, this was not observed. A hypothesis to these results is that since we interrogated the melanoma lesions at different development stages, the specific Warburg effect could not be observed at the average data. Furthermore, others molecules such as collagen and melanin may contribute to this change in the fluorescence lifetime observed. This data was also fitted for three

#214104 - $15.00 USD Received 16 Jun 2014; revised 8 Aug 2014; accepted 10 Aug 2014; published 22 Aug 2014

exponentials, but the parameters obtained did not improve our results. Anyway, these measurements showed a significant discrimination between normal skin and melanoma.

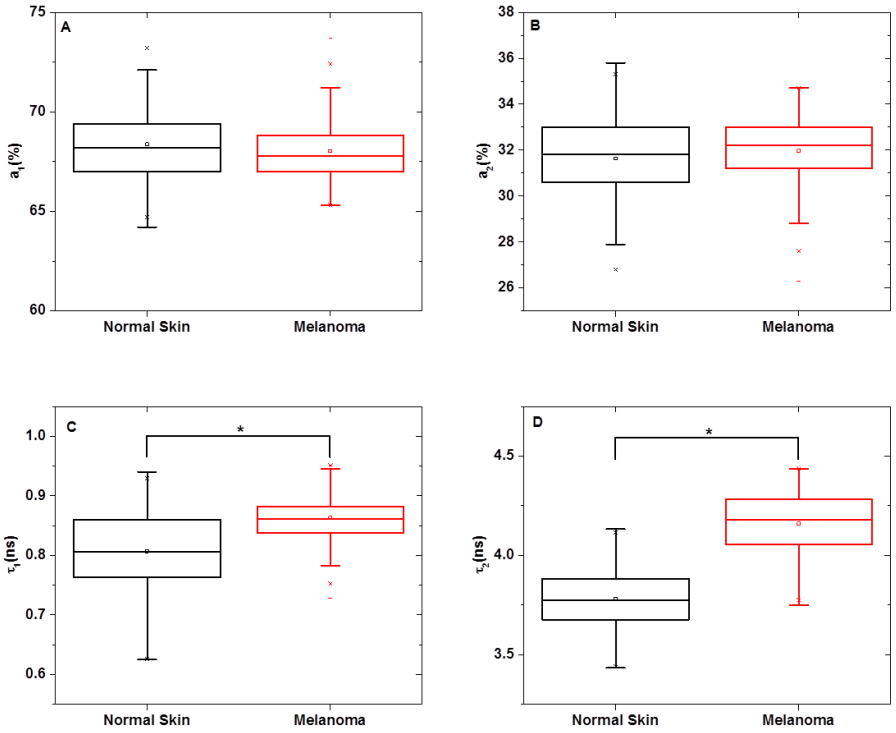

Fig. 2. Boxplot for the parameters obtained in the data analysis for 378 nm excitation: a_1, a_2, τ_1 and τ_2, respectively. Significant differences ($P < 0.001$) exist between normal vs. melanoma for the parameters τ_1 and τ_2(*).

Figure 3 shows the fluorescence lifetime parameters obtained for FAD excitation at 445nm. The parameters a_1 and a_2 represent the relative quantities of FAD molecules on both states, protein-bound and free, respectively. Figure 3(A) and 3(B) show that melanoma has more FAD in protein-bound state than normal skin. The opposite is also true: normal skin has more free FAD molecules than melanoma. If the glycolysis and oxidative phosphorylation ratio characteristic of melanoma were observed, melanoma would present higher amount of free FAD than in normal tissue. However, looking for the normal skin, the relative quantities of free and protein-bound FAD agree with the aerobic metabolism. These results may be explained by the system used for the measurements. Although FAD is the mainly excited molecule, it is not the unique one.

#214104 - $15.00 USD Received 16 Jun 2014; revised 8 Aug 2014; accepted 10 Aug 2014; published 22 Aug 2014

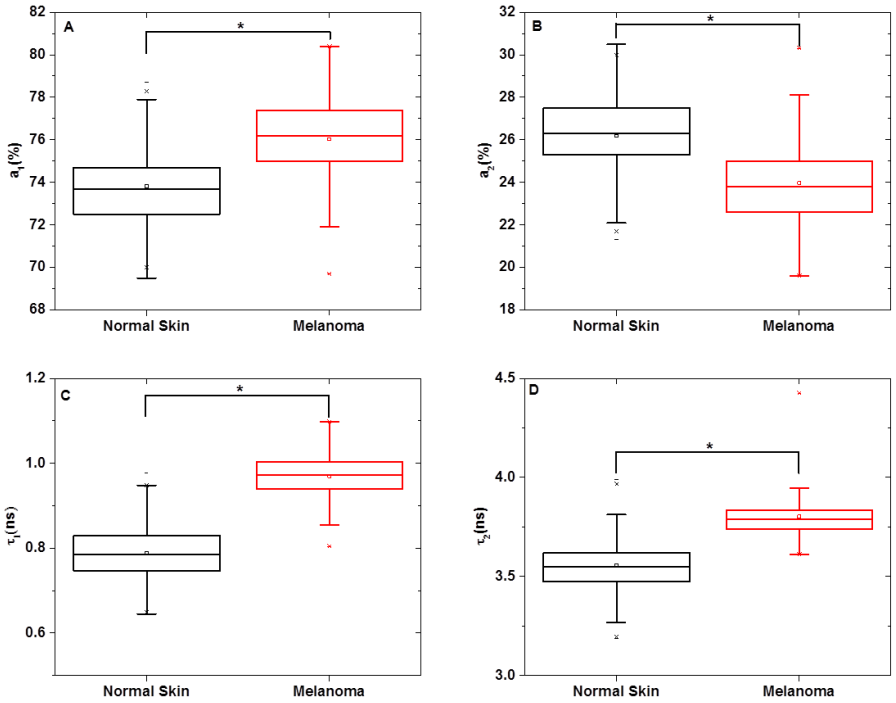

Fig. 3. Boxplot for the parameters obtained in the data analysis for 445 nm excitation: a_1, a_2, τ_1 and τ_2, respectively. Significant differences ($P < 0.001$) exist between normal skin vs. melanoma for all parameters (*).

The protein-bound FAD is part of the oxidative phosphorylation metabolism and its lifetime is smaller when compared to the free FAD state. Therefore, the short and long lifetime components describe the melanoma preference to glycolysis (Fig. 3(C) and 3(D)). These results agree with the melanoma metabolism changes described by Scott et al., 2011 [6]. Melanoma, even in the presence of oxygen, increases the energy generation by nonoxidative breakdown of glucose – glycolysis, instead of more energy-efficient oxidative respiration.

Data analysis: The data classification was performed using the parameters τ_1 for 445 nm excitation and τ_2 for 378 nm. These parameters were chosen based on the best results obtained in this study. The linear discriminant analysis was able to discriminate normal skin and melanoma with a sensitivity of 99.4%, specificity of 97.4% and accuracy of 98.4% (Fig. 4).

#214104 - $15.00 USD Received 16 Jun 2014; revised 8 Aug 2014; accepted 10 Aug 2014; published 22 Aug 2014

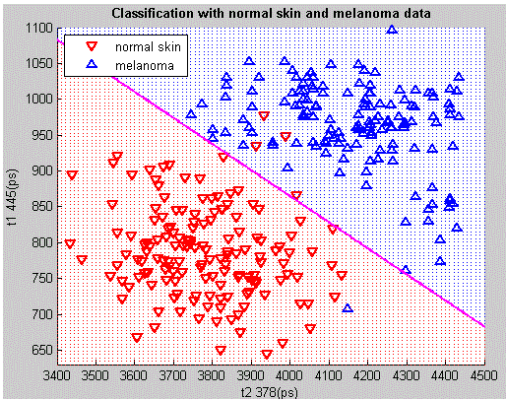

Fig. 4. Short lifetime component (τ_1) of 445 nm excitation against long lifetime component (τ_2) of 378 nm, the separating lines was performed using linear discrimination analysis.

The short lifetime component of FAD and long lifetime component of NADH provides information about the oxidative phosphorylation metabolism pathway. The aerobic respiration is present in both tissues following the Pasteur effect. Furthermore, it was an important parameter to distinguish normal skin and melanoma.

4. Discussion

Metabolism is an important parameter to evaluate the cell microenvironment. Nicotinamide adenine dinucleotide (NAD^+/NADH) is an important coenzyme involved in the energy metabolism of living cells. In the aerobic respiration, glucose is converted to lactate, NADH is oxidized to generate ATP through oxidative phosphorylation. NADH has a short and a long lifetime components, depending on whether it is in free or protein-bound state, respectively [6].

FAD is another coenzyme in living systems and is also present in two forms, referred to as protein-bound and free FAD. The protein-bound FAD state participates in oxidative phosphoylation and it is also important for tumor metabolism [6]. FAD also has, short and long lifetime components refer to protein-bound and free FAD state, respectively. Changes in the tumor's microenvironment such as the oxygen viability, pH, and temperature modify the metabolism process, and may be detected by time-resolved fluorescence lifetime measurements.

Results obtained in experimental melanoma model with excitation at 378nm were able to distinguish normal skin and tumor for both lifetime components. However, parameters a_1 and a_2 were not able to distinguish normal skin and melanoma. These components are related to the amount of NADH molecules in the free and protein-bound states and the measurements may be compromised due to the experimental melanoma development. A thin normal epidermis can be observed overlaying the melanoma lesion in the first three days after the cells injection. This tissue layer probably contributes to the amount of NADH measurements modifying the parameters a_1 and a_2. It also influences the long and short lifetime components, but it is not visible due to the average lifetime obtained. Therefore, both lifetime components distinguished the normal skin and melanoma. These results do not agree with the Warburg Effect that describes the tumor metabolism preference to glycolysis (Scott et al., 2011). If it happens, melanoma would present lower fluorescence lifetimes due to the free NADH state lifetime contribution. There are many reasons that may explain this, such as experimental melanoma development, tumor pH and oxygen. Some endogenous fluorophores such as tryptophan moieties, collagenase-digestible and pepsin-digestible collagen, cross-links, elastin cross-links, reduced NADH, oxidized flavins, porphyrin and keratin may contribute to change the NADH fluorescence lifetime in melanoma. Several studies using fluorescence lifetime

#214104 - $15.00 USD Received 16 Jun 2014; revised 8 Aug 2014; accepted 10 Aug 2014; published 22 Aug 2014

presented different behaviors for normal and malignant tissues that are neither all in agreement with the Warburg effect. Skala et al. (2007) evaluated the fluorescence lifetime in precancerous epithelia and showed a decrease in the NADH lifetime when comparing normal to low and high grade precancerous [8].

The experiments performed with the 445nm excitation showed statistical significance for all components evaluated. Melanoma presented a higher amount of protein-bound state FAD in comparison to normal skin. It does not reveal the expected, wherein the protein-bound state FAD is related to the oxidative phosphorylation metabolism. Although the relative quantities of FAD did not agree with the Warburg effect, the opposite was observed for the lifetimes. The protein-bound FAD state has a short lifetime, while the free FAD has a long lifetime. Results showed that the melanoma has a longer lifetime, related to the presence of free FAD molecules. On the other hand, the normal skin showed a shorter lifetime, related to the protein-bound FAD. These results agree with the tumor preference to glycolysis. pH is another parameter that may influence the FAD lifetime. Islam et al. (2013) described that acidic pH shift the fluorescence lifetime to higher values, while basic pH shifts the fluorescence lifetime to smaller values [9]. This shift to higher lifetime values was observed in melanoma measurements, and it may be related to the pH effect once there are several studies describing the melanoma acidic characteristic [10,11]. Our results based on an averaged of the fluorescence lifetime measured at distinct melanoma development stages may not be specifically explained by the Warburg effect. The analysis of the NADH and FAD, free and protein-bound states, has not been completely elucidated during at each step of the tumor development. Tumor metabolic pathways is a complex process involving many factors such as cell type and proliferation rate, temperature, experimental model including the animal and others [12]. Beyond that, it is not possible to measure the fluorescence lifetime of only NADH and FAD molecules. They are the mainly molecules present in tissue, but collagen, melanin, keratin and others molecules can be find and definitely contribute to the fluorescence lifetime. Tumor metabolic stages and the amount of molecules present in tissue may be the responsible of changes in the decays.

Butte et al. (2005) described the potential use of time-resolved fluorescence spectroscopy as an adjunctive tool for the intraoperative rapid evaluation of meningioma diagnosis. They evaluated the technique on *ex vivo* tissue specimens from patients undergoing brain tumor surgery and the results showed a sensitivity higher than 89%, specificity of 100% and an accuracy of classification around 92% [13].

Marchesini et al. (2002) reviewed the most important optical systems for melanoma detection. Video camera showed specificity from 55 to 91%, sensitivity from 80 to 90%. The best results were obtained for infrared and RGB gradient color [3, 14, 15]. Spectrophotometry techniques showed specificity from 46 to 91% and sensitivity from 80 to 89%. The best results were obtained for lesion area and spectral curve analysis [16]. Elbaum et al. 2001 investigated the potential of the multispectral dermoscopy to diagnose melanoma. Sixty-three cutaneous melanoma and 224 non-melanoma lesions were evaluated. In this study, the infrared and wavelet data were evaluated and 85% specificity and 100% sensitivity were obtained [17].

Multiphoton laser tomography and fluorescence lifetime was also evaluated for melanoma [4]. This technique was able to distinguish cell morphology such as keranocytes and melanocytes, although this technique did not distinguish melanoma and nevus.

The main advantage of time-resolved fluorescence lifetime comparing with steady-state fluorescence spectroscopy is the possibility to obtain metabolic information that is not dependent on tissue absorption and scattering [8]. This advantage is highly important for melanoma. It is also important for margin detection during a surgery resection.

Using the time-domain fluorescence lifetime, our results showed a sensitivity of 99.4%, specificity of 97.4% and accuracy of 98.4% when it was used a linear classification. These results refer to 42 experimental melanoma lesions induced in balb/c nude mice using the cell

#214104 - $15.00 USD Received 16 Jun 2014; revised 8 Aug 2014; accepted 10 Aug 2014; published 22 Aug 2014

line B16F10. Though these results were obtained with an experimental melanoma, the values of sensitivity, specificity and accuracy were significant when compared to other techniques.

Despite this study reveals that the fluorescence lifetime technique was able to distinguish normal and melanoma tissue, its potential use for melanoma and margins diagnostics must be defined based also on the discrimination of melanoma and others pigmented lesions.The investigation of the efficacy of this technique in cutaneous pigmented lesions will be performed in patients. Anyway, the differentiation of normal skin and melanoma is very important for margin detection in surgery, once melanoma is an extremely aggressive tumor with high rates of morbidity and mortality when metastasized. The possibility of using a fast measurement to determine the tumor site ressection may reduce the recurrence rate and then, improve the patient survival.

5. Conclusion

High rates of sensitivity, specificity, and accuracy of 99.4%, 97.4%, 98.4%, respectively, were obtained using time-domain fluorescence spectroscopy to detect cutaneous melanoma in an animal model. These results show the potential of lifetime fluorescence to aid in the cutaneous melanoma detection through a non-invasive technique.

Acknowledgments

This study was financially supported by the Brazilian Funding Agencies: Capes; CNPq (Universal 475322/2011-8, INOF – INCT 573587/2008-6); and São Paulo Research Foundation (FAPESP) grants: 1998/14270-8 (CEPOF), 2013/07276-1 (CEPOF). The authors also would like to thank the Centro de Bioterismo from Universidade de São Paulo.

Comparison between two portable devices for wide field PpIX fluorescence during Cervical Intraepithelial Neoplasia treatment

Fernanda M. Carbinatto[a]*, Natalia Mayumi Inada[a], Welington Lombardi[b], Natália Fernandez Cossetin[b], Cinthia Varoto[b], Cristina Kurachi[a], Vanderlei Salvador Bagnato[a].
[a] University of São Paulo, São Carlos Institute of Physics, São Carlos-SP, Brazil
[b] UNIARA, Medicine Faculty, Woman Health Ambulatory, Araraquara-SP, Brazil

ABSTRACT

The use of portable electronic devices, in particular mobile phones such as smartphones is increasing not only for all known applications, but also for diagnosis of diseases and monitoring treatments like topical Photodynamic Therapy. The aim of the study is to evaluate the production of the photosensitizer Protoporphyrin IX (PpIX) after topical application of a cream containing methyl aminolevulinate (MAL) in the cervix with diagnosis of Cervical Intraepithelial Neoplasia (CIN) through the fluorescence images captured after one and three hours and compare the images using two devices (a Sony Xperia® mobile and an Apple Ipod®). Was observed an increasing fluorescence intensity of the cervix three hours after cream application, in both portable electronic devices. However, because was used a specific program for the treatment of images using the Ipod® device, these images presented better resolution than observed by the Sony cell phone without a specific program. One hour after cream application presented a more selective fluorescence than the group of three hours. In conclusion, the use of portable devices to obtain images of PpIX fluorescence shown to be an effective tool and is necessary the improvement of programs for achievement of better results.

Keywords: Cervical Intraepithelial Neoplasia, portable electronic devices, Protoporphyrin IX, Photodynamic Therapy .

1. INTRODUCTION

The use of portable electronic devices, such as smartphones has become increasingly common place within the healthcare environment, using by healthcare professional and patients. Before the use of cellular devices was restricted in many healthcare environments but now these devices are used more freely for both the healthcare professional and patient [1]. Portable electronic devices can auxiliary diagnosis of diseases and monitoring treatments like topical Photodynamic Therapy such as Cervical Intraepithelial Neoplasia (CIN), precancerous condition of the cervix localized in the squamo-columnar junction [2].

Human papillomavirus (HPV) infections is main factor related to CIN, mainly high risk HPV types 16 and 18. The classification used to CIN is CIN 1: mild dysplasia, CIN 2: moderate dysplasia and CIN 3:severe dysplasia and carcinoma *in situ* (CIS) . However if CIN is diagnosed at an appropriate time before cervical cancer manifestation, it may be cured and cervical cancer avoided [2,3].

Biophotonics South America, edited by Cristina Kurachi, Katarina Svanberg, Bruce J. Tromberg, Vanderlei Salvador Bagnato, Proc. of SPIE Vol. 9531, 953140 · © 2015 SPIE
CCC code: 1605-7422/15/$18 · doi: 10.1117/12.2180914

Currently the detection of CIN lesions is made based on mass screening with cervical cytology and/or HPV testing and after identification of a subject at risk, colposcopy with acetic acid is used to evaluate the location, size and possible grade of the lesion, and to take guided biopsies from it. Colposcopy is a technique with high sensitivity (over 90%) but low specificity (50-60%).Therefore, new techniques are required which detect lesions with more efficiently [4].

Photodynamic Therapy (PDT) is a promising alternative for diagnosis and treatment of CIN and it is less damaging to normal tissues than surgery, radiation, or chemotherapy. Fluorescence diagnosis occurs through irradiation with light of a wavelength that matches the absorption peak of the photosensitizer, dysplastic or malignant tissue shows a characteristic fluorescence which can be used for lesion detection [3,4].

The application of cream with methyl aminolevulinate (MAL) in cervix lesion allows the penetration of MAL in the cell and allows entry into the biosynthetic pathway of heme, resulting in protoporphyrin IX (PpIX) formation. Studies have demonstrated that the production and accumulation of PpIX occurs more efficiently in altered and neoplastic cells than in normal cells. The PpIX molecule is highly fluorescent, or when it absorbs energy, the decay of the excited electronic state result in photon emission, or fluorescence [5].

As production and accumulation of PpIX is higher in altered cells if the tissue with CIN is treated with MAL cream and fluorescence is detected after the determined time, the visualization of the fluorescence has the potential to improve the identification and CIN treatment.

2. MATERIAL AND METHODS

2.1 Patient selection

Patients shows in cervical cytology testing and colposcopy diagnosis of CIN. Patients were selected and invited to participate in this study. The patients were subjected to photodynamic therapy (PDT) for diagnosis of CIN through the fluorescence images captured using two devices (a Sony Xperia® mobile and an Apple Ipod®) and these patients were divided in two groups: Group 1 with CIN 1(one hour with cream) and Group 2 with CIN 2 (three hours with cream).

2.2 Casuistry

The patient selection was consecutive, non-random, decided by the clinicians involved in the research and with biopsy confirmed by the CIN presence. Written informed consent was obtained following approval by the Human Medical Ethics Committee.

2.3 Application of cream with MAL

The applications of cream containing 20% MAL (w/w) was realize using a needleless syringe with 2 grams of the cream and after tampon was used to keep the cream in place for one (Group 1) and three hours (Group 2).

2.4 Portable devices

Portable devices used in this study were:

- Apple Ipod® touch 5th generation with iSight camera of 5 megapixel, hybrid IR filter and five-element lens
- Sony Xperia model "P" with 8 megapixel camera.

Fluorescence image using portable device Apple Ipod® were captured through of specific program for the treatment of images, ProCAM2.

2.5 Fluorescence images

After one hour (Group 1) and/or three hours (Group 2) of applications of cream containing MAL, fluorescence images of the photosensitizer protoporphyrin IX (PpIX) were obtained using the tip with laser emitting at 405 nm (CerCa 150 System®, MMOptics and Trubios) and fluorescence images were captured using two different devices (a Sony Xperia® mobile and an Apple Ipod®) and the images were compared. After the registration of images another tip of the Cerca System with LEDs (light-emitting diodes) emitting at 630 nm was anatomically positioned in cervix. The patients of the Group 1(with CIN I-one hour with cream incubation) were treated during 21 minutes, with an intensity of 80 mW/cm^2. The same time of application was did for the patients of the Group 2 (with CIN 2-three hours with cream incubation), with intensity of 120 mW/cm^2. After PDT, new fluorescence images were captured.

3. RESULTS AND DISCUSSION

Application of 2 grams of 20% MAL cream in cervix for one and three hours has been used for fluorescence diagnosis of CIN 1 and 2, respectively. Topical application of MAL, induces formation of the endogenous photosensitizer, PpIX in tissues where carcinogenesis has begun. The PpIX tend to accumulate in premalignant and malignant tissues and the illumination with light with appropriate wavelength beginning to excitation of PpIX fluorescence, which helps to localize PpIX-rich areas and identify potentially malignant tissues [6].

In this study was used a system (CerCa 150 System®) with the probe laser emitting at 405 nm and fluorescence images were captured, using two different devices (a Sony Xperia® mobile and an Apple Ipod®) after one and/or three hours, and the cevix demonstrated red fluorescent characteristic of the PpIX formation. After 21minutes of PDT was observed PpIX photodegradation, as seen in the green fluorescent imaging.

Panels A of the figures 1 and 2 shows the PpIX fluorescence imaging of cervix with CIN 1 using the Sony Xperia® and an Apple Ipod®, respectively.

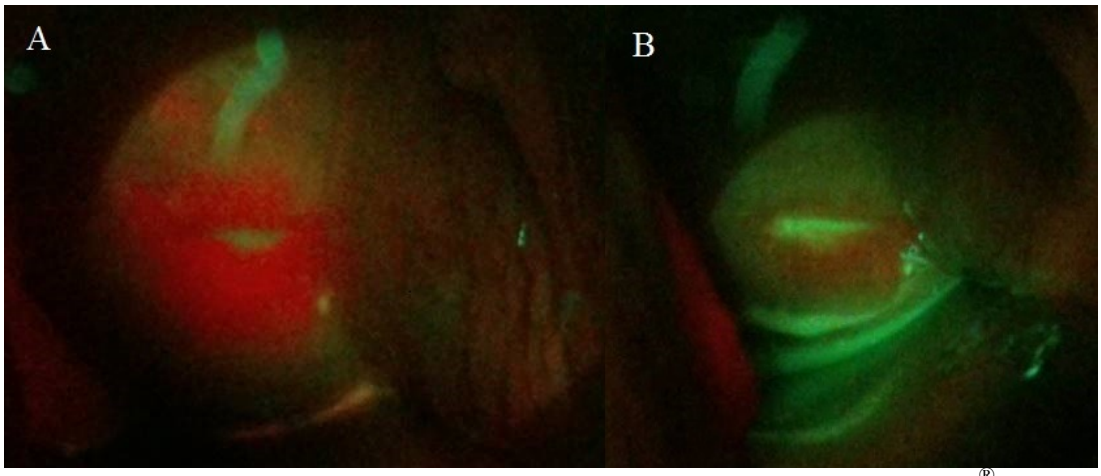

FIGURE 1: Cervix images of Group 1with one hour cream and acquired with Sony Xperia® model "P" device - Panel A: PpIX fluorescence in cervix. Panel B: Cervix fluorescence after PDT (LED 630nm, 80 mw/cm^2, during 21 minutes, total dose of 100 J/cm^2)

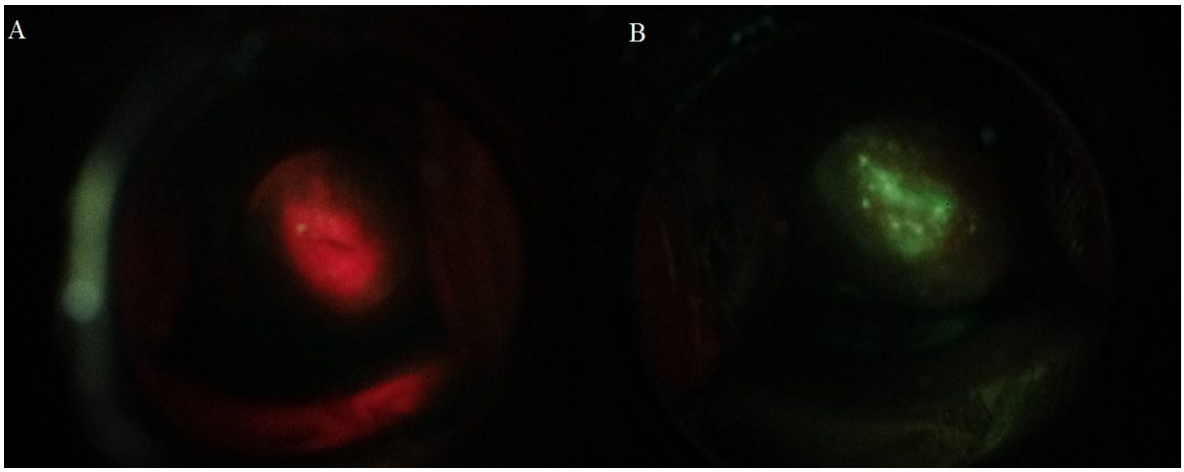

FIGURE 2: Cervix images of Group 1 with one hour of cream application and acquired with Apple Ipod®. - Panel A: PpIX fluorescence in cervix. Panel B: Cervix fluorescence after PDT (LED 630nm, 80 mw/cm^2, during 21 minutes, total dose of 100 J/cm^2)

Fluorescence images of the Group 1 were similar comparing the devices Sony Xperia® and Apple Ipod®, demonstrating selectivity in fluorescence with 1 hour of MAL cream (Figures 1 and 2, panels A).

After PDT of Group 1 (dose of100 J/cm²) a significant PpIX photodegradation was observed in both portable devices (Figures 1 and 2, panels B).

According to the images captured with Sony Xperia® and Apple iPod to the Group 2 patients (Figures 3 and 4, panels A) were observed greater intensity of fluorescence in comparison with patients of Group 1. Weingandt et al.

2002 [6] observed similar results and attributes that the increase fluorescence intensity is correlated to the severity of CIN.

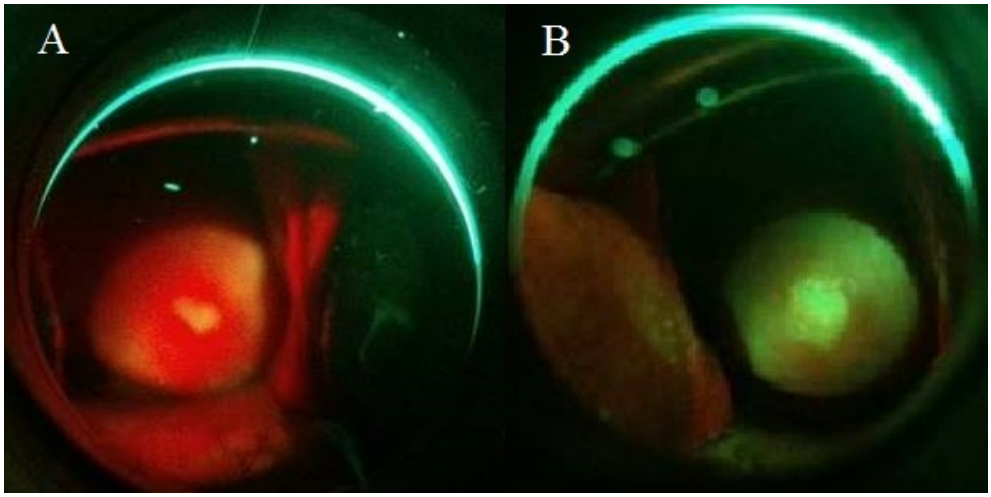

FIGURE 3: Cervix images of Group 2 with three hours of cream application and acquired with Sony Xperia® model "P" device. Panel A: PpIX fluorescence in cervix. Panel B: Cervix fluorescence after PDT (LED 630nm, 120 mw/cm^2, during 21 minutes, total dose of 150 J/cm^2)

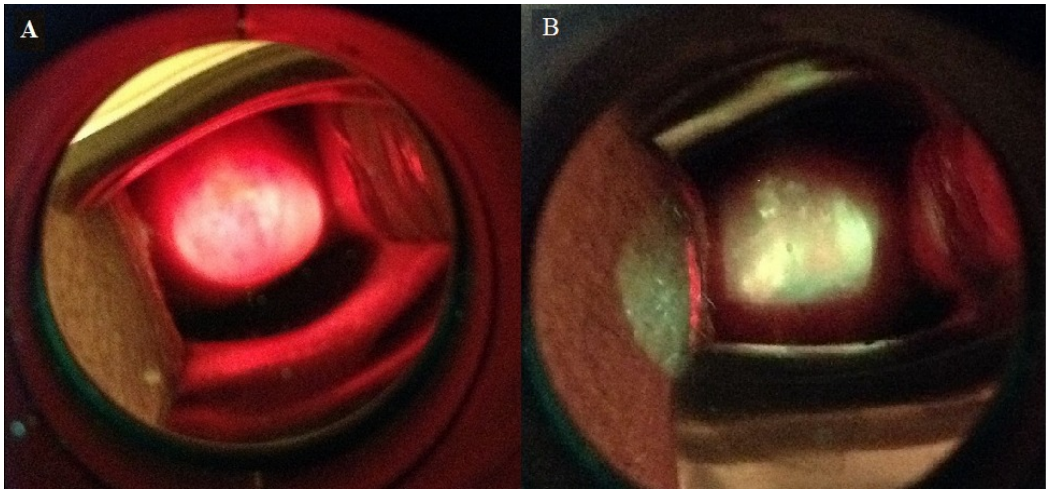

FIGURE 4: Cervix images of Group 1 with one hour of cream application and acquired with Apple Ipod®. Panel A: PpIX fluorescence in cervix. Panel B: Cervix fluorescence after PDT (LED 630nm, 120 mW/cm^2, during 21 minutes, total dose of 150 J/cm^2).

After PDT of Group 2 (final dose of150 J/cm²) also was observed a significant PpIX photodegradation forboth portable devices (Figures 3 and 4, panels B).

However, fluorescence images captured by Apple Ipod® device associated with a specific program called ProCam 2 demonstrated better resolution, possible due by the fact that this program allows the registering photography with Digital Single-lens reflex (DSLR) settings. DSLS have been shown to achieve remarkable low-light sensitivity using high-resolution and advanced noise reduction [7]

4. CONCLUSION

Fluorescence images obtained by portable devices (a Sony Xperia® model "P" mobile and an Apple Ipod®) demonstrated the possibility of fluorescence diagnostic by PpIX formation and monitoring the treatment of pre-malignant lesions through degradation of PpIX. However, is necessary the improvement of programs for achievement of better results.

5. ACKNOWLEDGEMENTS

This work was supported in part by CNPq (INOF – INCT grant: 573587/2008-6); FINEP (Grant n° 01.13.0430-00) and São Paulo Research Foundation (FAPESP) grant 2013/07276-1 (CePOF). FMC was supported by CNPq (Grant n° 383034/2014-0)

REFERENCES

[1] Page, K., Correia, A., l Wilson, M., Allan, E., Parkin, I. P. Light-activated antibacterial screen protectors for mobile telephones and tablet computers. Journal of Photochemistry and Photobiology A: Chemistry, 296, 19-24 (2015).

[2] Vansevičiūtė, R., Venius, J., Letautienė S., 5-Aminolevulinic acid-based fluorescence diagnostics of cervical preinvasive changes, medicina 50, 137-143 (2014)

[3] Tao, XH, Guanb Y, Shaoa D, et al. Photodiagnosis and Photodynamic Therapy, 2014, Article in press. http://dx.doi.org/10.1016/j.pdpdt.2014.02.012

[4] Hillemanns, P.; Soergel, P.; Davis and Loning, M. Fluorescence diagnosis and photodynamic therapy for lower genital tract diseases – A review. Medical Laser Application, 24, 10-17(2009).

[5] Rhodes LE, de Rie MA, Leifsdottir R, et al. Arch Dermatol, 143 (9), 1131-1136 (2007)

[6] Weingandt, H., Stepp H., Baumgartner R., Diebold J., Xiang W., Hillemanns P. Autofluorescence spectroscopy for the diagnosis of cervical intraepithelial neoplasia. BJOG: an International Journal of Obstetrics and Gynaecology 109, 947-951 (2002)

[7] Khoury, M.K., Parker, I., Aswad, D.W. Acquisition of chemiluminescent signals from immunoblots with a digital single-lens reflex camera. Analytical Biochemistry 397, 129–131 (2010)

Renewable Energy 46 (2012) 137–140

Contents lists available at SciVerse ScienceDirect

Renewable Energy

journal homepage: www.elsevier.com/locate/renene

Quantification of biodiesel content in diesel/biodiesel blends by fluorescence spectroscopy: Evaluation of the dependence on biodiesel feedstock

A.R.L. Caires [a,*], V.S. Lima [a], S.L. Oliveira [b]

[a] Grupo de Óptica Aplicada, Universidade Federal da Grande Dourados, CP 533, 79804–970 Dourados, MS, Brazil
[b] Grupo de Óptica e Fotônica, Universidade Federal de Mato Grosso do Sul, CP 549, 79070-900 Campo Grande, MS, Brazil

ARTICLE INFO

Article history:
Received 10 August 2011
Accepted 19 March 2012
Available online 8 April 2012

Keywords:
Fluorescence
Biodiesel
Diesel
Blend
Quantification
Vegetable oil

ABSTRACT

In a recent paper published by our group (M.D. Scherer et al. J. Fluoresc. 21 (2011) 1027–1031), we showed that fluorescence spectroscopy has a potential to be used to determine the biodiesel content in the diesel/biodiesel blends. However, this method presents some challenges that must be overcome to be successfully applied. For instance, the method must work with biodiesel produced from different vegetable oils and fats. In the present study, we evaluated the ability of fluorescence spectroscopy to quantify the biodiesel concentration in diesel/biodiesel blends prepared from different feedstocks. Four different blends prepared using biodiesel produced from four refined vegetable oils (canola, sunflower, corn, and soybean) were used in the present investigation. For all samples, the fluorescence spectra were collected between 300 and 800 nm when excited at 260 nm. Our results revealed that the four blends presented a similar emission profile with a maximum at 470 nm. Furthermore, the same fluorescence behavior (emission intensity as a function of biodiesel content) was observed for all blends. Therefore, the results showed that fluorescence-based method for quantifying the biodiesel content in the diesel/biodiesel blends is independent of the refined vegetable oil used in the biodiesel production.

1. Introduction

In recent years, a great attention has been given to the development of biofuels because they may be obtained from renewable sources, and are more environmentally friendly [1]. Among the biofuel options, biodiesel appears as a sustainable candidate to partly or completely substitute petroleum-derived diesel because its properties are quite similar to those of diesel fuel [2]. Biodiesel is a biodegradable fuel that can be obtained from vegetable oils as well as animal fats [3]. As a result of alternative strategies to reduce the emission amount of carbon dioxide [4], the use of diesel/biodiesel blends (DBB) has been increasing worldwide. Several countries have adopted DBB with different blending limits. The biodiesel percentage usually varies between 2 and 20% that depends on each national legislation. For instance, Brazil has required the use of 5% biodiesel by volume in the DBB [5]. Therefore, it is necessary to develop or improve methods to quantify the biodiesel content in DBB to ensure compliance with legislation. Moreover, it is desirable that the biodiesel content determination can be provided by a method that is easy to use, has a low cost per sample analysis, and provides rapid and accurate results.

A variety of analytical techniques have been developed for quantifying biodiesel content in DBB [6]. Methods based on Fourier transform mid-infrared (FT-IR) absorption spectroscopy [7,8], liquid and gas chromatography [9–11], nuclear magnetic resonance spectroscopy [6], ultraviolet absorption spectroscopy [12], near-infrared spectroscopy [6,13,14], saponification number [15], ester number [16], and radiocarbon analysis [17] have been reported. Despite the several proposed methods, the development of alternative methods that combine low cost, fast and accurate results, and portability is still the object of research. Portability is desirable to allow fuel measurements directly at the point of sale instead of the laboratory, reducing cost and analysis time. Aiming to develop a methodology that is able to meet all these requirements, we have recently demonstrated that fluorescence spectroscopy has a great potential to be used as tool to quantify the biodiesel content in DBB [18]. In that work, the authors showed that fluorescence method is as sensitive as the FT-IR spectroscopy method. The latter is the standard technique used to quantify the biodiesel content in DBB and its use is regulated by means of the NBR 15568 standard. The NBR was introduced by the Brazilian Association of Technical Standards (ABNT). Other international regulatory agencies, such as American Society for Testing and Materials and European

* Corresponding author. Tel./fax: +55 67 34102072.
E-mail address: andersoncaires@ufgd.edu.br (A.R.L. Caires).

0960-1481/$ – see front matter © 2012 Elsevier Ltd. All rights reserved.
doi:10.1016/j.renene.2012.03.026

Committee for Standardization, also make use of the method based on mid-infrared spectroscopy to quantify the biodiesel content in DBB by means of the ASTM D7371 and EN 14078, respectively. Besides the precision, the fluorescence method can be applied remotely and allowing biodiesel quantification without prior sample preparation. However, the method based on the fluorescence spectroscopy still presents some challenges that must be overcome to be successfully applied. As biodiesel can be produced from different vegetable oil feedstocks, an important question that needs to be evaluated is whether the method works with biodiesel produced from different vegetable oils.

Aiming to address this issue the fluorescence method, we evaluated four sets of blends prepared using biodiesel produced from four vegetable oils (canola, sunflower, corn, and soybean). Our results suggest that fluorescence-based method is independent of the vegetable oil feedstock.

2. Material and methods

Canola, sunflower, corn, and soybean biodiesel were produced via transesterification process from their respective refined oils using a 6:1 M ratio of methanol/oil, and NaOH as alkaline catalyst (0.4 wt.% with respect to oil). The NaOH was dissolved in methanol and then added to the preheated oil at 60 °C. The reaction was performed under constant stirring during 60 min at 60 °C. At the end of the reaction, the crude product was allowed to stand in separating funnels for 24 h and two phases were observed, one containing mainly biodiesel and other consisting of glycerol. Afterward, the phase rich in biodiesel was rotary evaporated under reduced pressure during 1 h at 70 °C to eliminate methanol. Then, the biodiesel was washed three times using tap water (3:1, v/v) at room temperature and intervals of 30 min. Subsequently, the samples were filtered through sodium sulfate to eliminate traces of water. The conversion oil to biodiesel was evaluated by FT-IR spectroscopy, monitoring the infrared absorption band at around 1746 cm^{-1} [19]. In addition to the FT-IR measurements, the biodiesel conversion process was monitored by viscosity measurements. As reported recently by Borges and co-workers [20], it is possible to estimate the fatty acid methyl esters content from the dynamic viscosity analysis. They showed that, after the conversion of vegetable oil to its biodiesel, the dynamic viscosity is usually reduced to values lower than 5 cP, depending on the type of raw material used. In our study, the soybean, sunflower, corn, and canola biodiesel presented a viscosity value of about 4.75, 4.70, 4.85, and 4.90 cP, respectively. Finally, the DBB was prepared using the diesel obtained from Petrobras (Petróleo Brasileiro S.A.). Henceforward, DBB is named B*X*, where *X* represents the volume percentage of biodiesel in the blend. Ten samples, from B1 to B10, were prepared in triplicate for each raw material.

Fluorescence measurements were performed in triplicate using a fluorescence spectrophotometer (Cary Eclipse, Varian) and right-angle geometry. UV light at 260 nm was used to excite the samples, and the fluorescence spectrum was collected in the spectral region between 300 and 800 nm. Finally, emission measurements of the blends (B1 to B10) and diesel (B0) without any dilution were performed to evaluate the biodiesel content. All fluorescence analyses were performed using 1-cm path length quartz cells at room temperature.

3. Results and discussion

Fig. 1 exhibits the fluorescence spectrum of diesel and soybean biodiesel under excitation at 260 nm. Although petroleum-derived diesel shows two fluorescence bands centered at about 470 and 585 nm, biodiesel presents two bands with fluorescence peaks at 470 and 660 nm. For better comparison, the spectra of diesel and soybean biodiesel showed in Fig. 1 were normalized. However, results corroborate that the fluorescence intensity at 470 nm from diesel is about five times higher than that from biodiesel [18]. The emission bands observed in diesel are principally due to the aromatic compounds in the fuel. In turn, it is reasonable to consider that the biodiesel emission bands are due to the remaining fluorophores from vegetable oil such as tocopherols and chlorophyll because biodiesel has a similar fluorescence spectral profile to that of the oil (data not shown), however the role of the fatty acid methyl esters may not be ruled out.

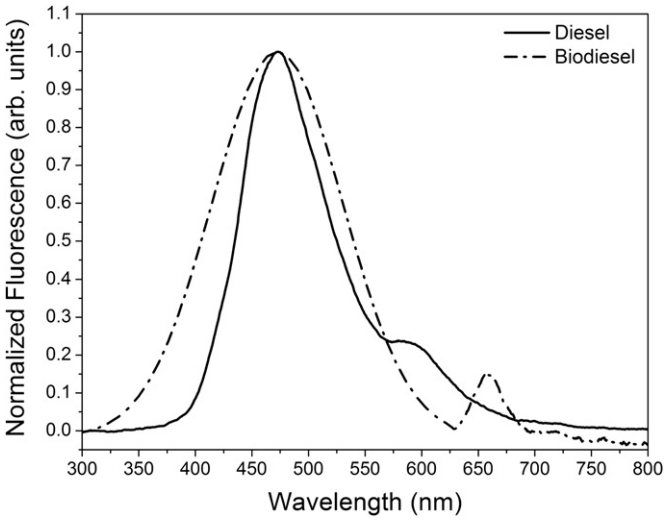

Fig. 1. Normalized fluorescence spectra of diesel and soybean biodiesel.

Fig. 2 displays an enhancement in the emission intensity of the blends as a result of the increase in the biodiesel content in the DBB. Furthermore, a linear dependence between fluorescence intensity and biodiesel content is observed, as shown in the inset of Fig. 2. As reported in Ref. [18], this fluorescence enhancement might be associated with the change in viscosity of the blend as the biodiesel content increases because an increase in the viscosity of the blend reduces, for instance, the collision frequency of the fluorophores,

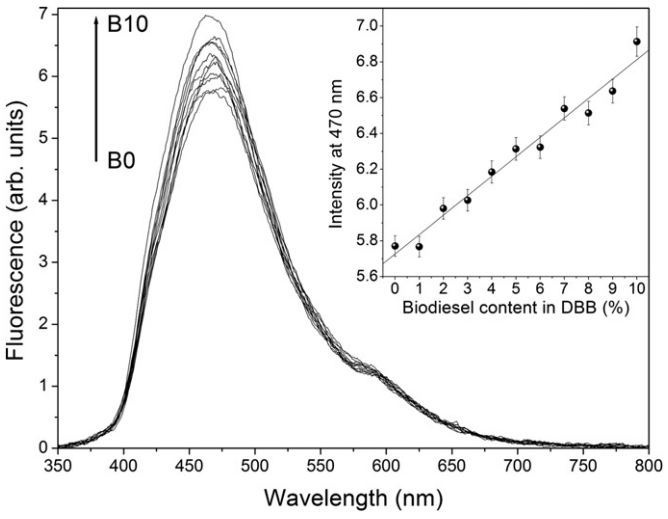

Fig. 2. Fluorescence spectra of the DBB prepared from corn biodiesel. The inset shows the fluorescence intensity at 470 nm as a function of biodiesel content in the DBB.

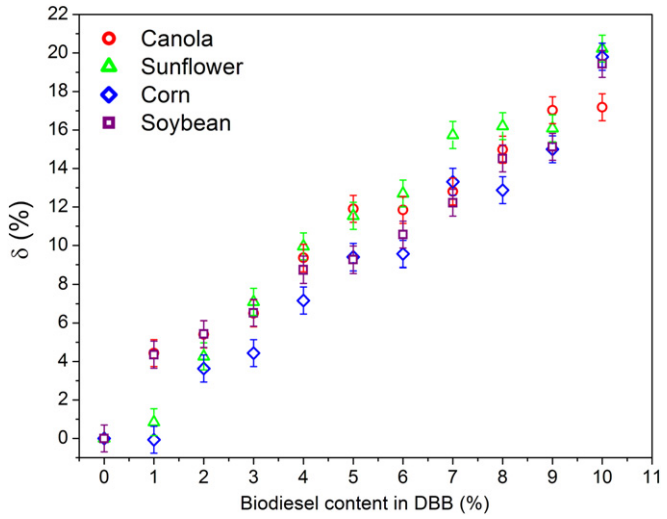

Fig. 3. δ as a function of biodiesel content in the DBB. The δ indicates the percentage variation of the fluorescence intensity at 470 nm. The error bars indicate the average deviation from the mean value.

decreasing the probability of the molecules in the excited state return to the ground state via nonradiative pathways.

To assess the applicability of the fluorescence method for quantifying the biodiesel content in different DBB, the emission intensity at 470 nm was determined for the samples of the four set of blends so that the δ parameter ($\delta = [(I - I_o)/I_o].100\%$, where I_o and I are the fluorescence intensity at 470 nm of the diesel (B0) and DBB samples, respectively) was calculated. This parameter indicates the relative change of the fluorescence intensity of each blend with respect to the fluorescence of the petroleum-derived diesel. Fig. 3 shows a similar increase of the δ with the increase in the biodiesel concentration for all blends. These data show that the addition of 10% (v/v) biodiesel to the blend yielded approximately 17–20% increase in the fluorescence intensity. A linear correlation (R^2) between fluorescence intensity and biodiesel content in DBB ratio bigger than 0.98 was determined for all DBB studied. The R^2 was 0.983, 0.984, 0.985, and 0.984 for the blend using canola, sunflower, corn, and soybean biodiesel, respectively.

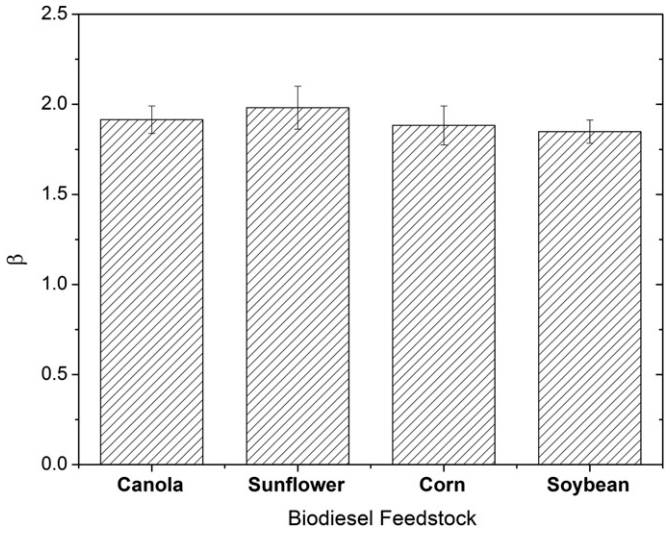

Fig. 4. Angular coefficient (β) obtained from Fig. 3.

Furthermore, Fig. 4 shows that the angular coefficients (β) are similar for all blends, where β was determined from the theoretical fit of the data shown in Fig. 3. These results show the fluorescence response of DBB was practically independent of the vegetable oil used for biodiesel preparation, although fluorescence changes in the different DBB within 2–3% of each other were observed.

4. Conclusions

In summary, the results pointed out that the DBB prepared from biodiesel produced from different vegetable oils present a similar fluorescence response as a function of biodiesel content. The finding reveals that all DBB samples exhibited an increase factor of about 17–20% in the fluorescence intensity at 470 nm when biodiesel content increased from B0 to B10. Furthermore, this enhancement of the emission intensity in the DBB was independent of biodiesel feedstock, suggesting that fluorescence spectroscopy can be successfully used to determine the biodiesel content in DBB. Therefore, the present results contribute to consolidate the fluorescence spectroscopy as a potential technique to be used as a sensitive method that allows biodiesel quantification in diesel without prior sample preparation.

Acknowledgments

We are grateful for financial support from CNPq, CAPES, and FUNDECT. The authors also acknowledge the support provided by the National Institute of Science and Technology of Optics and Photonics (INOF), and the National Institute of Science and Technology of Photonics (INFo).

References

[1] Kralova I, Sjoblom J. Biofuels-renewable energy sources: a review. J Dispersion Sci Technol 2010;31:409–25.
[2] Cheng JJ, Timilsina GR. Status and barriers of advanced biofuel technologies: a review, renew. Energy 2011;36:3541–9.
[3] Vyas AP, Verma JL, Subrahmanyam N. A review on FAME production processes. Fuel 2010;89:1–9.
[4] Xuea J, Grift TE, Hansena AC. Effect of biodiesel on engine performances and emissions. Renewable Sustainable Energy Rev 2011;15:1098–116.
[5] Ministry of Mines and Energy. Law Number 11097 (2009) and National Energy Policy Council. Resolution Number 6 (2009).
[6] Knothe G. Analyzing biodiesel: standards and other methods. J Am Oil Chem Soc 2006;83:823–33.
[7] Aliske MA, Zagonel GF, Costa BJ, Veiga W, Saul CK. Measurement of biodiesel concentration in a diesel oil mixture. Fuel 2007;86:1461–4.
[8] Guarieiro LLN, Pinto AC, Aguiar PA, Ribeiro NM. Determination of biodiesel percentage in biodiesel:diesel mixtures using mid-infrared spectroscopy. Quim Nova 2008;31:421–6.
[9] Bondioli P, Della Bella L. The evaluation of biodiesel quality in commercial blends with diesel fuel. Riv Ital Sostanze Grasse 2003;80:173–6.
[10] Foglia TA, Jones KC, Phillips JG. Determination of biodiesel and triacylglycerols in diesel fuels by LC. Chromatographia 2005;62:115–9.
[11] Kaminski M, Gilgenast E, Przyjazny A, Romanik G. Procedure for and results of simultaneous determination of aromatic hydrocarbons and fatty acid methyl esters in diesel fuels by high performance liquid chromatography. J Chromatogr 2006;A 1122:153–60.
[12] Zawadzki A, Shrestha DS, He B. Biodiesel blend level detection using ultraviolet absorption spectra. Trans ASABE 2007;50:1349–53.
[13] Pimentel MF, Ribeiro GMGS, da Cruz RS, Stragevitch L, Filho JGAP, Teixeira LSG. Determination of biodiesel content when blended with mineral diesel fuel using infrared spectroscopy and multivariate calibration. Microchem J 2006;82:201–6.
[14] Oliveira JS, Montalvao R, Daher L, Suarez PAZ, Rubim JC. Determination of methyl ester contents in biodiesel blends by FTIR-ATR and FTNIR. Talanta 2006;69:1278–84.
[15] Sastry GSR, Krishna Murthy ASR, Prasad PR, Bhuvaneswari K, Ravi PV. Identification and determination of bio-diesel in diesel. Energ Sourc Part A 2006; 28:1337–42.
[16] Birova A, Svajdlenka E, Cvengros J, Dostalikova V. Determination of the mass fraction of methyl esters in mixed fuels. Eur J Lipid Sci Technol 2002;104: 271–7.
[17] Reddy CM, Demello JA, Carmichael CA, Peacock EE, Xu L, Arey JS. Determination of biodiesel blending percentages using natural abundance

radiocarbon analysis: testing the accuracy of retail biodiesel blends. Environ Sci Technol 2008;42:2476–82.
[18] Scherer MD, Oliveira SL, Andrade LHC, Lima SM, Caires ARL. Determination of the biodiesel content in diesel/biodiesel blends: a method based on fluorescence spectroscopy. J Fluoresc 2011;21:1027–31.
[19] Zagonel GF, Peralta-Zamora P, Ramos LP. Multivariate monitoring of soybean oil ethanolysis by FTIR. Talanta 2004;63:1021–5.
[20] Borges ME, Diaz L, Gavin J, Brito A. Estimation of the content of fatty acid methyl esters (FAME) in biodiesel samples from dynamic viscosity measurements. Fuel Process Tech 2011;92:597–9.

Ampliando a visão bucal com fluorescência óptica

Recebido em: Abr/13
Aprovado em: Mai/13

Hérica Adad Ricci
Doutora em Ciências Odontológicas pela Faculdade de Odontologia de Araraquara-FOAr-UNESP. Pós-doutoranda do Grupo de Óptica do Instituto de Física de São Carlos, IFSC-USP, São Carlos, Brasil.

Sebastião Pratavieira
Mestre em Física Aplicada - Doutorando no Laboratório de Biofotônica - Grupo de Óptica do Instituto de Física de São Carlos, IFSC-USP, São Carlos, Brasil.

Aldo Brugnera Júnior
Doutor em Clinicas Odontológicas pela Universidade Federal do Rio de Janeiro, UFRJ. - Professor Doutor da Pós-graduação da Universidade Camilo Castelo Branco, Parque Tecnológico, São Jose dos Campos, Brasil.

Vanderlei Salvador Bagnato
Doutor em Física - Professor titular do Grupo de Óptica do Instituto de Física de São Carlos, IFSC-USP, São Carlos, Brasil.

Cristina Kurachi
Doutora em Ciências e Engenharia de Materiais – Professora Doutora do Grupo de Óptica do Instituto de Física de São Carlos, IFSC-USP, São Carlos, Brasil.

Autor para correspondência:
Hérica Adad Ricci
Universidade de São Paulo - Campus de São Carlos
Av. Trabalhador São-carlense, 400
Arnold Schimidt - São Carlos - São Paulo
13566-590
Brasil
hericaricci@yahoo.com.br

Improving the oral screening with optical fluorescence

RESUMO

A fluorescência óptica pode ser utilizada como um coadjuvante ao exame clínico bucal, uma vez que permite, por autofluorescência, a detecção de inúmeras alterações na cavidade bucal que poderiam passar despercebidas pelo cirurgião-dentista ou até mesmo de difícil percepção apenas pelo método visual. O objetivo do presente estudo foi demonstrar o uso do sistema de fluorescência óptica por imagem no diagnóstico de diferentes lesões da cavidade bucal, seja em tecido duro ou mole, de forma a familiarizar o cirurgião-dentista com o uso do equipamento. Para este estudo foi utilizado um equipamento constituído de um diodo emissor de luz (LED), com emissão na região do violeta e um conjunto de filtros ópticos (Evince - MMoptics, São Carlos, SP, Brasil). Para a aquisição das imagens foi acoplado ao equipamento uma câmera fotográfica (Nikon, D90, Bangkok, Tailândia) com o auxílio de um adaptador. O sistema de fluorescência bucal possibilitou observar alterações nos tecidos duros dentais como manchas, presença de placa e cálculo dental, lesões incipientes e infiltrações marginais, além de facilitar a diferenciação entre materiais restauradores como resina composta e cerâmica. Em tecidos moles foi possível detectar lesões potencialmente malignas e lesões tumorais. Portanto, pode-se concluir que o sistema de fluorescência óptica permite ao cirurgião-dentista diagnosticar e identificar estruturas e alterações na cavidade bucal de forma simples, não invasiva e em tempo real revelando lesões que não seriam facilmente detectados com a iluminação convencional.

Descritores: Fluorescência; Diagnóstico Bucal; Cavidade Oral

ABSTRACT

Fluorescence techniques can be used as an adjunct to clinical examination of the mouth, detecting tissue changes in oral mucosa or hard dental tissues, which might be unnoticed by the dentist or even difficult to detect under white light examination. The aim of this study was to demonstrate the use of wide-field fluorescence imaging in the diagnosis of various lesions of the oral cavity, either in hard or soft tissues, in order to familiarize the dentist with the use of the equipment. For this study we used an optical fluorescence system with emission in the violet region (Evince, MMOptics, São Carlos, SP, Brazil). For image acquisition, the fluorescence system was coupled to a digital camera (Nikon D90, Nikon, Bangkok, Tailândia). With the fluorescence system was possible to observe changes in hard dental tissues such as bright spots, dental plaque and calculus, incipient carious and marginal microleakage lesions. The system also facilitated the differentiation between restorative materials such as composite resin and ceramic. The fluorescence optical was also helpful in screening and detection of potentially malignant lesions and tumors could be observed. Therefore, we conclude that the fluorescence optical system allows the dentist to identify structures and alterations in the oral cavity in a simple, noninvasive, and in real-time procedure, revealing injuries that would not be easily detected with conventional illumination.

Descriptors: Fluorescence; Oral Diagnostics; Mouth

RELEVÂNCIA CLÍNICA

Neste trabalho sumarizamos diferentes situações clínicas onde imagens de fluorescência óptica auxiliam no diagnóstico, possibilitando uma melhor visualização de lesões da cavidade bucal, tornando-se um coadjuvante ao exame clínico bucal.

INTRODUÇÃO

Rotineiramente, no consultório odontológico, para o diagnóstico de lesões nas estruturas dentárias ou nos tecidos moles adjacentes, o cirurgião-dentista utiliza-se de uma boa anamnese, sendo considerado um ponto inicial no diagnóstico de uma doença, no qual o paciente é questionado de forma a discutir fatos que se relacionam com a doença. Em seguida, realiza-se exame físico intra e/ou extraoral, buscando-se através da inspeção visual os sinais e sintomas relacionados à queixa do paciente. Por fim, quando necessário, são solicitados exames complementares, no qual o exame radiográfico é essencial para suporte nas decisões diagnósticas de tecidos duros enquanto que o exame histopatológico (biópsias) é para os tecidos moles[1].

No entanto, em determinadas situações clínicas, o uso de exames complementares só permitem confirmações de diagnóstico quando a alteração tecidual já se encontra em estado considerado avançado, como é o caso de cáries incipientes, que não são visualizadas no exame radiográfico. No caso de lesões na mucosa bucal, onde é necessária a biópsia, este diagnóstico tende a ser mais tardio, pois a biópsia é um exame invasivo, embora indispensável. Além de ser um método invasivo, a biópsia não é realizada com frequência no consultório. Com isso, a maioria dos casos de lesões na mucosa é identificada já em fase avançada, apresentando alta mortalidade. No entanto, a detecção precoce de áreas displásicas e/ou neoplásicas aumenta significantemente as chances de sucesso do tratamento, assim como diminui a morbidade associada. Segundo dados do Instituto Nacional de Câncer (INCA), em 2012, aproximadamente 14.000 novos casos de câncer bucal foram diagnosticados no Brasil[2].

Atualmente, é cada vez maior o uso de técnicas modernas para auxílio do dentista no diagnóstico preventivo, especialmente de lesões em estágios iniciais, seja em tecidos duros ou moles da cavidade bucal. Dentre os métodos existentes, temos os mais caros e complexos como o raio-x digital e a tomografia computadorizada[3]. No entanto, outros métodos mais simples e capazes de serem utilizados diretamente pelo profissional da Odontologia podem auxiliar enormemente, e nesse sentido os sistemas de imagem de fluorescência óptica ganham destaque[4-6].

Fluorescência óptica é um fenômeno físico que ocorre em determinadas moléculas, denominadas fluoróforos. Várias moléculas que compõem nosso organismo são fluoróforos naturais. Os fluoróforos ao serem excitados por luz, ou seja, iluminados, absorvem a energia e depois emitem energia também na forma de luz, porém com uma cor diferente[7]. Um tecido sadio apresenta uma determinada fluorescência característica, porém ao sofrer uma alteração sua fluorescência natural se altera. Dessa forma, durante o desenvolvimento de uma lesão, os fluoróforos se alteram, mudam de concentração e de distribuição e, consequentemente, a fluorescência do tecido se altera[4,7-9].

Deste modo, ao realizar os procedimentos de rotina num paciente, a fluorescência pode ser usada pelo dentista para detectar possíveis alterações na cavidade bucal que não seriam facilmente detectadas com a iluminação convencional por aumentar o contraste de visualização dos tecidos alterados. Assim, além de detectar lesões pré-malignas e tumores malignos, essa técnica permite ao cirurgião-dentista detectar placa bacteriana, cálculo dental, lesões incipientes, desmineralização do esmalte dental, microtrincas, infiltrações marginais, e ainda auxilia na diferenciação de materiais restauradores estéticos como resina composta e cerâmica.

O presente trabalho teve como objetivo demonstrar o uso do sistema de fluorescência óptica por imagem no diagnóstico. Exemplos de diferentes lesões da cavidade bucal serão apresentados de forma a familiarizar o cirurgião-dentista com o uso dessa nova tecnologia disponível para auxiliar o exame clínico.

RELATOS DE CASOS CLÍNICOS

Para a visualização por fluorescência dos tecidos da cavidade bucal utilizou-se o sistema de imagem de campo amplo por fluorescência óptica EVINCE (MMOptics, São Carlos, SP, Brasil). O sistema é basicamente composto por arranjo de LEDs (Diodos Emissores de Luz), emitindo na região violeta-azul do espectro eletromagnético, e por um conjunto de filtros ópticos que permitem a visualização da fluorescência. Todo este conjunto forma uma peça de mão, por meio da qual é feita a observação direta da fluorescência no visor. O equipamento apresenta três níveis de irradiância (intensidade) de iluminação: alto, médio e baixo.

Para a aquisição das imagens foi acoplada ao equipamento uma câmera fotográfica digital Nikon D90 (Nikon, Bangkok, Tailândia) com o auxílio de um adaptador rosqueável, confecionado especialmente para este estudo.

Para comparação, imagens da mesma área foram capturadas com a iluminação convencional (luz ambiente) e, em seguida, uma imagem de fluorescência foi capturada com o sistema de fluorescência óptica.

Para a documentação de lesões pré-malignas e tumores malignos, os critérios de inclusão foram idade superior a 18 anos e inferior a 80 anos, com encaminhamento odontológico e/ou médico para avaliação no ambulatório de cabeça e pescoço do Hospital Fundação Amaral Carvalho (Jaú, SP, Brasil), por apresentarem suspeita de displasias e/ou neoplasias na região de cabeça e pescoço. Esses pacientes, em torno de 80, foram atendidos pela equipe médica local, sendo que apenas os casos restritos a lesões na cavidade bucal foram documentados, atingindo cerca de 10 casos, dos quais cinco estão descritos no presente estudo. A documentação dos casos de Dentística seguiram os mesmos critérios de inclusão quanto à idade e gênero acima referidos, porém apenas com finalidade de exame clínico rotineiro, sendo atendidos cerca de 30 estudantes pertencentes ao Instituto de Física de São Carlos – USP, dos quais cinco foram selecionados para documentação neste estudo. Todos os participantes autorizaram a publicação das imagens do caso.

Nas figuras de 1 a 4 são mostradas as imagens de luz branca e de fluorescência para diferentes situações clínicas envolvendo os

FIGURA 1A
Coroa de cerâmica no dente 21 (luz branca)

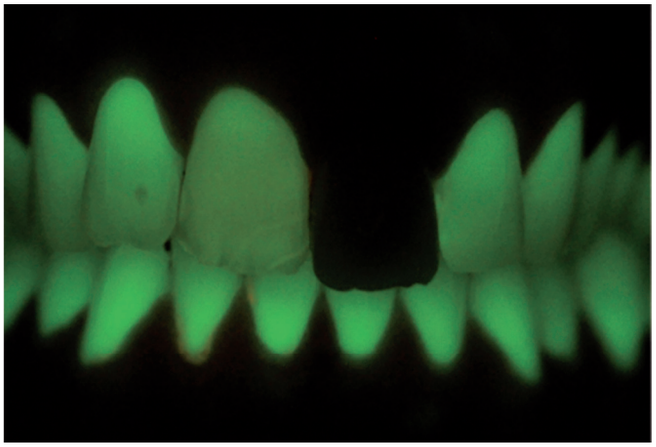

FIGURA 1B
Coroa de cerâmica no dente 21 (imagem por fluorescência)

FIGURA 2A
Restauração de resina composta (dente 46) e coroa de cerâmica (dente 47) (luz branca)

FIGURA 2B
Restauração de resina composta (dente 46) e coroa de cerâmica (dente 47) (imagem por flourescência)

FIGURA 3A
Placa e cálculo nos dentes anteriores inferiores (luz branca)

FIGURA 3B
Placa e cálculo nos dentes anteriores inferiores (imagem por fluorescência)

FIGURA 4A
Lesão incipiente em esmalte dental nos dentes 37 e 38 (luz branca)

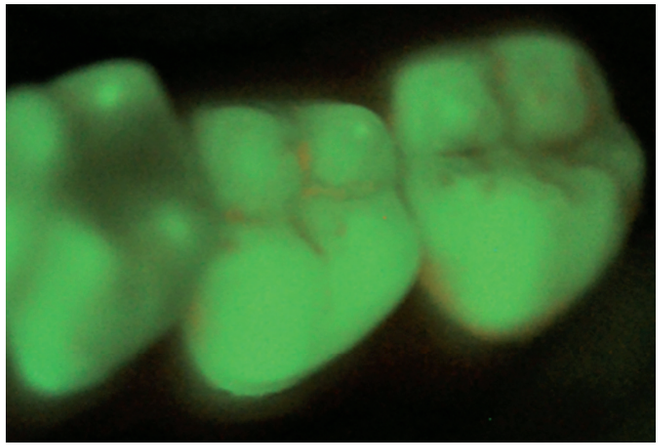

FIGURA 4B
Lesão incipiente em esmalte dental nos dentes 37 e 38 (imagem por fluorescência)

FIGURA 5A
Carcinoma basocelular com extensão para o lábio superior (luz branca)

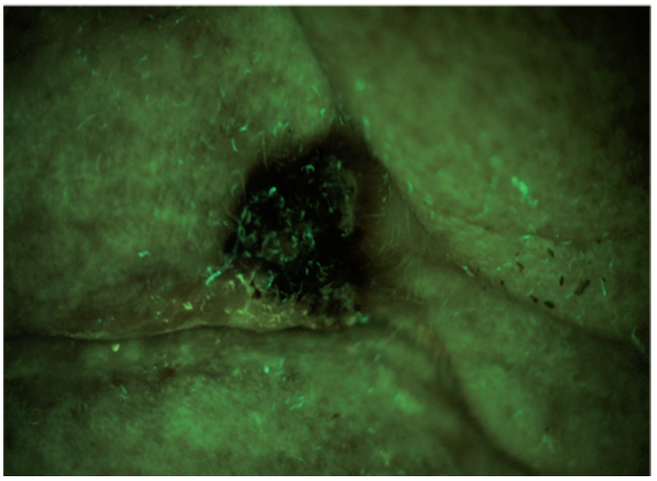

FIGURA 5B
Carcinoma basocelular com extensão para o lábio superior (imagem por fluorescência)

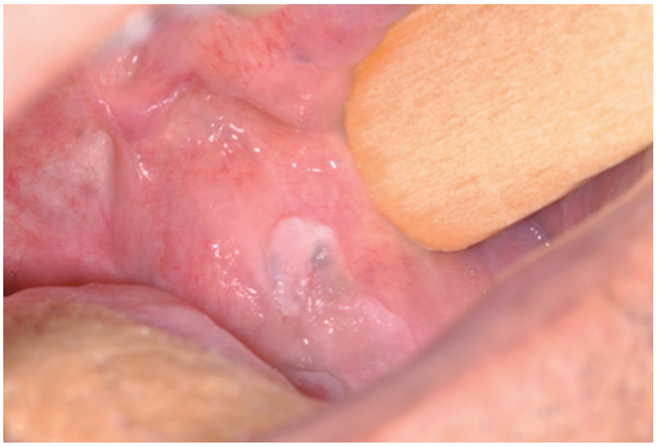

FIGURA 6A
Carcinoma espinocelular na região retromolar, lado esquerdo (luz branca)

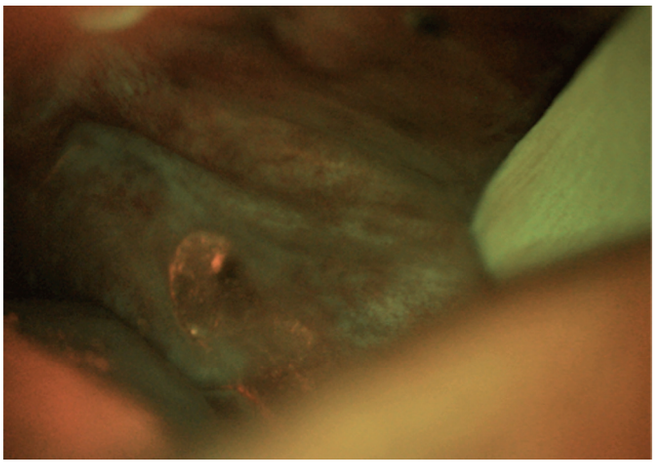

FIGURA 6B
Carcinoma espinocelular na região retromolar,
lado esquerdo (imagem por fluorescência)

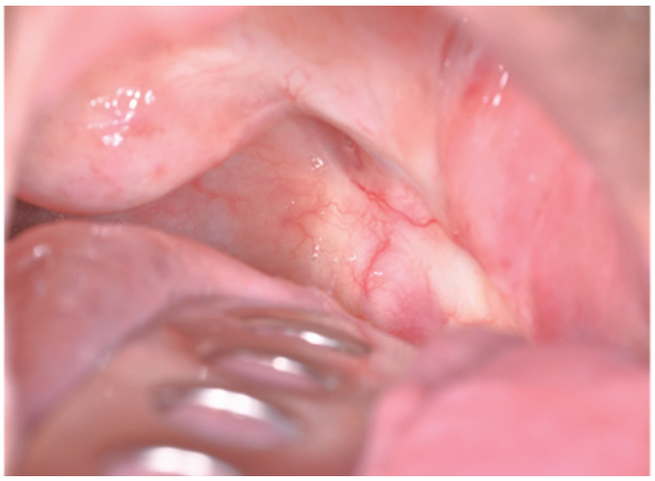

FIGURA 7A
Carcinoma espinocelular já tratado, na região de orofaringe, lado esquerdo, com áreas de fibrose (luz branca)

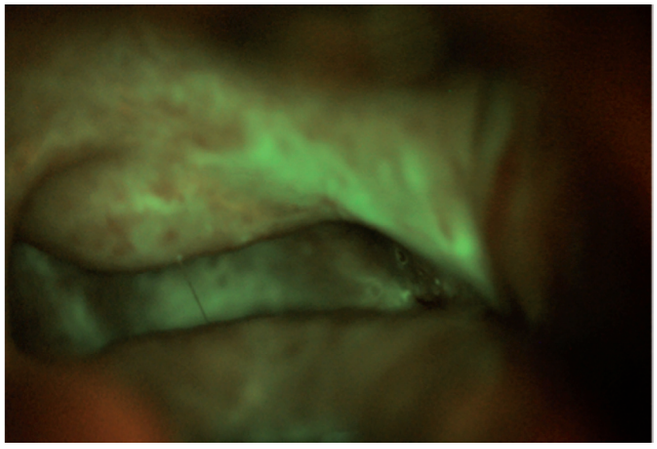

FIGURA 7B
Carcinoma espinocelular já tratado, na região de orofaringe, lado esquerdo, com áreas de fibrose (imagem por fluorescência)

FIGURA 8A
Lesão potencialmente maligna no lábio inferior (luz branca)

FIGURA 8B
Lesão potencialmente maligna no lábio inferior (imagem por fluorescência)

tecidos duros dentais. Enquanto que nas figuras de 5 a 8 apresentamos casos clínicos na mucosa bucal e lábios.

Para se obter um campo adequado de visualização de mucosa bucal por fluorescência é necessário um ambiente com pouca ou ausência de luz ambiente, pois somente a fluorescência do tecido deve ser observada, aumentando o contraste entre região normal e alterada. Outro fator importante para que se obtenha um bom sinal de fluorescência é que a fonte de luz emitida pelo equipamento tenha intensidade suficiente para atingir a superfície do tecido alvo. Os melhores resultados obtidos para estruturas dentárias foram com a menor intensidade de luz, o que já era suficiente para uma boa visualização, e a uma distância aproximada de 10cm. Enquanto que para os tecidos adjacentes foi necessário a intensidade máxima de emissão de luz, mantendo a mesma distância, em determinados casos de envolvimento de áreas posteriores uma distância menor foi exigida para melhor visualização.

Além disso, durante o exame bucal com equipamentos de fluorescência, é indispensável fornecer aos pacientes óculos de proteção específico com a função de evitar a exposição direta à luz, por ser considerada prejudicial ao olho humano. Quanto ao cirurgião-dentista, é dispensado o uso de tais óculos uma vez que a luz deve ser observada exclusivamente através do visor do equipamento.

DISCUSSÃO

Fluorescência é um fenômeno óptico que ocorre em diversos materiais, inclusive partes do corpo humano, como por exemplo: dente e mucosa bucal. A fluorescência é a emissão de luz por parte de um material ou tecido biológico. E cada material tem sua fluorescência característica. Por ser uma técnica com resposta imediata, a visualização é em tempo real, e não invasiva. Isso possibilitou observar alterações nos tecidos duros dentais como manchas, presença de placa, cálculo dental, lesões incipientes e infiltrações marginais, além de facilitar a diferenciação entre materiais restauradores como resina composta e cerâmica[7,8].

Com relação aos tecidos duros dentais, como mostrado nas figuras 1A e 1B, pode ser facilmente visualizada a fluorescência normal dos dentes e também ausência da fluorescência da coroa total em cerâmica no dente 21. Enquanto que nas figuras 2A e 2B, pode ser feita a diferenciação entre resina composta (dente 46) e a coroa de cerâmica (dente 47).

Essa diferença da fluorescência entre os diferentes materiais restauradores facilita a identificação e, consequentemente, a remoção restrita desses materiais. Desta forma, durante a troca de material restaurador o clínico consegue fazer uma remoção seletiva do material a ser trocado, preservando a estrutura dental sadia.

Em determinadas especialidades, como em ortodontia, após a finalização do tratamento, além do descolamento dos braquetes, é imprescindível a remoção completa dos resíduos do material resinoso, utilizado para colagem, da superfície do esmalte dental. Como a grande maioria das resinas compostas apresentam-se com alta fluorescência frente à excitação pela luz violeta, é permitido ao cirurgião-dentista diferenciar com facilidade áreas que ainda apresentam tais resíduos e desta forma fazer uma remoção adequada e completa, preservando ao máximo a estrutura dental.

Outra situação muito frequente é a presença de placa bacteriana, cálculo dental e lesões incipientes em esmalte dental. A presença de bactérias nessas áreas resulta na produção de porfirinas, substância produzida durante o metabolismo bacteriano. A porfirina, quando excitada pela luz violeta, emite fluorescência na cor alaranjada-vermelha[8,9]. Desta forma, as situação clínicas acima referidas podem ser facilmente detectadas pelo cirurgião-dentista frente à intensidade da coloração vermelha. Na figura 3B, representativa da imagem de fluorescência da figura 3A, placa bacteriana e áreas associadas com cálculo dental foram visualizadas pela fluorescência na coloração vermelha. Nos casos de placa bacteriana, alerta o cirurgião sobre áreas que o paciente está apresentando dificuldade de higienização adequada, já nos casos de cálculo dental, esta visualização auxiliará o dentista na remoção do mesmo. A motivação do paciente para os procedimentos de higienização também poderá ser melhor implementada, pois o paciente facilmente visualizará as áreas críticas e o resultado após uma efetiva higienização. Nas figuras 4A e 4B, são apresentadas lesões incipientes no esmalte dental dos elementos 37 e 38. Este tipo de lesão não é visualizado facilmente com luz branca, tornando-se uma área de alerta para um tratamento preventivo e/ou minimamente invasivo, tornando os procedimentos de Dentística menos restaurativos e mais preventivos e terapêuticos.

Em relação aos tecidos moles, o tecido bucal normal ao ser excitado com luz violeta emite uma luz em tom esverdeado. No entanto, quando há alguma alteração tecidual, essa característica também se altera. Em um tecido neoplásico geralmente ocorre diminuição da fluorescência, visualizada pelo equipamento como uma área mais escurecida, conforme ilustrado nas figuras 5A e 5B, um caso de carcinoma basocelular que se estendeu para o lábio superior.

As figuras 6A e 6B representam um caso diagnosticado, por biópsia, de carcinoma espinocelular na região retromolar, sendo importante ressaltar que a lesão estava associada ao uso de prótese. Na região alterada observamos uma diminuição da fluorescência verde natural do tecido, ainda acompanhada por pontos vermelhos de fluorescência que indicam a presença de microrganismos, fato comumente associado às lesões teciduais[7-9]. Vale ressaltar que as lesões inflamatórias apresentam também uma menor emissão de fluorescência verde, sendo que o clínico deve associar o exame clínico e histopatológico à visualização da fluorescência no seu diagnóstico final. A menor intensidade de fluorescência visualizada ocorre em função da maior quantidade de hemoglobina, principal biomolécula absorvedora presente no tecido inflamado.

Em alguns casos, onde há uma maior queratinização ou fibrose tecidual, geralmente ocorre um aumento da fluorescência na região verde, como nas figuras 7A e 7B. O paciente apresentava quadro de carcinoma espinocelular na região de palato mole estendendo-se para orofaringe, porém, quando foi feita a avaliação, ele já havia sido submetido ao tratamento cirúrgico apresentando área fibrosada, representada pela coloração verde mais intensa. Além disso, as ausências de áreas escurecidas permitiram confirmar o achado histopatológico de qualquer nova alteração.

Além do auxílio na detecção de lesões tumorais, também foi possível detectar lesões potencialmente malignas, como a lesão de lábio inferior apresentada nas figuras 8A e 8B, que teve maior evidenciação da sua extensão quando utilizado a fluorescência. Isso reforça o fato de que a técnica de imagem por fluorescência pode auxiliar o profissional na escolha de área adequada para a realização da biópsia, que nesse caso correspondeu não à área esbranquiçada visualizada na luz branca convencional, mas sim à área escura adjacente. A visualização da imagem também pode ser útil durante um procedimento cirúrgico para delimitação das bordas de uma lesão.

Com isso, foi demonstrado o grande potencial da fluorescência óptica no auxílio à detecção e distinção de lesões bucais, seja em tecidos duros ou moles. É importante também ressaltar a existência de vários outros equipamentos similares disponíveis no mercado. Neste estudo, utilizamos o EVINCE (MMOptics, São Carlos, SP, Brasil) como exemplo de sistema de fluorescência. Existem outros mais específicos somente para o diagnóstico de cárie, tais como: Inspektor Pro QLF (Inspektor Research Systems BV, Amsterdam, Holanda), VistaCam iX e/ou Vista- Proof (Dürr Dental, Bietigheim-Bissingen, Alemanha), Spectra (Air Techniques, Melville, NY, Estados Unidos) e o DIAGNOdent e/ou DIAGNOdent pen (KaVo, Biberach, Alemanha). Alguns destes equipamentos possuem softwares específicos para o auxílio neste diagnóstico[10-12]. Para o diagnóstico de lesões no tecido mole, podemos também citar o VELscope e/ou VELscope Vx (LED Dental, Burnaby, BC, Canadá), e o Identafi 3000 (Trimira LLC, Houston, Texas) que, além da fluorescência, usa diferentes cores para iluminar e analisar uma lesão suspeita[13,14]. Diversos estudos utilizando esses sistemas demostram igualmente a grande capacidade de imagens de fluorescência no auxílio ao profissional da odontologia.

CONCLUSÃO

Os exemplos mostrados neste trabalho demonstram a grande utilidade de imagens de fluorescência, sendo considerado um mé-

todo complementar ao exame clínico convencional realizado no consultório odontológico.

Concluímos que o sistema de fluorescência óptica permite ao cirurgião-dentista diagnosticar e identificar estruturas e alterações na cavidade bucal de forma simples, não invasiva e em tempo real, revelando lesões que não seriam facilmente detectados com a inspeção usando luz branca.

APLICAÇÃO CLÍNICA

O emprego da técnica de fluorescência óptica como método complementar, durante o exame clínico odontológico, é uma técnica recomendável na prática clínica por possibilitar, de maneira simples e eficaz, uma melhor visualização das alterações dos tecidos duros e moles bucais.

AGRADECIMENTOS

Agradecemos o apoio financeiro da Fapesp, CNPq e Capes. A Fapesp através do projeto CEPID - CePOF e bolsas de estudo. CNPq e Capes pelo projeto INCT – INOF e bolsas de estudo. Agradecemos o apoio clínico da cirurgiã-dentista Priscila Delamano Criado.

REFERÊNCIAS

1. Baptista Neto C. Exame clínico: anamnsese. Publicado em: Revista da APCD de São Caetano do Sul - Espelho Clínico; Ano IX, Nº50, p. 10-11, Jun 2005. Disponível em: <http://estomatologia-artigos.blogspot.com.br/2006/03/exame-clnico anamnese.html>
2. Inca –Instituto Nacional do Câncer. Rio de Janeiro, 2012. Estimativa 2012. Disponível em: Maio de 2013.
3. Kherlopian AR, Song T, Duan Q, Neimark MA, Po MJ, Gohagan JK. A Review Of Imaging Techniques For Systems Biology. BMC Syst Biol 2008; 2:74.
4. Roblyer D, Kurachi C, El-Naggar et al. Multispectral optical imaging device for in vivo detection of oral neoplasia. J Biom Optics. 2008; 13: 024019.
5. Araújo GS, Costa MM, Pereira LPC, Kurachi C, Bagnato VS. Dental Science Clínica e Pesquisa Integrada 2011; 5(13): 46-52.
6. Carvalho MT, Fernandes IQ, Pizelli HE, Chianfrone DJ, Ribeiro FMM, Bagnato VS. Tecnologias emergentes para laserterapia, terapia fotodinâmica e fotodiagnósticos aplicados à Odontologia. Rev Implantnews 2012; 9(1a): 68-74.
7. Pratavieira S, Andrade CT, Cosci A, Kurachi C. Diagnóstico óptico em Odontologia. Rev Implantnews 2012; 9(1a): 20-3.
8. Roblyer D, Kurachi C, Stepanek V, Williams MD, El-Naggar AK, Lee JJ et al. Objective detection and delineation of oral neoplasia using autofluorescence imaging. Cancer Prev Res. 2009; 2 (5): 423-431.
9. Betz CS, Mahlmann M, Rick K, Stepp H, Grevers G, Baumgartner R et al. Autofluorescence imaging and spectroscopy of normal and malignant mucosa in patients with head and neck cancer. Laser Surg. Med 1999; 25(4): 323-34.
10. Gomez J, Zakian C, Salsone S, Pinto SC, Taylor A, Pretty IA et al. In vitro performance of different methods in detecting occlusal caries lesions. J Dent. 2013; 41 (2): 180 -6.
11. Jablonski-Momeni A, Liebegall F, Stoll R, Heinzel-Gutenbrunner M, Pieper K. Performance of a new fluorescence camera for detection of occlusal caries in vitro. Lasers Med Sci. 2013; 28(1): 101-9.
12. Pretty IA. Caries detection and diagnosis: novel technologies. J Dent. 2006; 34(10): 727-39.
13. Patton LL, Epstein JB, Kerr AR. Adjunctive techniques for oral cancer examination and lesion diagnosis: a systematic review of the literature. J Am Dent Assoc. 2008; 139(7): 896-905.
14. Lane P, Follen M, MacAulay C. Has fluorescence spectroscopy some of age? A case series of oral precancers and cancers using white light, fluorescent light at 405 nm, and reflected light at 545 nm using the Trimira Identafi 3000. Gend Med. 2012; 9(1): S25-35.

ELSEVIER

Evaluation by Fluorescence Spectroscopy of the Most Appropriate Renal Region for Obtaining Biopsies: A Study in the Rat

M.F. Cassini, M.M. da Costa, V.S. Bagnato, L.F. Tirapelli, G.E.B. Silva, A.C.P. Martins, and S. Tuccl Jr

ABSTRACT

Introduction. Renal puncture biopsies are directed at the lower poles of the organ to decrease the risk of hemorrhage and complications.

Objectives. To evaluate by fluorescence spectroscopy (FS) the most appropriate renal region (in terms of metabolic changes) to obtain a biopsy.

Materials and methods. The kidneys of 33 *Rattus norvegicus* rats were submitted to FS detection in the upper and lower poles and in the middle third. Excitations were generated with lasers at wavelengths of 408, 442, and 532 nm. Animals were divided at random into groups of warm ischemia (30, 60, and 120 minutes), whose kidneys were again analyzed by FS, as well as after 5 minutes of reperfusion using the same excitation beams in the same renal regions. Then the kidneys underwent histologic preparation and examination.

Results. The middle third area of the rat's kidneys proved to be significantly more sensitive to ischemic and reperfusion changes than the renal poles, as determined by FS ($P < .001$).

Conclusions. The middle third of the kidney was the most appropriate site for a renal biopsy to monitor a transplanted organ.

RENAL TRANSPLANTATION is the best treatment for patients who require replacement therapy.[1] During the post-transplant period, an inappropriate clinical evolution, a delayed recovery of function, or suspicion of acute rejection indicate the need for a graft biopsy. In general, renal puncture or open surgery biopsies are directed at the poles (especially the lower one) of the organ because of the reduced risk of hemorrhage or other complications due to the procedure. The renal poles are believed to have less exuberant vascularization, presenting a lower risk of bleeding and a greater sensitivity to ischemic injury. When no acute tubular necrosis (ATN) is present in the poles, ATN is not considered to be present in the other regions. Similarly, the absence of signs of acute rejection in a polar biopsy reassures the medical team regarding the organ as a whole.[2]

Fluorescence spectroscopy measures changes in tissues by quantitating differences in spectral properties. Biological tissues can absorb, emit, and dissipate light at various wavelengths. The measurements can be performed rapidly with no manipulation of the organ, in contrast to a biopsy, which provides only a static, focal evaluation. Evaluations by fluorescence spectroscopy do not suffer interference by methods of hypothermic preservation because they do not involve enzymatic activities. Photodetection by fluorescence offers an alternative technique to differentiate biological tissues, not only for the diagnosis of tumors, but also for the investigation of changes in the metabolic status of cells.[3–7]

When a material is photo-excited, the energy received in the form of photons causes electrons to be transferred from a layer of lower to a layer of higher energy. This state is unstable and the excited electrons will decay, soon returning to the layer of lower energy and releasing the excess energy. One of the permitted forms of the decay process is a radioactive phenomenon called fluorescence (ie, the re-emission of photons).[8–10]

Fluorescence spectroscopy is based on the detection of photons emitted by fluorescent species when excited from a source of photons of well-known energy, usually the laser

From the Division of Urology, Department of Surgery and Anatomy, Ribeirao Preto Medical School, University of Sao Paulo, Brazil.

Address reprint requests to Marcelo Ferreira Cassini, PhD, MD, Division of Urology, Department of Surgery and Anatomy, Ribeirao Preto Medical School, University of Sao Paulo (USP), Av. dos Bandeirantes 3900–Monte Alegre, Ribeirao Preto, Sao Paulo, Brazil 14.049-900. E-mail: marcelo.cassini@globo.com

0041-1345/–see front matter
http://dx.doi.org/10.1016/j.transproceed.2013.01.059

due to one of its main properties (ie, monochromaticity, the characteristic of a source that emits photons of well-determined wavelength). Biological tissues contain enormous amounts of chromophores, molecules that interact differently with light. Three main types of chromophores are present in tissues: fluorophores (chemical groups that can convert the light absorbed to fluorescence—tryptophan and structural proteins, for example); absorbers (chemical groups that absorb light and do not produce fluorescence—hemoglobin, for example), and scatterers (structures that alter the direction of the incident photon but conserve its energy such as the refraction gradient between the intra- and extracellular environments).

In the presence of metabolic changes, such as acidosis, that increase or reduce deoxyhemoglobin or cell structure changes, there is an early modification of the characteristics of tissue fluorescence. Thus spectroscopy may be more sensitive than histologically observed by standard light microscopy.

The objective of the present study was use fluorescence spectroscopy (FS) to assess the most appropriate renal region, to obtain a renal biopsy.

MATERIALS AND METHODS

Thirty-three adult male albino Wistar rats (*Rattus norvegicus*) weighing 200 to 250 g were anesthetized by an intraperitoneal injection of thiopental (20 Un/100 g weight) before a median longitudinal laparotomy to reach the left kidney. The 33 kidneys first underwent FS detection (control group) of the cortex. The laser tip was placed on the upper and lower poles and the middle third of the kidney. Excitations were generated with laser beams of 408-, 442-, and 532-nm wavelengths. The renal vascular pedicles were then dissected, isolated, and occluded with a vascular mini-clamp. The animals were then divided randomly into groups subjected to warm ischemia for 30, 60, or 120 minutes (groups 1, 2, and 3), respectively. During the specific ischemic period the kidneys underwent cortical readings in the upper and lower poles and in the middle third using excitation laser beams of the same wavelengths (408, 442, and 532 nm). New readings were obtained after 5 minutes of complete reperfusion using the same excitation lasers in the same renal regions. The animals were observed for the presence of a renal artery pulse, patency of the renal vein and complete, uniform reperfusion of the kidney with a return to the initial color. The left kidneys then were processed for histologic studies.

Four animals were selected at random for a contralateral nephrectomy. The excised kidneys were used for histologic study; their warm ischemia time was 0.

The study followed the norms of the Brazilian College of Animal Experimentation and was approved by our Ethics Committee (protocol no. 041–2010).

Histologic and Statistical Analysis

After staining with hematoxylin and eosin or Masson trichrome, ischemic injuries of proximal tubular cells were classified according to the grading proposed by Goujon et al.[11,12] This method is based on seven basic morphologic patterns typical of proximal tubular lesions: vacuolization of the apical cytoplasm, tubular necrosis, tubular dilatation, cell detachment, brush border integrity, intracellular edema, and basement membrane denudation, using a 5-point scale: 1 (no abnormality), 2 (mild injuries to 10%), 3 (10% to 25% tissue), 4 (25% to 50%), 5 (more than 50%).

Light-View-Med (LVM.exe) software was used to acquire spectroscopy data, together with the Origin-Lab (8.lnk) software to produce and store the graphs.

The statistical analysis was performed using the GraphPad PRISM software, version 4.0 (GraphPad Software Inc, San Diego, Calif, USA). Continuous variables were compared by the nonparametric Kruskal-Wallis test followed by the Dunn multiple comparisons post-test, associations between parameters were analyzed by linear regression. One-way analysis of variance was used to evaluate renal damage, examining correlation coefficients with multiple comparisons analyzed after Bonferroni post-tests. The level of significance was set at $P < 0.05$.

RESULTS

To validate the fluorescence spectroscopy method, we first analyzed the mean graphic readings obtained during autofluorescence, ischemia, and renal reperfusion (Fig 1). The post hoc Bonferroni test revealed a significantly higher mean result of autofluorescence ($P < .001$) than ischemia or reperfusion. The reperfusion phase, in turn, showed a significantly higher mean result compared with the ischemic phase.

Next, we calculated the correlation between ischemia time and fluorescence data. With increasing ischemic time (for example, from 30 to 60 minutes), there was a significant fall in the peaks of the curves during reperfusion. The fall was more significant the longer the ischemia (Fig 2).

A correlation coefficient calculated to assess the relation between histologic grading and ischemia time was positive of high magnitude ($r = 0.81$), that is, the longer the ischemia time, the greater the ischemic injury by histologic grading (Table 1).

The fluorescence laser reading obtained using spectroscopy of three renal regions (upper and lower poles and

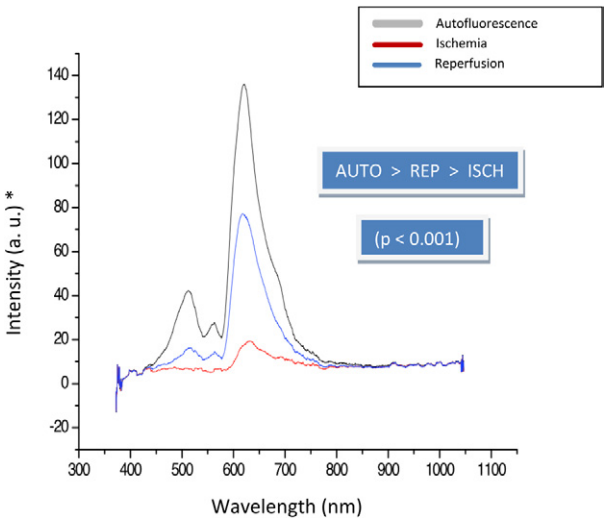

Fig 1. Mean renal fluorescence values obtained—autofluorescence (AUTO). ischemia (ISCH), and reperfusion (REP)—regardless of the laser excitation wavelength. (*a.u., arbitrary unity).

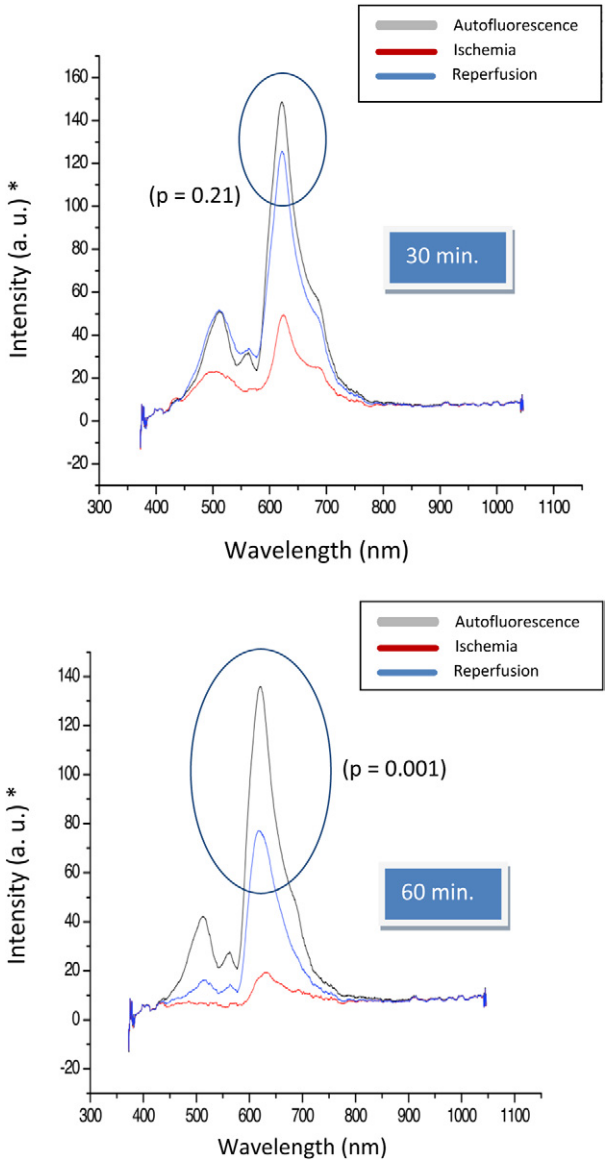

Fig 2. Reperfusion curve showing a significant decrease with an increased of the ischemia time from 30 to 60 minutes, compared with the control curve (autofluorescence). a.u., arbitrary unity.

middle third) were analyzed to determine the most reliable sector (Table 2). The post hoc Bonferroni test revealed a significant difference: the renal middle third showed a

Table 1. Correlation Between Ischemia Time and Histologic Graduation

Histological graduation	Correlation coefficient	1.000
	Significance (2-tailed)	
	n	37
Ischemia time	Correlation coefficient	.806[a]
	Significance (2-tailed)	.000
	n	33

[a]Significative correlation at level of 0.01 (r = .81).

Table 2. Correlation Between Kidney Regions and Data From Fluorescence Spectroscopy

			95% Confidence Interval	
Region (Kidney)	Mean	Standard Error	Lower Bound	Upper Bound
SP	2.069	0.026	2.015	2.123
M	2.234	0.036	2.131	2.337
IP	2.070	0.026	2.017	2.124

SP, Superior pole; IP, inferior pole; M, middle area.

significantly higher mean value than the upper or lower pole (region: $F(1.60, 47.91) = 63.04$; $P < .001$).

The histologic analysis (Fig 3) was unable to characterize distinct patterns of ischemic tubular injuries at the various ischemic times, when the renal poles were compared to each other and to the middle third of the kidney. At a given ischemic time the histologic changes were similar regardless of the different evaluated renal region.

DISCUSSION

The use of spectroscopy to study ischemia is not new. Spectroscopy for tissue analysis was introduced by Chance and Williams in 1955.[13] They evaluated alterations in tissue fluorophores, such as mitochondrial NADH, during the process of cellular respiration leading to production of adenosine triphosphate. The principles used to obtain pulse oximetry, for example, employ spectrophotometry as a method that uses the difference in light absorption by oxyhemoglobin compared with carboxyhemoglobin. The pulse oximeter determines the peripheral oxygen saturation by the emission of red and infrared light by hemoglobin. It measures the changes in light absorption during the pulsatile cycle since hemoglobin in its oxygen-bound or unbound forms is recognized as one of the major absorber chromophores of biological tissues. For this purpose, the oximeter has a sensor fitted with a light photoemitter on one side and a photoreceptor on the other.[14]

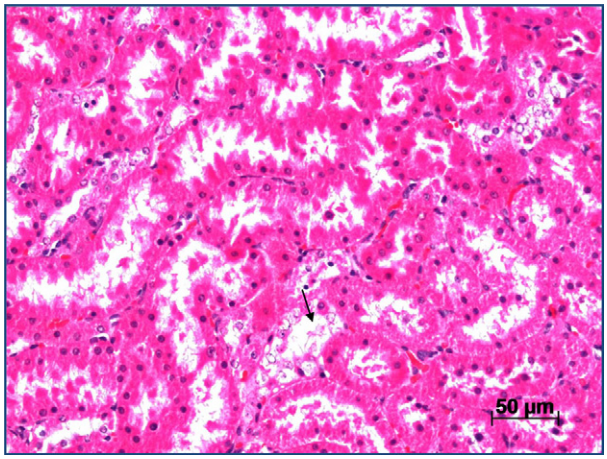

Fig 3. Acute tubular necrosis with cell desquamation into the light of the proximal tubules and tubular dilatation (arrow) hematoxylin and eosin 400 ×).

A question always raised when laser-induced FS is applied is the depth of penetration of the excitation laser into the renal tissue of the rat, and whether the molecules that compose the renal capsule can somehow interfere to significantly compromise the readings. The excitation laser penetrates the renal parenchyma in an extremely superficial manner (100 μm), but it is in this region not the medullary one that the targets of main interest are located, that is, the glomeruli and the proximal convoluted tubules, which are also the objectives of open or puncture biopsies.[15] Laser propagation in tissue is known to depend on light intensity, on the type of tissue studied, and on the wavelength used. The ability of tissue penetration increases with higher excitation wavelengths.[16–18]

Several studies have shown minimal interference by the renal capsule with FS measurements. The capsule is composed of the collagen and elastin do not undergo early changes during ischemia, in contrast to the renal parenchyma, which is formed by cells that are metabolically more active and sensitive to changes in the levels of hemoglobin, NADH, FAD, pH, and other fluorescent compounds.[19]

However, the renal capsule of humans is thicker than that of rats. In terms of the clinical applicability of the method described herein, it is important to confirm the depth of excitation laser penetration into the human kidney. This determination would assess the reliability of the information by analyzing the interference of the renal capsule in the results, and only later to validate the method in question.[17]

The present study showed that laser-induced FS could evaluate the changes among the phases of normal perfusion (autofluorescence), ischemia, and reperfusion of rats renal tissue. A statisticall significant difference was detected among the declines from the peaks of the curves during the ischemic phase, followed by recovery during the reperfusion phase, both of which depended on the ischemia time (Fig 1). A fall in fluorescence was observed with increasing ischemia time regardless of the excitation wavelength, as also reported by Fitzgerald et al in 2004.[17] This result suggests that all biological fluorophores, regardless of the wavelengths evaluated, behave in a similar manner in response to ischemia, possibly as a consequence of the intense changes in pH, which reduce the efficiency of fluorescence emission by fluorescent biological compounds.[20] In addition, the organ examined during ischemia becomes excessively rich in carboxyhemoglobin (cyanotic), increasing even more the absorptive properties of hemoglobin compared to the same organ under normal perfusion.[19] The origin of the changes in signal intensity during the ischemic and reperfusion phases has not been fully identified; it may require monitoring of additional parameters such as dispersal of excitation and emission or even intracellular pH.[21]

An important result also obtained in the present study was that, with increasing time of ischemia (for example, from 30 to 60 minutes), there was a significant fall in the peaks of the fluorescence curves during reperfusion, with a more significant fall being observed with longer ischemia times (Fig 2). This observation shows continuous and progressive molecular changes in ischemic tissue. A progressive increase in absorber chromophores such as carboxyhemoglobin occurs with time, as well as worsening of metabolic acidosis, which reduce fluorescence at the expense of the tissue fluorophores (fluorescent structures).

We cannot completely exclude an influence on laser propagation caused by morphologic and structural tissue changes secondary to the ischemia time. Fitzgerald et al[22] investigated fluorescence induced by a 335-nm laser in the kidneys of rats subjected to 18 or 85 minutes of warm ischemia followed by reperfusion. They detected a reduction of fluorescence to 78% and 65% of the initial values, respectively. After 18 to 50 minutes of reperfusion, there was a return of fluorescence to baseline preischemia values. No eventual change in fluorescence was detected among the group of rats subjected to 85 minutes of ischemia.

Due to the heterogeneity of ischemia throughout the kidney, the FS data obtained from a small site may not represent the totality of the surface. Multiple measurements are necessary to considered their mean value. For this reason, in the present study we opted to make measurements in three renal regions (ie, the upper and lower poles and the middle third). When these regions were compared, a post hoc Bonferroni test showed a significant difference. The middle third of the kidney presenting significantly higher mean values than the upper and lower poles (Table 3). This fact was not analyzed by Tirapelli et al[18] in a similar study, which, however, did not use the 408-nm laser.

Our results suggested that, to reach the conclusions as the present study, it would be sufficient to determine fluorescence only in the middle third of the kidney, with no need for an analysis of the upper and lower poles.

These observations lead us to some questions: could the renal circulation, with vessels of greater caliber in the central region of the hilus, have affected the findings of FS, causing the middle third of the kidney to be more sensitive to the effects of ischemia? Why do we obtain routine biopsies preferentially from the renal poles when the more sensitive changes may be located in the middle third of the organ?

In general, practical, and accepted terms, puncture or open biopsies are routinely directed at the poles because of the lower risk of hemorrhage and complications. The renal poles are believed to be a little less vascularized, to present a lower risk of bleeding, and for this reason to be even more sensitive to ischemic injuries. A practical thought is that if there is no ATN injury in the poles, there will also be no injuries in the middle third of the kidney. This was not the result obtained in the present study: the middle third of rat kidneys was more sensitive to ischemic and reperfusion changes as determined by FS. Although the hypothesis should be raised that the histologic changes provoked by ischemia are relevant but many of them are transitory, showing full recovery. Early metabolic changes, much more sensitive to FS light, should be investigated. These changes

appear to occur more intensely in the middle third of the kidney and may activate a series of humoral immunologic mechanisms invisible by standard light microscopy, culminating in severe long-term consequences such as chronic graft nephropathy.

The circulation is not believed to be the only factor responsible, since the excitation laser penetrates the renal parenchyma in a superficial manner at the extreme periphery of the cortex and analyzes a region in the middle third as with vessels as fine those at the renal poles in the same peripheral position. It should be remembered that FS is also affected by metabolic cell changes such as acidosis that modify the absorptive and fluorescent properties of the molecules.

In conclusion, the most appropriate site for a renal biopsy from the metabolic point of view is the middle third.

REFERENCES

1. Nankivell BJ, Kuypers DR. Diagnosis and prevention of chronic kidney allograft loss. *Lancet*. 2011;378(98):1428–1437.

2. Williams WW, Taheri D, Tolkoff-Rubin N, Colvin RB. Clinical role of the renal transplant biopsy. *Nat Rev Nephrol*. 2012;8(2):110–121.

3. Georgakoudi I, Jacobson BC, Müller MG, et al. NAD(P)H and collagen as in vivo quantitative fluorescent biomarkers of epithelial precancerous changes. *Cancer Res*. 2002;62:682–687.

4. Tsai T, Chen HM, Wang CY, Tsai JC, Chen CT, Chiang CP. In vivo autofluorescence spectroscopy of oral premalignant and malignant lesions: distorsion of fluorescence intensity by submucous fibrosis. *Lasers Surg Med*. 2003;33:40–47.

5. Zuluaga AF, Utzinger U, Durkin A, et al. Fluorescence excitation emission matrices of human tissue: a system for in vivo measurement and method of data analysis. *Appl Spectrosc*. 1999;53(3):302–311.

6. Wang CY, Tsai T, Chen HM, Chen CT, Chiang OP. PLS-ANN based classification model for oral submucous fibrosis and oral carcinogenesis. *Lasers Surg Med*. 2003;32:318–326.

7. Müller MG, Valdez TA, Georgakoudi I, et al. Spectroscopic detection and evaluation of morphologic and biochemical changes in early human oral carcinoma. *Cancer*. 2003;97(7):1681–1692.

8. Ramanujam N. Fluorescence spectroscopy in vivo. In: Meyers RA, ed. *Encyclopedia of Analytical Chemistry.* Chincherster, England; John Wiley & Sons Ltd; 2000:20–56.

9. Lakowicz JR. *Principles of Fluorescence Spectroscopy.* 2nd ed. New York, NY: Plenum Press; 1–49.

10. Georgakoudi I, Feld MS, Müller MG. Intrinsic fluorescence spectroscopy of biological tissue. In: Mycek MA, Pogue BW. *Handbook of Biomedical Fluorescence.* New York, NY: Marcel Dekker; 2003;109–142.

11. Goujon JM, Hauet T, Menet E, et al. Histological evaluation of proximal tubule cell injury in isolated perfused pig kidneys exposed to cold ischemia. *J Surg Res*. 1999;82:228–233.

12. Solez K, Colvin RB, Racusen LC, Sis B, Halloran PF, Birk PE, et al. Banff's 2005 meeting report: differential diagnosis of chronic allograft injury and elimination of chronic allograft nephropathy ("CAN"). *Am J Transplant*. 2007;7(3):518–526.

13. Chance B, Williams GR. Respiratory enzymes in oxidative phosphorylation in the kinetics of oxygen utilization. *J Biol Chem*. 1955;217:383.

14. Carlson KA, Jahr JS. A historical overview and update on pulse oximetry. *Anesthesiol Rev*. 1993;20:173–181.

15. Demos SG, Alfano RR. Optical polarization imaging. *Appl Opt*. 1997;36:150.

16. Melo CA, Lima AL, Brasil IR, et al. Characterization of light penetration in rat tissues. *J Clin Laser Med Surg*. 2001;19:175–179.

17. Fitzgerald JT, Demos S, Michalopoulou A, Pierce JL, Troppmann C. Assessment of renal ischemia by optical spectroscopy. *J Surg Res*. 2004;122:21–28.

18. Tirapelli LF, Trazzi BFM, Bagnato VS, et al. Histopathology and laser autofluorescence of ischemic kidneys of rats. *Lasers Med Sci*. 2009;24:397–404.

19. Gryczynski Z, Gryczynski L, Lakowicz J. Fluorescence sensing methods. *Methods Enzymol*. 2003;360:44.

20. Lin HJ, Herman P, Lakowicz J. Fluorescence lifetime-resolved pH imaging of living cells. *Cystometry.* 2003;52(a):77.

21. Raman RN, Pivetti CD, Matthews DL, Troppmann C, Demos SG. Quantification of in vivo autofluorescence dynamics during renal ischemia and reperfusion under 355 nm excitation. *Opt Express*. 2008;16(7):4930–4944.

22. Fitzgerald JT, Michalopoulou A, Pivetti CD. Real-time assessment of in vivo renal ischemia using laser autofluorescence imaging. *J Biomed Opt*. 2005;10(4):44018(1)–44018(7).

cepof.ifsc.usp.br

Grupo de Óptica / CePOF, Instituto de Física de São Carlos, Universidade de São Paulo
Av. Trabalhador Sancarlense, 400, Centro, CP 369, 13560-970, São Carlos - SP
Telefones: (16) 3373-9810; 3373-9823 - Fax: 3373-9811